VILNIUS UNIVERSITY
CENTER FOR PHYSICAL SCIENCES AND TECHNOLOGY

STEPONAS RAIŠYS

TUNING EXCITON DIFFUSION IN ORGANIC OPTOELECTRONIC MATERIALS

Doctoral Dissertation
Physical Sciences, Physics (02P)

Vilnius, 2017

The dissertation was prepared at Vilnius University in 2013 – 2017.

Scientific supervisor – dr. Karolis Kazlauskas (Vilnius University, Physical sciences, Physics – 02P).

VILNIAUS UNIVERSITETAS
FIZINIŲ IR TECHNOLOGIJOS MOKSLŲ CENTRAS

STEPONAS RAIŠYS

EKSITONŲ DIFUZIJOS VALDYMAS ORGANINĖS OPTOELEKTRONIKOS MEDŽIAGOSE

Daktaro disertacija
Fiziniai mokslai, fizika (02P)

Vilnius, 2017 metai

Disertacija parengta 2013 – 2017 metais Vilniaus universitete.

Mokslinis vadovas – dr. Karolis Kazlauskas (Vilnius universitetas, fiziniai mokslai, fizika – 02P).

List of abbreviations

A – molecular separation constant

a – radius of the fluorophore's cavity

C – concentration

c – speed of light

CT – charge transfer

°C – degrees Celsius

3D – three dimentional

D – exciton diffusion coefficient

d – intermolecular distance

D-A – donor - acceptor

DMPE – 2,2-di(4-methoxyphenyl)ethenyl)

DPA – 9,10-diphenylanthracene

DPE – 2,2-diphenylethenyl

eq – equation

$[E]_{x,t}$ – exciton concentration as a function of distance x and time t

F – collision frequency

Δf – orientation polarizability

f – oscillator strength

f_a – fraction

f_i – fractional contribution to the total fluorescence intensity

F_D – normalized fluorescence spectrum

FL – fluorescence

FRET – Förster resonance energy transfer

$G_{x,t}$ –exciton generation rate

h – hour

HOMO – highest occupied molecular orbital

h – Planck's constant

I_0 – emission intensity without quencher

IM – naphthalimide

IME – naphthalimide-ethenyl

I_q – emission intensity with a quencher

IRF – instrument response function

ISC – intersystem crossing

I_{th} – intensity threshold

I_{UC} – upconversion intensity

$I_{UC(q)}$ – upconversion intensity with a quencher

$J(\lambda)$ – spectral overlap integral

k – intrinsic exciton decay rate

k_F – Förster energy transfer rate

k_q – exciton quenching rate

K_{SV} – Stern-Volmer constant

L_D – exciton diffusion length

LED – light emitting diode

λ – wavelength

λ_{ex} – excitation wavelength

λ_{FL}^{max} – fluorescence band maximum

λ_{abs}^{max} – absorption band maximum

LUMO – lowest unoccupied molecular orbital

M – molecule

M^* – excited molecule

$\Delta\mu$ – change in the dipole moments of excited and ground states

μ_E – dipole moment of excited state

μ_G – dipole moment of ground state

MPE – 2-methyl-2-phenylethenyl

n – refraction index

N_A – Avogadro's number

$\bar{\nu}_A$ – absorption maxima in cm^{-1}

$\bar{\nu}_F$ – fluorescence maxima in cm^{-1}

OLED – organic light emitting diode

OSC – organic solar cell

P – probability

P3HT – poly(3-hexylthiophene-2,5-diyl)

PCBM – [6,6]-phenyl-C61-butyric acid methyl ester

PE – pyreneethynylene derivative

PL – photoluminescence

$PL_{(blend)}$ – photoluminescence transients with a certain PCBM concentration

$PL_{(pristine)}$ – photoluminescence transients without PCBM

PMMA – poly(methyl methacrylate)

PS – polystyrene

PtOEP – platinum octaethylporphyrin

Q – relative quenching efficiency

Q_C – quencher molecule

$[Q_c]$ – quencher concentration

r – reaction radius

R_0 – Förster radius

R_a – annihilation radius

ρ – density

SSET – singlet-singlet energy transfer

SED – singlet exciton diffusion

t – time

TED – triplet exciton diffusion

THF – tetrahydrofuran

TPA – triphenylamine

TPD – triphenylamine dimer

TTA – triplet – triplet annihilation

TTET – triplet-triplet energy transfer

$[T]_t$ – triplet exciton concentration as a function of time

UC – light upconversion

wt% – percentage by weight

Z – dimensionality constant

γ – second order annihilation rate

ε' – absorption intensity at

ε – dielectric constant

κ – dipole orientation factor

σ_A – absorption cross-section

τ – exciton lifetime

τ_q – exciton lifetime in a presence of quencher

$<\tau>$ – average emission lifetime

Φ_{FL} – fluorescence quantum yield

Φ_{Ph} – phosphorescence quantum yield

Φ_{UC} – upconversion quantum yield

1 Introduction

Mostly composed of carbon atoms organic materials have almost unlimited possibilities for tunability of their electrical and optical properties through chemical engineering.[1] Moreover, molecular structure of organic compounds predetermines their intermolecular interactions and thus distinctive molecular packing in the solid state resulting in unique mechanical properties. These properties allow producing lightweight, flexible, stretchable, thin, transparent, large area and potentially cheap optoelectronic devices, which in fact boosted the existing popularity of organic semiconductors.[2,3] Solution processability of organic materials enables implementation of a variety of printing technologies, such as inkjet printing or stamping, and thus allows fabricating large area devices from roll to roll at low cost. The synergy of electrical and mechanical properties led to the development of unique organic devices, in many aspects outperforming inorganic semiconductor-based analogs. The spectrum of such devices is very broad and covers multiple areas of potential applications e.g. integrated circuits,[4] general lighting,[5] displays,[6] sensing,[7] xerography,[8] solar harvesting[9] and many others.[10] However, a large variety of potential applications does not guarantee a successful commercialization, on the contrary, it requires extensive research to make organic electronic devices competitive on the market. Although intensions to reduce the consumption of fossil fuel and steadily increasing world's energy demand intensely pushes the development of organic photovoltaics, relatively low durability and efficiency of OSCs are serious issues remaining to be solved.[11]

The solar energy harvesting in OSCs is ensured by a series of cascading processes, i.e. absorption of solar light, exciton generation, exciton diffusion to the donor-acceptor interface, exciton dissociation into free carriers, drift of the electrons and holes towards the electrodes as

well as carrier extraction from the material. Since all of these processes occur sequentially, the efficiency of each process must be maximized to achieve the highest possible device performance. It has been demonstrated that power conversion efficiency of OSC directly correlates with exciton diffusion length in donor material, since it is one of the primary processes in operation of solar cell.[12] Exciton diffusion length in disordered organic materials usually does not exceed 10 nm, while the absorption depth of the solar light in donor and acceptor materials is typically higher than 100 nm. This implies exciton relaxation before reaching donor-acceptor interface, where it could dissociate and further contribute to the photocurrent. To this end, the research of materials possessing long exciton diffusion length and the ways of enlarging it by chemical engineering are of great importance.

Another important factor determining efficiency of OSCs is the capability to harvest full spectrum of solar radiation. Since the solar spectrum is broad, extending from visible to infrared region, it is virtually impossible to create organic compound capable of absorbing all of the sunlight. One possible way is to combine several organic materials possessing different bandgaps and stack them in tandem solar cells. An alternative approach is to exploit light upconversion phenomenon, which enables conversion of low energy photons to higher energy ones, thus ensuring utilization of broader spectral range of solar radiation for OSC.[13] Light upconversion has the advantage over tandem OSC that it does not require diligent adjustment of the layers in the cells to keep balanced photocurrent and avoid potential barriers for charge carriers. The light upconversion mediated by triplet-triplet annihilation (TTA-UC) in organic semiconductors can be achieved under incoherent excitation and at relatively low excitation power densities (~10 mW/cm^2), which are directly available from the sun.[14] The quantum yield of TTA-UC in solution or liquid medium exceed 26%,[15] however for practical applications solid

state materials are preferred, which, demonstrate one order of magnitude lower Φ_{UC}.[16] The reduced efficiency in the solid films compared to solutions is typically ascribed to insufficient triplet exciton diffusion. However, no systematic studies of triplet exciton diffusion in the solid upconverting films have been carried out so far.

1.1 Aim and objectives of the dissertation

The dissertation is aimed at achieving tunability of exciton diffusion in organic solid films of triphenylamine (TPA) and 9,10-diphenylanthracene (DPA) compounds, and thereby enhancing their performance for organic optoelectronic applications like solar cells, light upconverters etc. To achieve the goal the following tasks were formulated:

1. To perform photophysical measurements of phenylethenyl-substituted TPA compounds and determine the photophysical processes ongoing in these compounds in various environments as a function of number and type of phenylethenyl sidearms.
2. To quantitatively evaluate exciton diffusion in the TPA films by time-resolved fluorescence bulk-quenching technique followed by Monte Carlo simulations as a function of the number of different phenylethenyl and naphthalimide sidearms.
3. To determine fluorescence concentration quenching, energy transfer efficiency, emission quantum yield in light upconverting DPA polymeric films as a function of emitter concentration.
4. To estimate singlet and triplet exciton diffusion in light upconverting DPA polymeric films as a function of emitter concentration.
5. To assess the influence of concentration of triplet exciton sensitizer to the TTA-UC quantum yield.
6. To evaluate potential of singlet exciton sink approach for enhancing TTA-UC in the solid films.

1.2 Novelty and relevance

In the dissertation the photophysical properties and energy transfer studies of the new phenylethenyl-substituted TPA derivatives are described. It is found that in solid films of branched TPA derivatives a dense network of the sidearms is formed, which results in prolonged exciton diffusion length. Such effect has not been observed before. Research disclosing materials with long diffusion length is very important for the development of efficient solar cells or other optoelectronic devices.

The film formation technology by melt-processing followed by rapid cooling allows achieving high concentrations (up to 40 wt%) of DPA in the polymer matrix with low fluorescence quenching (up to 65% of the initial efficiency). Films with such high DPA concentrations and small aggregation were not demonstrated before. A large concentration of the emitter ensures efficient exciton diffusion and relatively high light upconversion efficiency in the solid state. Moreover, time-resolved emission bulk-quenching method was applied to determine triplet exciton diffusion length by utilizing light upconversion signal as a probe for the first time. Triplet and singlet exciton diffusion length measurements in the light upconverting solid films were performed and their impact on the light upconversion efficiency was assessed. Such exciton diffusion experiments in light upconverting films have not been carried out before and are new. A possibility to enhance TTA-UC quantum yield by utilizing singlet exciton sink approach, which allows achieving record high upconversion efficiency in the amorphous solid films was also demonstrated. High TTA-UC efficiency is exceptionally relevant to the practical applications of light upconverting TTA-UC films for enhancing performance of the solar cells and other TTA-UC based optoelectronic devices.

1.3 Statements of the dissertation

1. Tuning of singlet exciton diffusion length in the films of TPA compounds can be accomplished *via* incorporation of different number and type of phenylethenyl or naphthalimide sidearms, which form a dense network of exciton hopping sites in the amorphous TPA films and facilitate exciton diffusion.
2. Triplet exciton diffusion length in DPA polymeric films increases (from 22 to 60 nm) with emitter content (from 20 to 35 wt%) and is not the main limiting factor of TTA-UC efficiency. Lowered TTA-UC performance is caused by energy back-transfer of singlet excitons from emitter to sensitizer and diffusion-enhanced non-radiative decay of triplet excitons at higher DPA loadings (>25 wt%).
3. UC signal originating from TTA can be used as a probe for quantitative evaluation of triplet exciton diffusion.
4. Singlet exciton sink approach is suitable for enhancing green to blue TTA-UC efficiency in sensitized DPA polymeric films.

1.4 Publications related to the dissertation

1. S. Raisys, K. Kazlauskas, S. Jursenas, Y. Simon, The role of triplet exciton diffusion in light-upconverting polymer glasses, *ACS Applied Materials and Interfaces*, 8, 15732-15740 (2016).
2. R. R. Reghu, J. Simokaitiene, J. V. Grazulevicius, S. Raisys, K. Kazlauskas, S. Jursenas, V. Jankauskas, A. Reina, Synthesis and properties of hole-transporting triphenylamine-derived dendritic compounds, *Dyes and Pigments*, 115, 135-142 (2015).
3. S. Raisys, K. Kazlauskas, M. Daskeviciene, T. Malinauskas, V. Getautis, S. Jursenas, Exciton diffusion enhancement in triphenylamines via incorporation of phenylethenyl sidearms, *Journal of Materials Chemistry C*, 2, 4792-4798 (2014).

4. M. Cekaviciute, J. Simokaitiene, V. Jankauskas, S. Raisys, K. Kazlauskas, S. Jursenas, J. V. Grazulevicius, Structure-properties relationship of phenylethenyl-substituted triphenylamine, *The Journal of Physical Chemistry C*, 117, 7973–7980 (2013).
5. T. Malinauskas, M. Daskeviciene, G. Bubniene, I. Petrikyte, S. Raisys, K. Kazlauskas, V. Gaidelis, V. Jankauskas, R. Maldzius, S. Jursenas, V. Getautis, Phenylethenyl-substituted triphenylamines: efficient, easily obtainable and inexpensive hole-transporting materials, *Chemistry – A European Journal*, 19, 15044–15056 (2013).

1.5 Other publications

1. A. Ivanauskaite, R. Lygaitis, S. Raisys, K. Kazlauskas, G. Kreiza, D. Volyniuk, D. Gudeika, S. Jursenas, J. V. Grazulevicius, Structure-properties relationship of blue solid state emissive phenanthroimidazole derivatives, *Physical Chemistry Chemical Physics,* 19, 16737–16748 (2017).
2. E. Stanislovaityte, J. Simokaitiene, S. Raisys, H. A. Al-Attar, J. V. Grazulevicius, A. P. Monkman, V. Jankus, Carbazole based polymers as hosts for blue iridium emitters: synthesis, photophysics and high efficiency PLEDs, *Journal of Materials Chemistry C*, 1, 8209–8221 (2013).
3. V. N. Kozhevnikov, Y. Zheng, M. Clough, H. A. Al-Attar, G. C. Griffiths, K. Abdullah, S. Raisys, V. Jankus, M. R. Bryce, A. P. Monkman, Cyclometalated Ir(III) complexes for high-efficiency solution-processable blue PhOLEDs, *Chemistry of Materials*, 25, 2352–2358 (2013).

1.6 Conference presentations

1. S. Raišys, G. Bučytė, K. Kazlauskas, S. Juršėnas, Enhanced upconversion efficiency *via* emitter structural modification, E-MRS 2017 Spring Meeting. (Strasbourg, France, May 22-26, 2017).
2. G. Bučytė, S. Raišys, P. Adomėnas, K. Kazlauskas, S. Juršėnas, Optimization of modified anthracene compounds for light upconversion, 60th Scientific Conference for Young Students of Physics and Natural Sciences - Open Readings 2017, Programme and Abstracts (Vilnius, Lithuania, March 14-17, 2017) p. 259.
3. S. Raišys, K. Kazlauskas, S. Juršėnas, Y. C. Simon, Role of triplet exciton diffusion in light-upconverting polymer glasses, 2nd International Caparica Conference on Chromogenic and Emissive Materials. Proceedings book (Caparica, Portugal, September 5-8, 2016) p. 134.
4. S. Raišys, K. Kazlauskas, S. Juršėnas, Y. Simon, Triplet exciton diffusion in light up-converting diphenylantracene/poly(methyl methacrylate) films, Conference Functional Materials and Nanotechnologies. Abstract book (Vilnius, Lithuania, October 5-8, 2015) p. 138.
5. S. Raišys, K. Kazlauskas, S. Juršėnas, Y. Simon, Sensitizer-limited exciton diffusion in light-upconverting diphenylanthracene/PMMA films, 4th International Conference on the Physics of Optical Materials and Devices. Book of Abstracts (Budva, Montenegro, September 31-August 4, 2015) p. 116.
6. S. Raišys, K. Kazlauskas, S. Juršėnas, Y. Simon, Triplet exciton diffusion: impact to light upconversion efficiency in polymer films, 41st Lithuanian national physics conference, (Vilnius, Lithuania, June 17-19, 2015).
7. S. Raišys, G. Kreiza, S. Grigalevičius, K. Kazlauskas, S. Juršėnas, Bifluorene derivatives for fluorescence organic nanoaggregates, 7th

International conference on Molecular Electronics, (Strasbourg, France, August 24-29, 2014).

8. S. Raišys, K. Kazlauskas, M. Daškevičienė, T. Malinauskas, V. Getautis, S. Juršėnas, Manipulation of exciton diffusion length in triphenylamine compounds, XVth International Krutyn Summer School "Challenges to open up the new era of organic photonics and electronics from material to market - from Asian perspective", (Krutyn, Masurian Lake District, Poland, June 8-14, 2014).
9. K. Kazlauskas, S. Raišys, D. Tomkute-Luksiene, M. Daškevičienė, T. Malinauskas, V. Getautis, S. Juršėnas, Exciton diffusion length in triphenylamine with different number of phenylethenyl sidearms, 11th International symposium on functional pi-electron systems. Program (Arcachon, Aquitaine, France, June 2-7, 2013) p. 9.
10. S. Raišys, K. Kazlauskas, M. Daškevičienė, T. Malinauskas, V. Getautis, S. Juršėnas, Enhancement of exciton diffusion: by attaching phenylethenyl side groups, 40th Lithuanian national physics conference, (Vilnius, Lithuania, June 10-12, 2013) p. 70.
11. S. Raišys, K. Kazlauskas, M. Daškevičienė, T. Malinauskas, V. Getautis, S. Juršėnas, Exciton diffusion in triphenylamine based compounds, 56th Scientific Conference for Young Students of Physics and Natural Sciences - Open Readings 2013, Programme and Abstracts (Vilnius, Lithuania, March 20-23, 2013) p. 22.
12. S. Raišys, K. Kazlauskas, M. Daškevičienė, T. Malinauskas, V. Getautis, S. Juršėnas, Exciton diffusion length in thriphenylamine derivatives, 3rd young scientists conference “Interdisciplinary research of physical and technology science”, (Vilnius, Lithuania, February 12, 2013).

1.7 Participation in scientific projects and internships

1. January 2013 – September 2015. "Control of the photophysical properties of multifunctional molecular systems", (Global Grant, The Research Council of Lithuania, 2012-2015).
2. May 2013 – November 2014. "Flexible structure bearing bifluorene compounds for optoelectronics industry, BiFluorenas", (EU structural funds, 2013-2015).
3. November 2014 – April 2015. Six months internship at Adolphe Merkle Institute, Fribourg University, Switzerland (Scientific Exchange Programme NMS-CH). Project "Triplet Diffusion in Sensitized Upconversion". Supervised by dr. Yoan C. Simon (group of prof. C. Weder).

1.8 Author's contribution

The author carried out all the experiments described in the dissertation, performed necessary calculations and simulations. The author was very active in interpretation of the results and preparation of the drafts of publications.

Synthesis of the new materials presented in the dissertation was carried out by research groups leaded by prof. Vytautas Getautis (Kaunas University of Technology), prof. Juozas V. Gražulevičius (Kaunas University of Technology) and prof. Suresh Valiyaveettil (National University of Singapore) to whom author is very grateful.

1.9 Layout of the dissertation

The dissertation is organized as follows. In Chapter 1 the introduction of the dissertation is presented, in which the importance of exciton diffusion in organic optoelectronic materials is emphasized,

followed by the aim and objectives of the dissertation, novelty and relevance, statements of the dissertation, list of publications related to the dissertation, other publications, list of presentations in the conferences, participation in scientific projects and internships and author's contribution to the dissertation.

In Chapter 2 an overview of the methods of exciton diffusion measurements is presented, highlighting the three main methods used in the dissertation.

Chapter 3 describes preparation of samples and experimental techniques in detail. These include fluorescence, delayed fluorescence and phosphorescence spectroscopy, emission quantum yield measurements as well as emission transients using variable optical window method and time correlated single photon counting.

Chapter 4 presents experimental results and discussion with two main sections. Section 1 begins with the overview of the TPA derivatives used in the optoelectronic devices, followed by the photophysical properties of the three groups of phenylethenyl-substituted TPA derivatives. Thereafter, the exciton diffusion measurements, simulations and theoretical calculations of the three groups of TPA compounds (phenylethenyl-substituted TPA monomers and dimers, and naphthalimide-substituted triphenylamines) are presented. Section is completed with the summary of Section 1. Section 2 starts with the overview of the latest achievements of the TTA based light upconversion. Here follows fluorescence concentration quenching measurement of the PMMA films with heavily doped DPA. Thereafter, the triplet-triplet energy transfer efficiency of light upconverting PMMA films as well as TTA-UC quantum yield measurements is presented. Further, triplet exciton diffusion length is determined in the DPA/PtOEP/PMMA films with increasing DPA concentration. Also the upconversion quenching by the triplet exciton sensitizer is analyzed in great detail, followed by singlet

exciton diffusion measurement by Monte Carlo and Stern-Volmer methods. Finally, the way to increase light upconversion efficiency by utilizing fluorescent singlet exciton sink is demonstrated. Section is completed with the summary of Section 2.

In Chapter 5 conclusions of the dissertation are formulated.

2 Methods for evaluation of exciton diffusion

Excitons in disordered organic medium travel by a random walk and during their lifetime can diffuse only a certain distance. That distance can be expressed as an average diffusion length

$$L_{\mathrm{D}} = \sqrt{ZD\tau}, \tag{1}$$

where D is the diffusion coefficient, τ is the exciton lifetime, and Z is dimensionality constant, which can be 1, 2 or 3 for one-dimensional, two-dimensional and three-dimensional diffusion, respectively.

There are several methods for the determination of exciton diffusion length. These methods include fluorescence surface quenching,[12,17] time-resolved fluorescence bulk-quenching,[18,19] exciton-exciton annihilation,[20] photocurrent modeling,[21,22] time-resolved microwave conductivity,[23] direct imaging of exciton migration[24] and Förster resonance energy transfer calculation[25]. Each of them has its own advantages and drawbacks, e.g. sample preparation, performance of experiments or data analysis, etc.[26]

Surface quenching method is based on fluorescence quenching by a thin layer of quencher on top of the organic material. Excitons generated in the organic material diffuse toward quenching surface where they are quenched by the charge or energy transfer into the quencher. The exciton quenching efficiency of the samples with different thickness of organic layer can be determined by either steady-state or time-resolved fluorescence measurements. For the steady-state measurement the amount of absorbed light and the optical interference effects should be taken into account, whereas for the time-resolved method these could be ignored. In both cases, efficient quencher, the sharp interface between quencher and organic material and precise film thickness is necessary for the accurate determination of exciton diffusion length. The following diffusion equation is used for the determination of D:

$$\frac{\partial [E]_{x,t}}{\partial t} = G_{x,t} + D\frac{\partial^2 [E]_{x,t}}{\partial x^2} - k[E]_{x,t} - k_q[E]_{x,t}, \quad (2)$$

where $[E]_{x,t}$ is exciton concentration depending on the distance x from the quenching surface and time t, $G_{x,t}$ is the exciton generation rate, k is the intrinsic exciton decay rate measured in the film of the same thickness without quenching surface and k_q is the surface quenching rate.

Exciton-exciton annihilation method allows determining L_D by measuring time-resolved emission at variable excitation power densities. At the certain excitation fluence excitons experience diffusion limited collision and annihilation. Exciton-exciton annihilation dominates at high exciton densities therefore high excitation power densities are required for experiments. Concentration of excitons changes over time according to kinematic equation:

$$\frac{d[E]_{x,t}}{dt} = G_{x,t} - k[E]_{x,t} - \gamma[E]_{x,t}^{\ 2}, \quad (3)$$

where γ is annihilation rate. For the time-independent annihilation the rate is expressed as follows:

$$\gamma = 4\pi R_a D, \quad (4)$$

where R_a is radius at which annihilation between excitons occurs. The annihilation takes place in bulk organic material therefore three-dimensional diffusion is assessed.

Photocurrent modeling takes into account that in OSCs charges are generated after diffusion of excitons to a heterojunction. In a planar heterojunction solar cell, the excitons created further than diffusion length from heterojunction will not be able to participate in photocurrent generation. In this case the photocurrent of the device is linked to exciton diffusion length. By changing the film thickness and excitation wavelength the exciton diffusion length can be estimated.[21,22]

Using time-resolved microwave conductivity the exciton diffusion in non-fluorescent materials can be evaluated. The planar

heterojunction is used for charge carriers' generation and a microwave probe to measure the conductivity increase in the sensing layer when excitons reach heterojunction and the charges are injected. Only excitons within a diffusion length of the heterojunction can contribute to photoconductivity, therefore L_D can be determined.[23]

Direct imaging of excitons is rather simple method wherein the organic material is excited with a focused laser beam and the images of resulting fluorescence at different delay times after excitation are captured. Experimental realization of this method is quite complicated as excitation laser beam spot in many cases is larger than exciton diffusion length, therefore it has been applied only for materials with long L_D such as organic crystals.

Bulk (or volume) quenching method similar to surface quenching method is also based on fluorescence quenching, but instead of quenching surface the homogeneously distributed quenchers in organic material are used. Exciton quenching efficiency versus quencher concentration in the blend films is measured. For the accurate determination of L_D the homogeneous distribution of quencher should be ensured, otherwise L_D might be underestimated. The emission quenching data can be analyzed by a Monte Carlo simulation[18] or using Stern–Volmer analysis[19].

In Förster resonance energy transfer (FRET) theory the exciton energy is transferred through the Coulomb coupling between transition dipole moments of neighboring molecules. Exciton diffusion coefficient is calculated from the Förster radius and the distance between interacting molecules. FRET enables relatively easy estimation of L_D, however, this method requires a number of specific parameters, such as the average dipole orientation, intermolecular distance and index of refraction which are often difficult to obtain experimentally.[26]

Fluorescence bulk-quenching analyzed by a Monte Carlo simulation and the Stern–Volmer theory and FRET calculations will be explained in more detail as these methods will be used in this dissertation for diffusion length determination.

2.1 Monte Carlo simulations

The method allows to determine exciton diffusion length in organic materials by blending them with a low concentration of [6,6]-phenyl-C61-butyric acid methyl ester (PCBM), which has low laying singlet (lowest absorption band at 697 nm) ant triplet energy levels and acts as an efficient exciton quencher (Fig. 1).[18,27] Experimentally measured photoluminescence (PL) decays of blends then are modeled using a Monte Carlo simulation of 3D exciton diffusion. The measured decay of organic material and PCBM blends with increasing PCBM concentration shows accelerated PL decay. The reduction of the PL decay time is a result of the diffusion limited exciton quenching by the PCBM quencher. When the

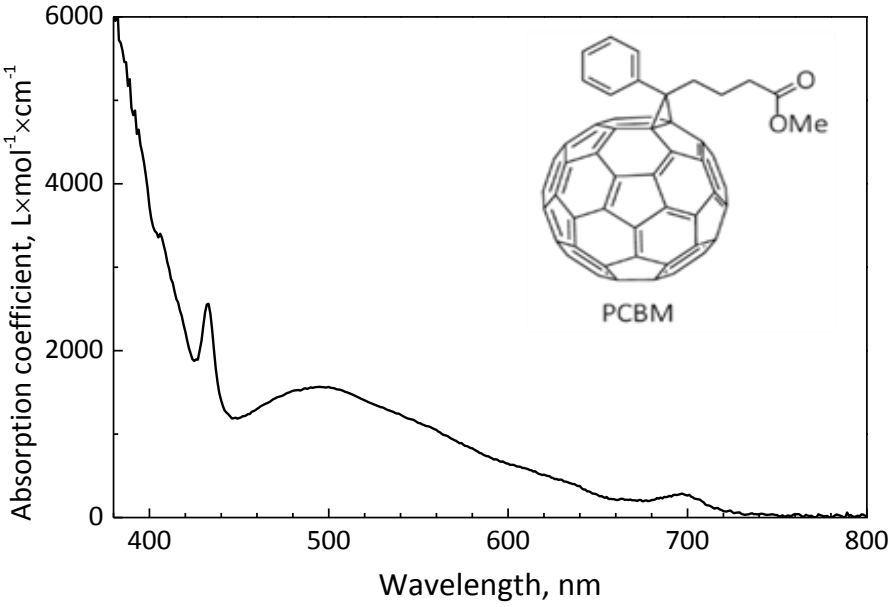

Fig. 1. Absorption spectrum of PCBM in poly(methyl methacrylate) and its molecular structure.

average distance between PCBM molecules is similar to the exciton diffusion length significant quenching is observed. In this case the measured PL decay time represents the average diffusion time to quenchers, rather than the natural decay time. It is very important to assure that PCBM molecules do not aggregate and form clusters in the organic material, otherwise PL decay will show slower quenching due to reduced effective quenching. Fortunately, for the conduction of experiments low PCBM concentrations (0 – 2 wt%) were sufficient, which consequently lowered probability of PCBM aggregation. However, this method is not very suitable for the crystalline or polycrystalline organic materials. According to Monte Carlo simulation non-interacting excitons undergo a random walk in the medium and decay non-radiatively if they reach a quencher during their lifetime. In the simulations the input parameters are fluorescence decay time of the pristine film and relative quenching efficiency (Q) at a given PCBM concentration in the blend. The Q is calculated from the following equation:

$$Q = 1 - \frac{\int PL_{(blend)}\mathrm{d}t}{\int PL_{(pristine)}\mathrm{d}t}. \quad (5)$$

Here $PL_{(\mathrm{blend})}$ and $PL_{(\mathrm{pristine})}$ is photoluminescence transients at a certain and 0 wt% PCBM concentration, respectively.

As an output the PL decay, i.e. the number of radiatively decayed excitons versus time is obtained. The simulation is repeated with the adjusted exciton diffusion coefficient, which is the only one fitting parameter, until the simulated and experimental PL decay curves converge.

The simulation is performed in a cubic box in which PCBM quenchers are placed. This simulation box has the edge length of 50 nm and periodic boundary conditions. PCBM molecules are assumed to be spheres with the radius of 0.5 nm. The size of the excitons is assumed to be equal to the size of PCBM molecules.[18]

At room temperature exciton hopping in organic material can be described by normal diffusion equation:[28]

$$\frac{\partial [E]_{x,t}}{\partial t} = D\frac{\partial^2 [E]_{x,t}}{\partial x^2} - k[E]_{x,t}, \quad (6)$$

where $[E]_{x,t}$ is exciton concentration as a function of the distance x and time t, D is diffusion coefficient, k is the intrinsic exciton decay rate. According to the Einstein's theory of random walks the normal diffusion can be described as a random walk with constant step size.[18] Exciton is moved in a random direction by a fixed distance δs after time interval δt. The latter is related to the diffusion coefficient D by:

$$D = \frac{\delta s^2}{6\delta t}. \quad (7)$$

The L_D then can be calculated using equation 1. The δt should be short enough in order for δs would be several times smaller than the quencher size. In the simulation the exciton is quenched if its position overlaps with quencher site. Radiative relaxation of the exciton is assumed if an exciton after time t_i did not reach quencher. For this t_i is fixed at the beginning of the simulation by:

$$t_i = -\tau \ln(w_i), \quad (8)$$

where w_i is a random number between 0 and 1.

This fluorescence bulk-quenching method is rather simple, requires no special sample preparation and complicated modeling with many fitting parameters, therefore is convenient for the estimation of D and L_D.[18]

2.2 Förster resonance energy transfer calculations

FRET calculations can be employed to estimate L_D. For this analytical method the absorption and fluorescence spectra, as well as fluorescence quantum yield, fluorescence lifetime, molecular orientation factor, intermolecular distance and refraction index of a single pristine

film should be measured. According to the Förster's theory, the rate of energy transfer (k_F) between two weakly coupled dipoles is expressed as:[29]

$$k_F = \frac{1}{\tau}\left(\frac{R_0}{d}\right)^6, \tag{9}$$

where τ is the exciton lifetime and d is the intermolecular distance. The Förster radius for energy transfer (R_0), which shows the distance where the energy transfer efficiency is 50%, is expressed as:

$$R_0^6 = \frac{9\Phi_F\kappa^2}{128\,\pi^5 n^4}\int \lambda^4 F_D\,(\lambda)\sigma_A(\lambda)d\lambda = \frac{9\Phi_F\kappa^2}{128\,\pi^5 n^4}\,J(\lambda), \tag{10}$$

where Φ_{FL} is the fluorescence quantum yield, κ is dipole orientation factor, n is the refraction index, λ is the wavelength, F_D is the normalized fluorescence spectrum, σ_A is absorption cross-section, and $J(\lambda)$ is spectral overlap integral. The κ is often assumed to be $0.845\sqrt{2/3}$ for amorphous film with randomly oriented dipoles.[30] Exciton diffusion length can be defined in terms of k_F as:[31,32]

$$L_D^2 = AZ\tau d^2 k_F, \tag{11}$$

where A is a constant, which accounts for the distribution of molecular separation in an amorphous film and Z - describes dimensionality of the diffusion process. Combining equations (9), (10) and (11) L_D can be written as follows:

$$L_D = \sqrt{AZ}\,\frac{R_0^3}{d^2} = \frac{\sqrt{AZ}}{d^2}\sqrt{\frac{9\Phi_F\kappa^2}{128\,\pi^5 n^4}J(\lambda)}\,. \tag{12}$$

2.3 Stern-Volmer quenching analysis for determination of triplet exciton diffusion *via* TTA-UC

In Stern-Volmer approach[19,33] emission transients of a photophysical intermolecular deactivation processes are analyzed with a presence of emission quencher. This quenching process follows the reaction scheme:

$$M^* + Q_c \rightarrow M + Q_c \quad (13)$$

where M is molecule, Q_C is emission quencher and * designates an excited state. The kinetics of this process follows the Stern–Volmer relationship:

$$\frac{I_0}{I_q} = 1 + K_{SV}[Q_C], \quad (14)$$

here I_0 is the emission intensity without a quencher, I_q is the intensity with a quencher, K_{SV} is Stern-Volmer constant and $[Q_C]$ is quencher concentration. Instead of emission intensity the emission quantum yield or lifetime can be used. In the case when only a fraction (f_a) of the molecules M is accessible to the quencher due to its aggregation at higher concentrations the "hindered access model" is applied.[19] Then quenching efficiency can be expressed as follows:

$$\frac{I_0 - I_q}{I_0} = \frac{\tau - \tau_q}{\tau} = f_a - \frac{f_a}{1 + K_{SV}[Q_c]}. \quad (15)$$

Stern-Volmer constant is quenching rate coefficient (k_q) multiplied by exciton lifetime (τ):

$$K_{SV} = k_q \tau. \quad (16)$$

The exciton quenching rate is proportional to the probability (P) that a quenching reaction will occur when exciton collides with the quencher and the frequency (F) of these collisions:

$$k_q = PF. \quad (17)$$

The collision frequency is directly proportional to diffusion constant D:

$$F = 4\pi r D N_A, \quad (18)$$

where r is the reaction radius of the two colliding species and N_A is Avogadro's number.

It has been demonstrated that Stern-Volmer quenching theory can be applied for both singlet and triplet excitons,[19,26] however triplet excitons unlike singlets are very weakly emissive, therefore fulfillment of the experiments for triplet exciton diffusion length measurement using Stern-Volmer approach is often complicated. When molecules exhibit

efficient TTA, the upconversion signal can be used in Stern-Volmer analysis to estimate triplet exciton diffusion.

Taking into account that the TTA-UC is bimolecular process, i.e. that the delayed UC emission originates from TTA, its intensity I_{UC} is proportional to the square of the concentration of emitter triplets ($[T]_t$):[34]

$$\frac{d\sqrt{I_{UC}(t)}}{dt} \propto \frac{d[T]_t}{dt} = -k[T]_t - \gamma[T]_t^2, \quad (19)$$

where k is the first-order decay constant, which is a combination of the intrinsic radiative and non-radiative decay of the triplet excitons and other possible quenching processes, whereas γ is the second-order decay constant originating from the triplet exciton depopulation *via* TTA process only. Thus, by measuring delayed I_{UC} from the singlet state at later times when I_{UC} over time is proportional to the double lifetime of triplet excitons it is possible to probe indirectly triplet exciton dynamics. [35] In such a way triplet exciton quenching efficiency (Q) can be evaluated by using the following relation:

$$Q = 1 - \frac{\int \sqrt{I_{UC(q)}}dt}{\int \sqrt{I_{UC}}dt}, \quad (20)$$

here $I_{UC(q)}$ and I_{UC} stand for UC transients measured with and without quencher, respectively.

3 Experimental setup

3.1 Sample preparation

For the measurements of photophysical properties of dilute solutions of the investigated TPA compounds they were dissolved in spectral grade organic solvents (acetone, acetonitrile, chloroform, cyclohexane, tetrahydrofuran and toluene) at 10^{-4} or 10^{-5} M concentrations. PS films with 0.1 wt% concentration of investigated compound were prepared by mixing the dissolved compound and PS in toluene at the appropriate ratio and casting the solutions on pre-cleaned quartz substrates under ambient conditions. Drop casting from toluene or THF solutions (10^{-3} M) was also employed to prepare neat films of the compounds.

For the singlet exciton diffusion measurements the blends of TPA compounds with different concentration of PCBM quenchers were prepared from chlorobenzene solutions (1.75×10^{-2} M) by drop-casting method on pre-cleaned glass substrates to produce ~1 µm thick amorphous films. The TPA:PCBM blends were prepared under nitrogen atmosphere inside the glovebox and encapsulated by using an epoxy resin and another glass plate on top. The encapsulation was essential for protecting films from ambient, and especially from oxygen, which is an effective excitation quencher. No post-annealing of the blends has been carried out.

The preparation procedure of the light upconverting films by melt processing was the following: PMMA (30 mg), DPA (0 – 40 wt%) and PtOEP (0 – 13.5 wt%) were dissolved at the appropriate ratio in chlorobenzene solvent (300 µL) by stirring for 4 h at 65°C. For evaluation of triplet exciton diffusion in DPA/PtOEP/PMMA films, varying amounts of PCBM quencher (0 – 2 wt%) were additionally introduced. The mixture of

all the compounds was drop casted on pre-cleaned 150 μm thick glass substrate at 200°C and left for half an hour to evaporate solvent. Thereafter the samples were covered with second glass substrate and hot-pressed with Carver press at 240°C under the pressure of ~100 kg/cm^2 for 5 min. After the hot-pressing samples were immediately cooled down in the ice-bath.

3.2 Spectroscopic characterization

Absorption spectra of the compound dilute solutions, PS, PMMA and neat films were recorded on a UV-vis–NIR spectrophotometer Lambda 950 (Perkin–Elmer).

Steady state fluorescence measurements of the investigated compounds dilute solutions, PS, PMMA and neat films were performed by exciting them with a 365 nm light emitting diode (Nichia), 405 nm and 532 nm wavelength semiconductor laser diodes or Xenon lamp coupled to a monochromator and measured by using a back-thinned charge-coupled device (CCD) spectrophotometer PMA-11 (Hamamatsu).

The Φ_{FL} of the solutions were estimated by comparing wavelength-integrated photoluminescence intensity of the compound solutions to that of quinine sulfate in a 0.1 M aqueous solution of H_2SO_4, which served as a reference (Φ_{FL} =53 ± 2.3).[36] Optical densities of the reference and sample solutions were kept below 0.05 to avoid reabsorption effects. Φ_{FL} of the neat and PS films were estimated by using the integrated-sphere method.[37]

Fluorescence nanosecond transients of the samples were measured by using a time-correlated single-photon-counting system PicoHarp 300 (Pico- Quant), which utilizes a pulsed semiconductor laser diode (repetition rate – 1 MHz, pulse duration – 70 ps, $\lambda_{emission}$ – 375 nm)

or light-emitting diode (repetition rate – 1 MHz, pulse duration 500 ps, $\lambda_{emission}$ – 330 nm) as an excitation source.

Delayed fluorescence and phosphorescence transients were recorded using time-gated intensified CCD camera New iStar DH340T (Andor) coupled with spectrograph SR-303i (Shamrock), while frequency-doubled (532 nm) Nd^{3+}:YAG laser (EKSPLA) with a pulse duration of 25 ps and a repetition rate of 10 Hz served as an excitation source. Phosphorescence measurements at 10 K temperature were performed using closed cycle helium cryostat 204N (Cryo Industries) with sample in helium exchange gas.

4 Experimental results and discussion

4.1 Photophysical properties and singlet exciton diffusion in TPAs

TPA derivatives represent one of the largest and one of the most widely studied classes of organic electroactive materials.[38–40] They were successfully employed as hole-transporting layers[41] and as hosts of the triplet-emitting layers in OLEDs,[42] electrophotographic photoreceptors,[8] electrochromic devices,[43] organic field-effect transistors[44] as well as in bulk-heterojunction,[45] dye-sensitized[46] and perovskite-based[47] solar cells.

TPA compounds presented in this chapter are exceptional in that they demonstrate superior hole drift mobilities (up to 0.017 $cm^2 V^{-1} s^{-1}$) in the amorphous films, are solution-processable, and moreover, feature simple one-step synthesis route from inexpensive commercial starting materials.[48–53] These features expand the possibilities for exploitation of these TPA derivatives in organic optoelectronic devices, as in a vast majority of the applications the ability to transport charges is necessary. However, to comply with all parameters required for the practical applications thorough knowledge of the photophysical properties of the TPA derivatives is required and therefore, detailed photophysical characterization of this class of organic materials is of great importance.

Exciton diffusion is one of the key photophysical parameters and plays an essential role in the operation of various optoelectronic devices. For example, in OSCs it determines the fraction of excitons that reach donor – acceptor (D-A) interface and subsequently split into electron-hole pairs, which later contribute to the extracted photocurrent, and so to the photoconversion efficiency of the solar cells.[9,18,25,54–59] Typical exciton diffusion lengths (L_D) in the amorphous films of organic semiconductors are one order of magnitude shorter than the optical

absorption length (~100 nm). Since only excitons generated within the diffusion length of the interface provide photocurrent, short L_D in the donor restricts exciton migration to the dissociating D-A interface, and thus, hampers performance of OSCs.[55] Although the problem was solved to a greater extent by introducing bulk heterojunction solar cells containing interpenetrating D-A networks,[9,25,54,60] for the blends like P3HT:fullerene charge generation still remained largely dependent on exciton diffusion in the polymer.[61,62] Generally in bulk heterojunction solar cells, short L_D defines the slow part of charge generation, which extends to 100 ps[61,63] and sets limits on the acceptable length scale of D-A phase-separated regions.[64] Obviously, enhanced L_D could permit use of coarser blends with enhanced charge collection[65] and would also make simple planar heterojunction solar cells more efficient.[25]

The ability to control L_D was also recognized to offer new opportunities in the design of organic light emitting diodes.[66,67] For example, the management of singlet and triplet exciton diffusion was found to be important for white OLEDs composed of fluorescent blue and phosphorescent green and red dopants.[67] As in the case of charge mobility, the exciton diffusion length was demonstrated to improve with the extent of crystallinity.[66]

In this chapter the photophysical properties for the series of TPA derivatives with the special emphasis on exciton diffusion will be presented.

4.1.1 Photophysical properties of phenylethenyl-substituted TPA derivatives

Propeller shape-like structure of the TPA core with highly twisted (~50°) phenyls around C-N bonds implies effective C-N stretching vibrations and phenyl torsions, which greatly affect $n\pi$ conjugation, and

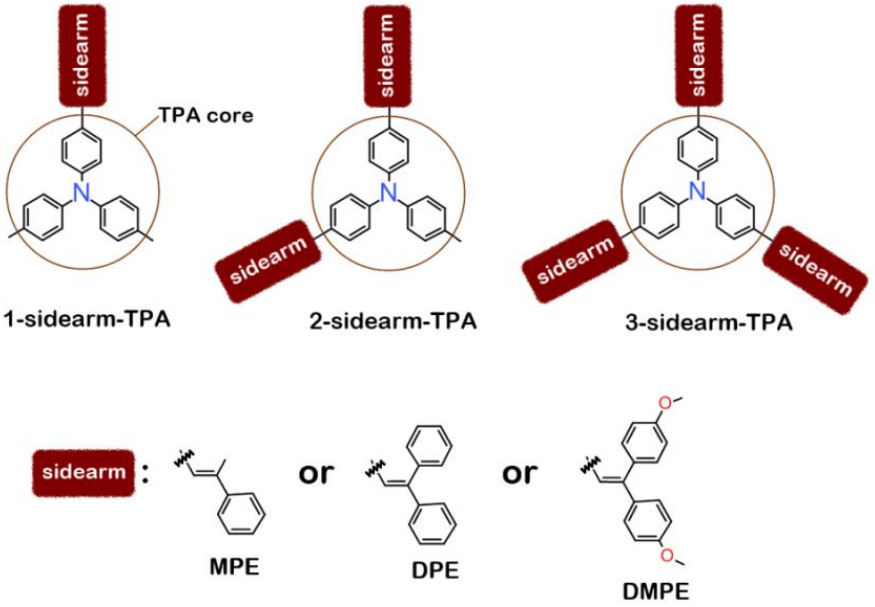

Fig. 2. Chemical structure of the series of nine TPA compounds with different number (one, two and three) and different type of sidearms (MPE, DPE and DMPE).

thus, spectroscopic properties of the TPA and TPA-derived compounds.[68,69] On the other hand, the non-planar TPA geometry predefines intricate molecular packing in the solid state resulting in non-trivial optical properties of the TPA compounds. Generally, the attachment of phenylethenyl sidearms to the phenyl groups of TPA core is expected to hinder phenyl vibrations/torsions, and consequently, by systematically varying the number and type of the sidearms, tune optical properties of the compounds (Fig. 2). To differentiate between the intramolecular motions and intermolecular effects the TPA compounds were investigated in different media (solution, rigid polymer matrix and neat film).

Figure 3 displays absorption and fluorescence spectra of the structurally modified TPA derivatives with one, two and three phenylethenyl (stilbene-like) sidearms. The optical properties of the compounds are summarized in Table 1. Even in the presence of one stilbene-like sidearm (compound 1-MPE-TPA), the lowest-energy absorption band with a maximum at ~350 nm is considerably redshifted

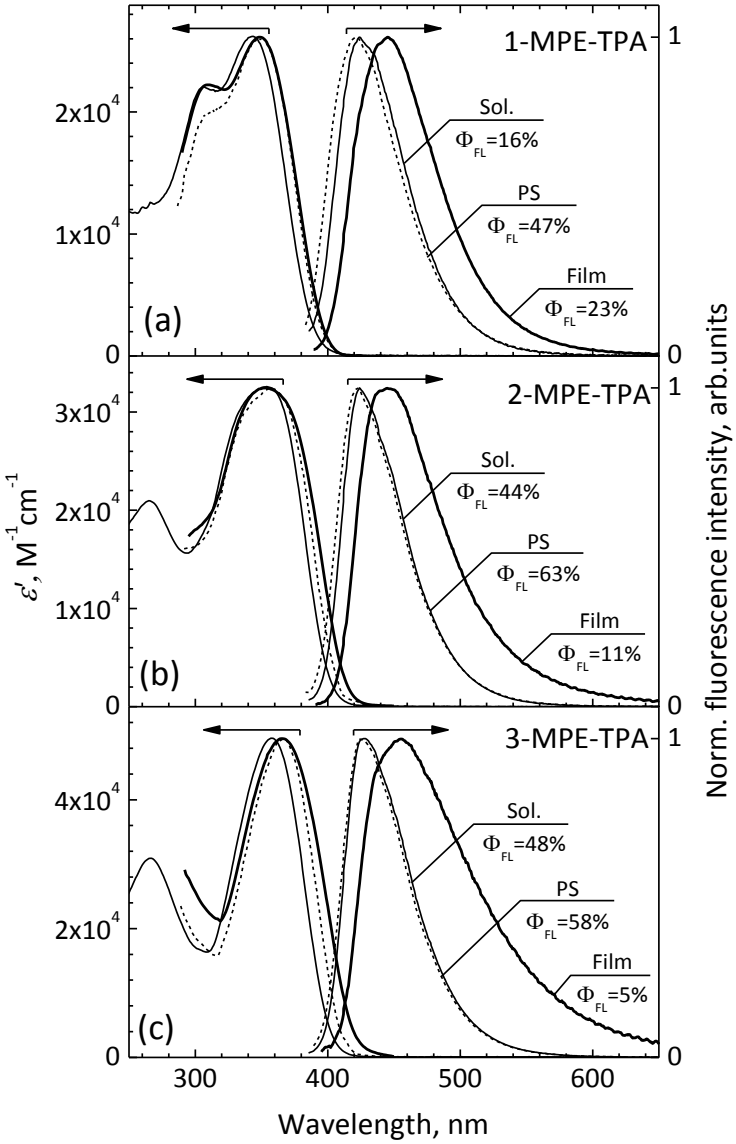

Fig. 3. Absorption and fluorescence spectra of different number of phenylethenyl sidearms containing TPA derivatives (a) 1-MPE-TPA, (b) 2-MPE-TPA and (c) 3-MPE-TPA in 10^{-5} M toluene solutions (thin solid line), PS matrixes at 0.1 wt% concentration (dashed line) and neat films (thick solid line). Fluorescence quantum yield values indicated. Absorption spectra of the compounds in PS matrixes and neat films are normalized to the spectra of compound solutions, which are presented in absolute values.

conjugation over the core and sidearm, which becomes more prominent with increasing number of MPE sidearms. To compare, the redshift for the three sidearms containing compound 3-MPE-TPA is 16 nm larger than for the compound 1-MPE-TPA possessing only one sidearm. An increase in the

number of sidearms is also followed by enhanced absorbance, i.e. a factor of 1.2 and 1.9 enhancement for compounds 2-MPE-TPA and 3-MPE-TPA, respectively, as compared to the absorbance of 1-MPE-TPA. Since two-fold and three-fold enhancement of absorbance as a result of doubling and tripling the number of MPE sidearms is only possible for decoupled side-chromophores, the considerably smaller enhancement demonstrates that the conjugation between the twisted MPE sidearms in the ground state is indeed maintained through the TPA core. The absorption spectra of the MPE-TPA compounds dispersed in different media (toluene solution, polystyrene (PS) matrix and neat film) are very similar. Small spectral shifts observed may be induced by different polarity of the surrounding media.

In contrast to the absorption spectra dynamics, the fluorescence band maximum of the TPA derivatives 1-MPE-TPA – 3-MPE-TPA is found to be independent of the number of MPE sidearms and is located at ~426 nm. Nearly identical spectra of the compound solutions and those of the compounds dispersed in PS matrixes point out that planarization of the non-interacting molecules 1-MPE-TPA – 3-MPE-TPA in the solution in the excited state is unlikely.[71] Bearing out-of-plane twisted MPE sidearms, likewise the phenyl moieties in the propeller-shaped unsubstituted TPA molecule, the TPA derivatives can undergo planarization in a solution, which otherwise is suppressed in a rigid polymer matrix. Since the planarization is accompanied by an extension of the π-conjugation, experimentally evidenced as a spectral shift to longer wavelengths, the absence of this shift in the fluorescence spectra of the compound solutions indicates that the planarization is improbable. Similar argumentation rules out possible altering in the electron-vibron coupling with increasing number of MPE sidearms.

In spite of the similar fluorescence spectra, fluorescence quantum yield (Φ_{FL}) of the TPA compounds in dilute solutions increases

Table 1. Optical characteristics of the TPA derivatives

	Solution				0.1wt% PS film				Neat film			
	λ_{abs}^{max}[a] ε'[b]	λ_{FL}^{max}[c]	Φ_{FL}	τ[d]	λ_{abs}^{max}	λ_{FL}^{max}	Φ_{FL}	τ[d]	λ_{abs}^{max}	λ_{FL}^{max}	Φ_{FL}	τ[d]
Compd.	nm (M^{-1} cm^{-1})	nm	%	ns	nm	nm	%	ns	nm	nm	%	ns
1-MPE-TPA	348 (2.62×10^4)	424	16	0.61 [91%] 4.55 [9%]	349	422	47	1.66 [87%] 4.05 [13%]	349	446	23	0.30 [24%] 1.06 [61%] 4.08 [15%]
2-MPE-TPA	358 (3.26×10^4)	424	44	1.25	357	422	63	1.06 [34%] 1.80 [66%]	353	445	11	0.15 [55%] 0.52 [39%] 2.03 [6%]
3-MPE-TPA	364 (4.96×10^4)	428	48	0.74 [22%] 1.42 [78%]	367	424	58	1.89 [98%] 10.2 [2%]	366	455	5	0.10 [62%] 0.56 [30%] 2.05 [8%]
1-DPE-TPA	374 (4.25×10^4)	476	1	0.01 [74%] 1.69 [5%] 5.05 [21%]	380	453	45	0.55 [3%] 1.92 [60%] 2.87 [37%]	377	478	11	0.20 [56%] 0.67 [41%] 2.72 [3%]
2-DPE-TPA	393 (4.45×10^4)	469	5	0.02 [68%] 0.21 [23%] 2.10 [9%]	394	457	53	0.23 [3%] 1.49 [30%] 2.29 [67%]	396	480	8	0.08 [85%] 0.35 [13%] 2.68 [2%]
3-DPE-TPA	396 (6.97×10^4)	474	10	0.27 [81%] 2.34 [19%]	401	461	54	1.33 [24%] 2.28 [76%]	395	481	4	0.07 [84%] 0.40 [13%] 3.00 [3%]
1-DMPE-TPA	371 (4.02×10^4)	477	5	0.17 [93%] 4.73 [7%]	377	451	62	0.52 [2%] 1.97 [68%] 3.03 [30%]	374	479	18	0.19 [49%] 0.80 [45%] 3.40 [6%]
2-DMPE-TPA	384 (3.97×10^4)	464	12	0.03 [21%] 0.47 [72%] 2.63 [7%]	382	451	62	0.80 [6%] 1.97 [87%] 3.39 [7%]	384	479	12	0.12 [70%] 0.49 [26%] 2.84 [4%]
3-DMPE-TPA	382 (5.77×10^4)	462	13	0.08 [14%] 0.51 [79%] 2.19 [7%]	383	451	55	0.19 [3%] 1.68 [65%] 2.63 [32%]	382	480	6	0.10 [75%] 0.46 [21%] 2.82 [4%]

[a] Absorption band maximum measured in 10^{-4} M THF solution.
[b] Absorption intensity at λ_{abs}^{max}.
[c] Fluorescence band maximum in 10^{-5} M toluene solution.
[d] Fluorescence lifetime measured at λ_{FL}^{max}. Fractional contribution to the total fluorescence intensity is given in the parentheses.

with the number of sidearms from 16% for the compound 1-MPE-TPA with one sidearm to 48% for the compound 3-MPE-TPA with three sidearms (Fig. 4a). Evidently, the enhancement of Φ_{FL} is evoked by the sidearms hindering vibrations/torsions of the phenyls constituting the TPA core, and thus, considerably reducing torsion-activated non-radiative relaxation pathway. This result is confirmed by high Φ_{FL} obtained for the compounds 1-MPE-TPA – 3-MPE-TPA in rigid PS matrixes, where intramolecular vibrational/torsional motions of the phenyls are suppressed irrespectively of the presence of adjoining sidearms (Fig. 4b).

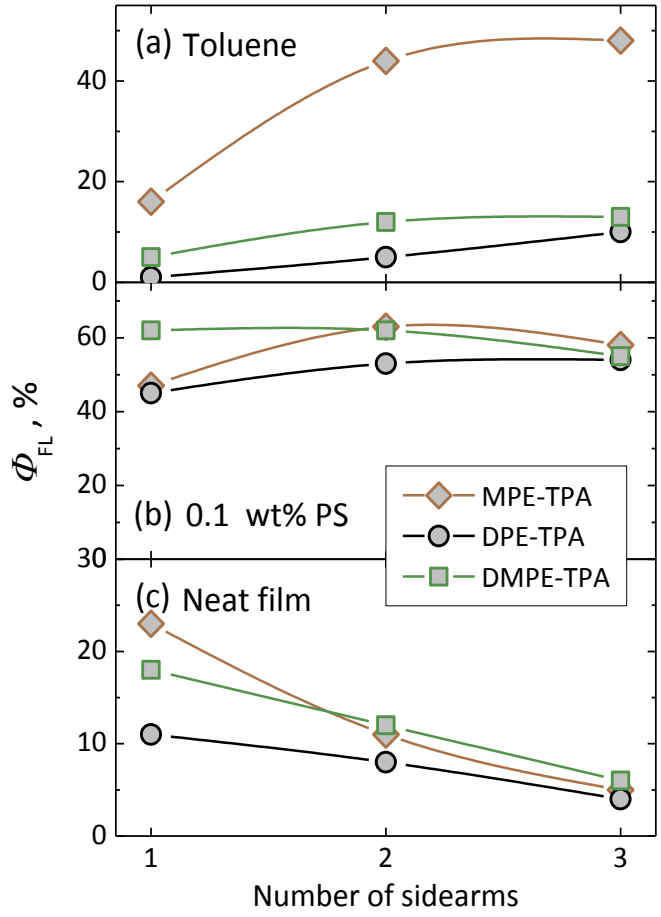

Fig. 4. Fluorescence quantum yield of the TPA derivatives *vs* number of TPA sidearms in (a) 10^{-5} M toluene solutions, (b) PS matrixes at 0.1 wt% concentration and (c) neat films.

Consequently, Φ_{FL} varies insignificantly (47-63%) in respect to the number of MPE sidearms attached. However, at least one sidearm is required for attaining such high Φ_{FL}, since the unsubstituted TPA molecules incorporated in PS matrix exhibit Φ_{FL} of only ~4%.

Fluorescence spectra of the neat films of the TPA derivatives 1-MPE-TPA – 3-MPE-TPA are broadened and redshifted as compared to those of the compound solutions, which is in correspondence with enhanced intermolecular interaction in a solid state (Fig. 3). These features are the most pronounced for the compound 3-MPE-TPA bearing three sidearms, what suggests MPE sidearms to play a major role in the molecular packing leading to increased intermolecular interaction. Unlike

in solutions, increasing number of the sidearms diminishes Φ_{FL} in the MPE-TPA neat films (Fig. 4c). Φ_{FL} continuously decreases from 23% in the compound 1-MPE-TPA to 5% in the compound 3-MPE-TPA. Intuitively, the incorporation of more branches into the TPA molecule is supposed to prevent molecule aggregation in the solid state resulting in enhanced Φ_{FL}, however, in this particular case, MPE sidearms most likely arrange in a densely overlapping pattern, which facilitates exciton migration and migration induced relaxation at non-radiative decay sites. Similar trends of the optical properties versus the number of sidearms were also observed for the rest of the TPA compound series DPE-TPAs and DMPE-TPAs**.** Introduction of the second phenyl into the stilbene-like sidearm (DPE-TPA compounds) resulted in the redshifted absorption and fluorescence bands by 20-50 nm. A similar behavior was also observed for diphenylethenyl sidearms with methoxy groups (DMPE-TPA compounds), which indicated an extension of π-conjugation caused by the second phenyl group (Fig. 5). Although extended conjugation conditioned nearly 2-fold enhanced absorbance, additional phenyl moiety detrimentally affected Φ_{FL} of the DPE-TPA and DMPE-TPA compounds in solution (Fig. 4a). For the compounds with one sidearm Φ_{FL} dropped from 16% down to 1% for 1-DPE-TPA and to 5% for 1-DMPE-TPA. This drastic reduction of Φ_{FL} is attributed to the second phenyl induced steric hindrance effect, which activates phenyl vibrations/torsions, and thus, promotes radiationless decay.[72] The reduction of Φ_{FL} for the DMPE-TPA compounds is smaller than for DPE-TPAs, since the phenyl motions are somewhat impeded by the presence of methoxy moieties. Likewise in MPE-TPAs, increasing number of the sidearms in DPE-TPA and DMPE-TPA compounds increased Φ_{FL} (Fig. 4a). However, in contrast to the MPE-TPA compounds, the fluorescence spectra of the DPE-TPA and DMPE-TPA compounds dispersed in PS matrixes are blueshifted in respect to the spectra of the compound solutions (Table 2). This result points out that

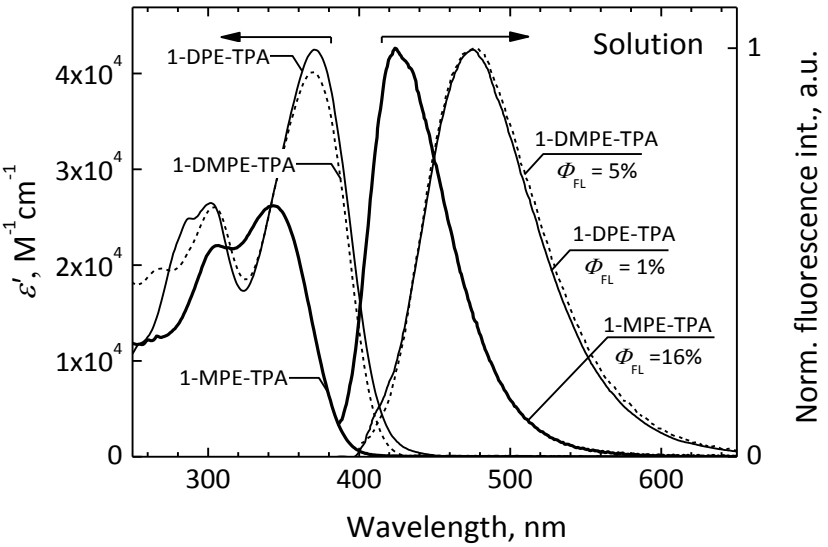

Fig. 5. Absorption and fluorescence spectra of the one sidearm containing TPA derivatives 1-MPE-TPA, 1-DPE-TPA and 1-DMPE-TPA in 10^{-5} M toluene solutions. Fluorescence quantum yield values are indicated.

the additional phenyl group in diphenylethenyl sidearms provokes planarization of the molecules in the excited state.[69] Incorporation of the DPE-TPA and DMPE-TPA compounds in PS matrixes strongly diminished non-radiative relaxation rate by suppressing phenyl torsions, and therefore, boosting Φ_{FL} up to 45-54% and 55-62%, respectively. These Φ_{FL} values are very similar to those obtained for the MPE-TPA compounds bearing stilbene-like sidearms and are roughly independent of the number of sidearms attached (Fig. 4b).

Fluorescence spectra of the neat films of DPE-TPAs and DMPE-TPAs were found to be slightly redshifted as compared to those of the compounds in solutions or PS matrixes, however the spectral shape remained unchanged and contained no traces of vibronic structure, thus verifying an amorphous character of the films formed. Likewise in the series MPE-TPA**,** a monotonous decrease of Φ_{FL} from 11% to 4% and from 18% to 6% in the neat films of DPE-TPAs and DMPE-TPAs, respectively, with increasing number of the sidearms highlighted the key role of

diphenylethenyl sidearms in facilitating exciton migration and migration-induced non-radiative deactivation at quenching sites (distortions, defects etc.) (Fig. 4c).

Interestingly, that measured fluorescence spectra of the compounds with different number of sidearms in various media do not show any steady spectral shifts, contrary to absorption spectra, which constantly redshift while increasing number of sidearms. Clarifying such spectral dynamics, absorption and fluorescence spectroscopy of all nine TPA compounds in a different polarity solvent was performed. The fluorescence spectra of MPE-TPAs in different solvents are displayed in Figure 6. The obtained data indicate negligible changes of the absorption spectra and significant redshift of the fluorescence spectra with increasing polarity of the solvent. Similar spectral shifts also were observed for DPE-TPA and DMPE-TPA compounds. To quantify solvent polarity induced changes, the estimated Stokes shift was plotted against orientation polarizability (Δf):

$$\Delta f = \frac{\varepsilon - 1}{2\varepsilon + 1} - \frac{n^2 - 1}{2n^2 + 1}, \tag{21}$$

which characterizes solvent by its refractive index (n) and dielectric constant (ε). According to Lippert-Mataga equation, the Stokes shift ($\bar{\nu}_{\mathrm{A}} - \bar{\nu}_{\mathrm{F}}$) can be expressed as a function of Δf and the change in the dipole moments ($\Delta\mu$) of excited and ground states, μ_{E} and μ_{G}, respectively,

$$\bar{\nu}_{\mathrm{A}} - \bar{\nu}_{\mathrm{F}} = \frac{2}{hc}\Delta f \frac{(\mu_{\mathrm{E}} - \mu_{\mathrm{G}})^2}{a^3}. \tag{22}$$

Here $\bar{\nu}_{\mathrm{A}}$ and $\bar{\nu}_{\mathrm{F}}$ are absorption and fluorescence maxima in cm^{-1}, h is Planck's constant, c – speed of light, a is the radius of the cavity in which the fluorophore resides. The plots of Stokes shift versus Δf are presented in Figure 7. It is worth mentioning that compounds 3-MPE-TPA, 3-DPE-TPA and 3-DMPE-TPA possess symmetrical chemical structure and therefore the dipole moment of these compounds should be small or even close to zero. Figure 7 illustrates that the slopes of the plots, which are

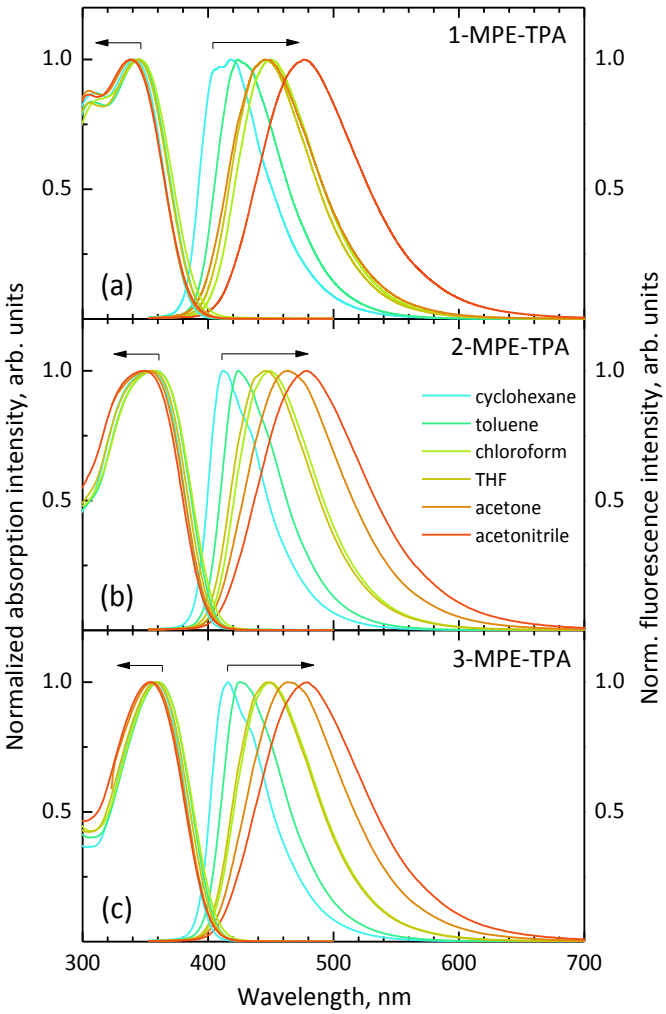

Fig. 6 Absorption and fluorescence spectra of the compounds (a) 1-MPE-TPA, (b) 2-MPE-TPA, (c) 3-MPE-TPA in different polarity solvents.

proportional to $\Delta\mu^2$ (according to equation 22) are very similar for the TPA compounds bearing the same type but different number of sidearms. This is only possible for the compounds exhibiting similar dipole moments, and thus, for these compounds can be achieved if the excited state is localized on one of the sidearms. To compare, relatively small spectral shifts *vs* solvent polarity, and thus minimal slope have been obtained for the unsubstituted TPA (Fig. 7a, Fig. 8). The continuous redshift of the absorption band and almost unaffected fluorescence band with increasing number of the sidearms in the dilute solutions of the MPE-TPA, DPE-TPA and DMPE-TPA compounds can be explained by treating

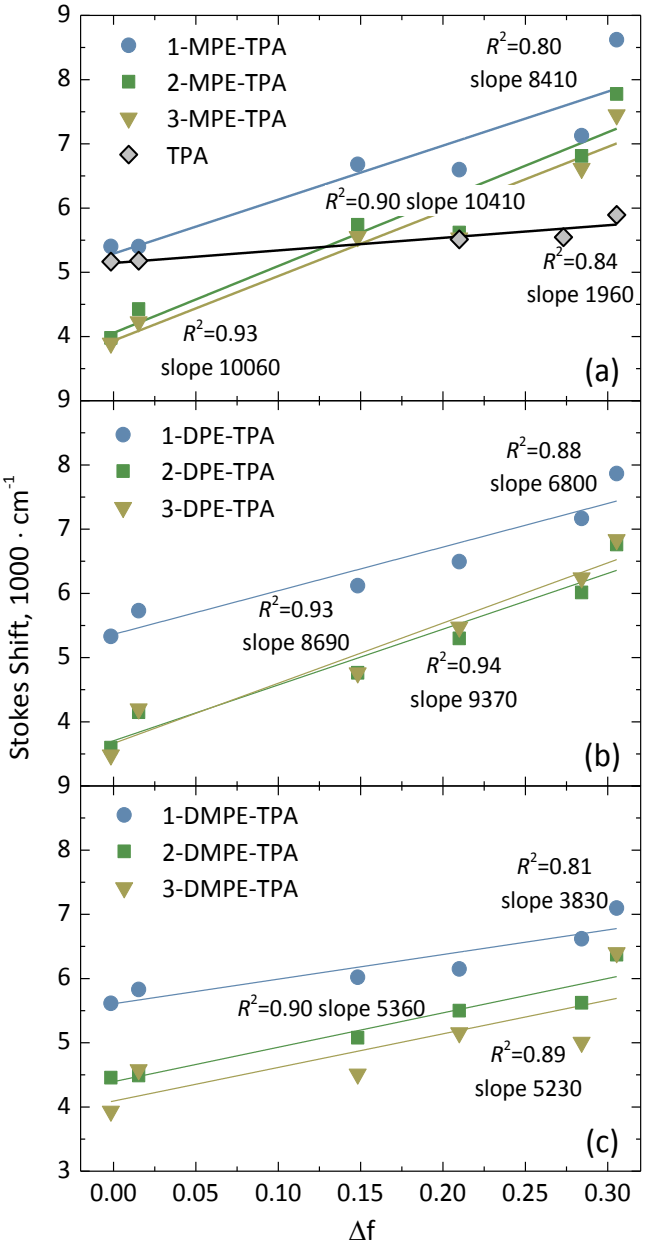

Fig. 7. Stokes shift as a function of orientation polarizability for the TPA compounds as well as for the unsubstituted TPA. Slopes and R^2 are indicated. R^2 shows the accuracy of the linear fit (R^2=1 indicates perfect fit).

the absorbing state as delocalized Frenkel exciton state and the emitting state as localized on one of the sidearms in agreement with the analogous behavior reported for structurally similar TPA compounds.[73,74] According to the proposed localization model, multidimensional intramolecular charge transfer (CT) takes place from the donating TPA moiety to the periphery of the branched molecules upon excitation, while fluorescence

stems from an excited state localized on one of the sidearms in the TPA compounds.[73]

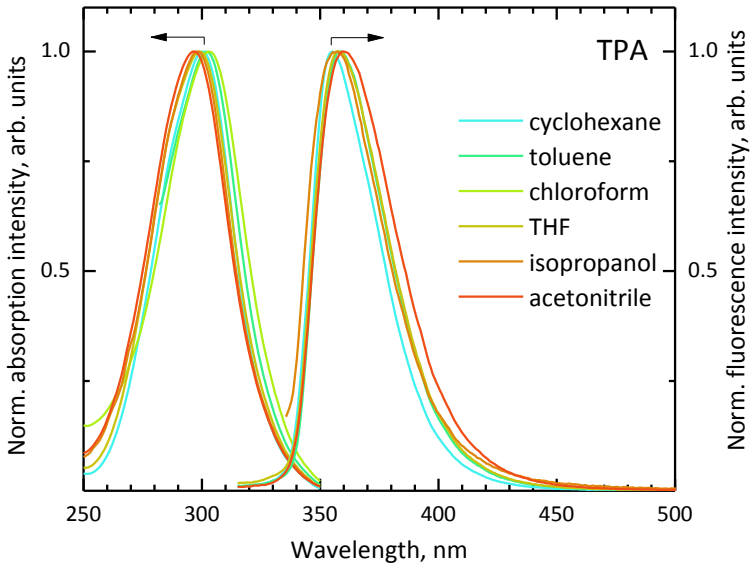

Fig. 8. Absorption and fluorescence spectra of the unsubstituted TPA in different polarity solvents.

Assumption of the increasing/decreasing a with increasing the number of sidearms is improbable, since this would result in the enhanced/reduced conjugation, and thus, in the fluorescence spectrum shift, which was not observed (Fig. 3).

Generally, the fluorescence transients of the TPA derivatives with MPE sidearms (Fig. 9) as well as of DPE-TPAs and DMPE-TPAs demonstrate multi-exponential decays resulting from various molecular conformations, which are feasible due to the labile phenyl groups. For a quantitative comparison of decay rates of multi-exponential transients the dominant decay time component with the largest fractional intensity was used. The transients fairly well reflected the tendencies of Φ_{FL} evaluated in different media (dilute solution, PS or neat film) as a function of the number and type of phenylethenyl sidearms. Increasing number of the sidearms caused prolonged τ in compound solutions in agreement with enhanced Φ_{FL} implying suppression of the phenyl torsions in the TPA core.

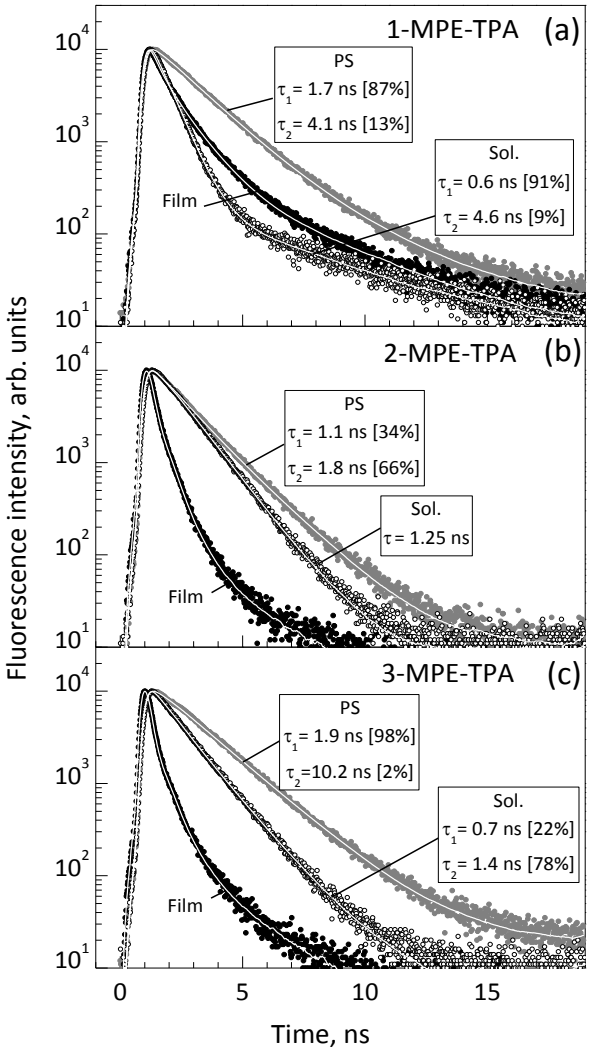

Fig. 9 Fluorescence transients of different number of phenylethenyl sidearms containing TPA derivatives (a) 1-MPE-TPA, (b) 2-MPE-TPA and (c) 3-MPE-TPA in 10^{-5} M toluene solutions (unfilled circles), PS matrixes at 0.1 wt% concentration (grey points) and neat films (black points). Lines mark single and double exponential fits to the experimental data. Fluorescence decay time constants indicated.

The increase of τ with the number of sidearms was observed irrespectively of the type of phenylethenyl sidearms attached, though the presence of the second phenyl in diphenylethenyl moieties (DPE-TPA and DMPE-TPA compounds) strongly activated phenyl torsions, and thus, torsion-induced non-radiative decay thereby reduced τ considerably. The reduction of τ from 0.6 ns (in 1-MPE-TPA) to <0.07 ns (in 1-DPE-TPA) for

one sidearm containing compounds is evidenced in Figure 10. Initial fluorescence decay of the compounds 1-DPE-TPA and 1-DMPE-TPA having sterically hindered phenyl groups is so rapid that it approaches the temporal resolution (0.07 ns) of experimental setup. On other hand, suppression of phenyl torsions by incorporating the TPA derivatives in rigid PS matrixes significantly increases τ up to 1.7-2.4 ns regardless of the number and type of the sidearms used (Fig. 9 and Table 1). This behavior again perfectly correlates with the enhanced Φ_{FL} observed upon the incorporation of the derivatives in PS matrixes and also with the independence of this enhancement on the type and number of phenylethenyl sidearms (Fig. 4b).

In the neat films of the MPE-TPA, DPE-TPA and DMPE-TPA compounds fluorescence transients become very fast and for the two- and three-sidearms containing compounds they are close to the instrument response function (IRF) of the experimental setup. Likewise in dilute

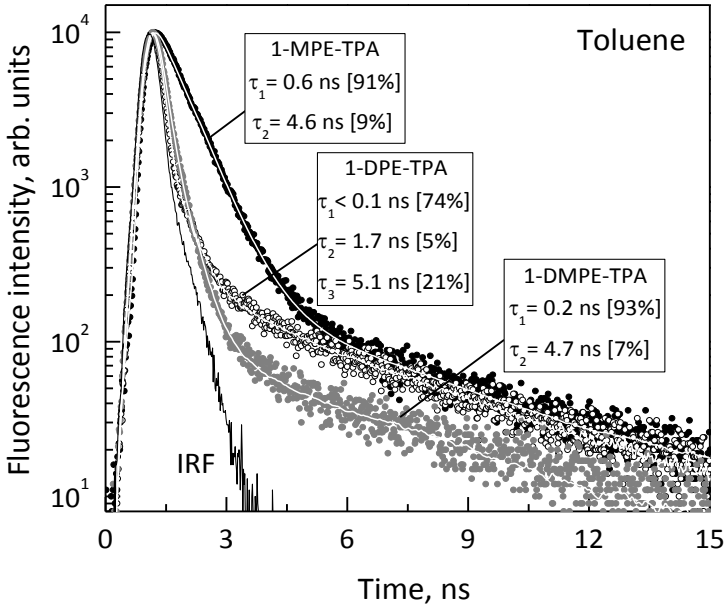

Fig. 10 Fluorescence transients of the single sidearm containing TPA derivatives 1-MPE-TPA, 1-DPE-TPA and 1-DMPE-TPA in 10^{-5} M toluene solutions. IRF – instrument response function. Lines mark double exponential fits to the experimental data. Fluorescence decay time constants indicated.

(0.1 wt%) PS matrixes, the phenyl torsions are severely inhibited in the neat films of the compounds, however, as opposed to the polymer matrix, the condensed phase enables exciton migration, which facilitates exciton quenching at non-radiative decay sites. This is the main cause of the fast excited state decay observed in the compound neat films. Moreover, a general tendency of the shortening of τ with increasing number of phenylethenyl sidearms, irrespectively of their type, indicates more favorable arrangement of the molecules with more sidearms resulting in more efficient exciton migration. The latter result is in agreement with decrease of Φ_{FL} observed in the compound neat films with increasing number of the sidearms due to enhanced exciton migration (Fig. 4c).

4.1.2 Photophysical properties of methoxy-substituted TPA derivatives with phenylethenyl sidearms

In previous section it was demonstrated that less likely exciton quenching is observed in the neat films of the compounds containing diphenylethenyl sidearms with methoxy groups at *para*-position. However, it was also demonstrated that methoxy groups attached at the *para*-position may induce better electronic coupling of methoxy-substituted TPA compounds as compared to the non-substituted one resulting in lower ionization potential and enhanced hole drift mobility.[75] Therefore, a series of phenylethenyl-substituted TPA compounds with methoxy groups attached at the TPA core were designed and investigated. A series of TPA compounds with one or two methoxy groups at TPA core are presented in Figure 11.

Optical and photophysical properties of the methoxy-TPA derivatives possessing different number (none, one and two) and different type MPE and DPE of sidearms (Fig. 11) were investigated in different media, i.e. dilute solution, rigid polymer matrix, and in the form of neat

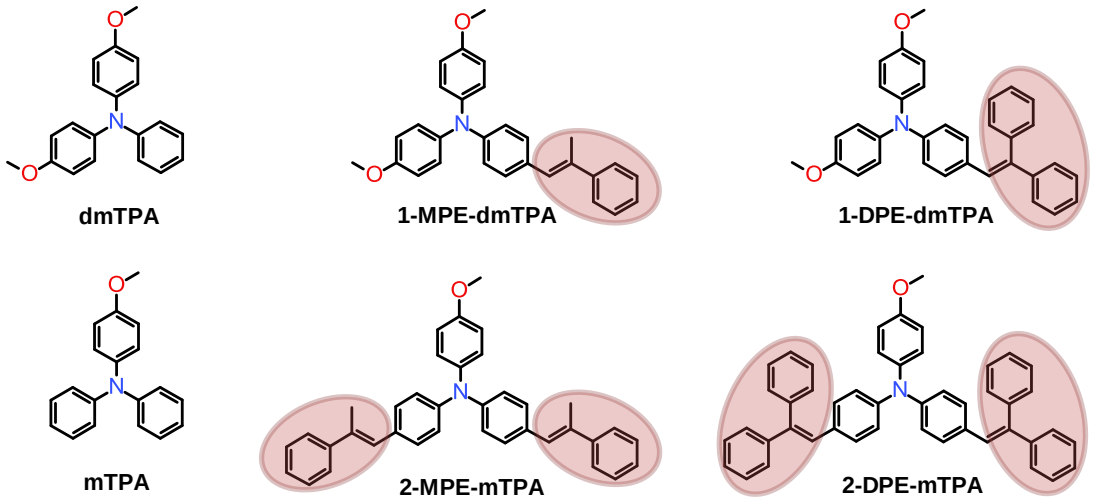

Fig. 11. Chemical structure of methoxy-substituted TPA compounds with different number (none, one and two) of MPE or DPE sidearms.

films in order to differentiate between the intramolecular and intermolecular effects, and thus, to assess molecular and solid state properties of these compounds. Figure 12a-d displays absorption and fluorescence spectra of the investigated compounds. The optical and photophysical characteristics of the compounds are summarized in Table 2. Introduction of additional phenylethenyl groups to the parent mTPA and dmTPA compounds causes redshift of the lowest-energy absorption bands indicating increased π-conjugation (cf. 2-MPE-mTPA with 1-MPE-dmTPA and 2-DPE-mTPA with 1-DPE-dmTPA). However, 30 nm larger redshifts induced by the DPE sidearms as compared to the MPE sidearms signify a higher impact of the former sidearms to the extension of conjugation. The introduction of the second phenylethenyl substituent into the TPA core is also followed by 1.6-fold enhanced absorbance of the disubstituted compounds 2-MPE-mTPA and 2-DPE-mTPA as compared to that of monosubstituted compounds 1-MPE-dmTPA and 1-DPE-dmTPA. The absorption spectra of the methoxy-TPA derivatives dispersed in different media (toluene solution, PS matrix) are similar to those of the neat films (Fig. 12a-d). Slight modifications of the

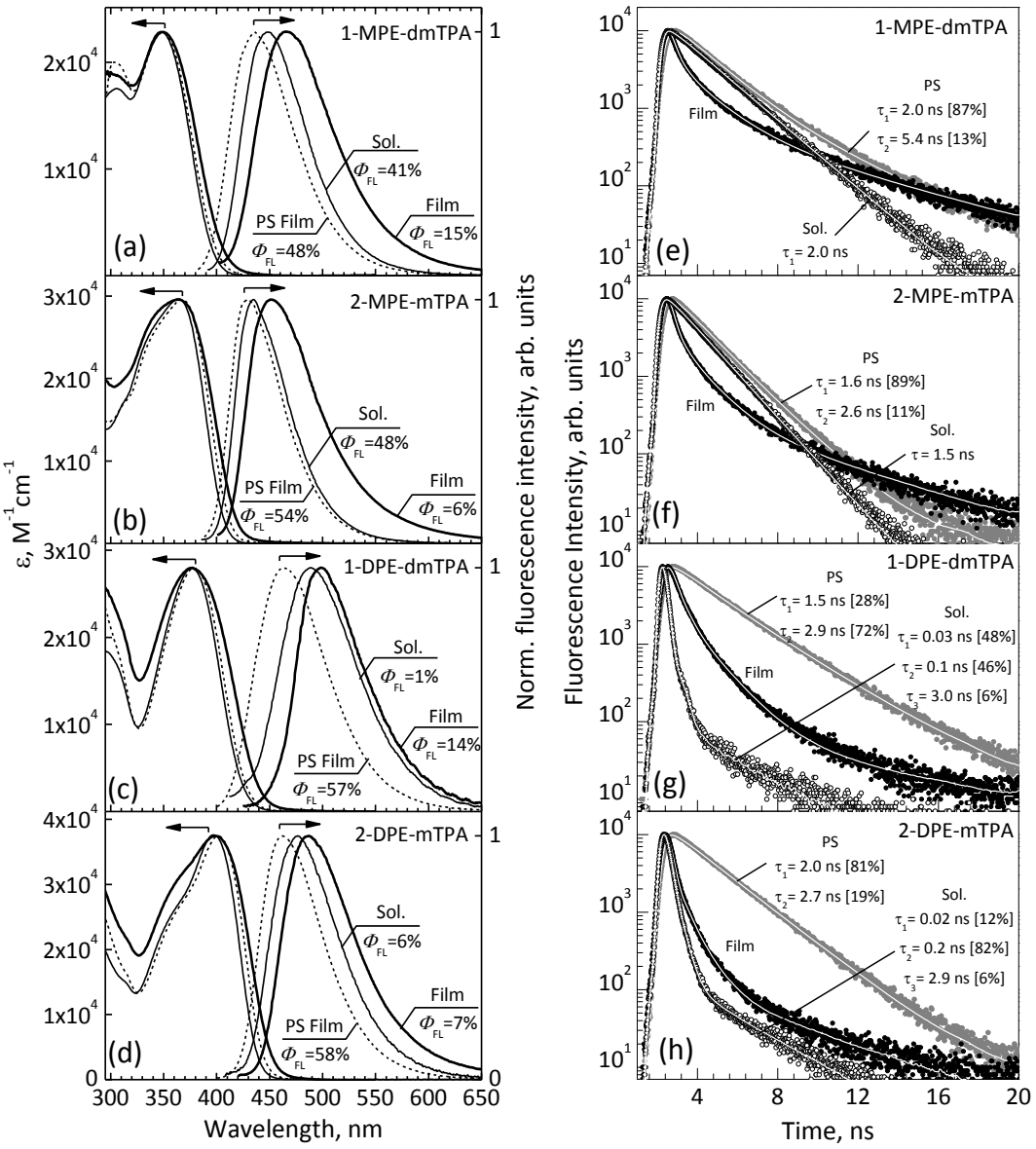

Fig. 12. Absorption and fluorescence spectra (a-d) and fluorescence transients (e-h) of dilute (10^{-5} M) solutions in toluene (thin solid lines), low concentration (0.1 wt%) PS films (dashed lines) and neat films (thick solid lines) of the methoxy-TPA derivatives: 1-MPE-dmTPA (a, e), 2-MPE-mTPA (b, f), 1-DPE-dmTPA (c, g) and 2-DPE-mTPA (d, h). Fluorescence quantum yield values are indicated. Absorption spectra of the compounds in PS matrixes and of the neat films are normalized to the spectra of compound solutions, which are presented in absolute values. Lines at fluorescence transients mark exponential fits to the experimental data. Fluorescence decay time constants are indicated.

spectra may be related to the changes of intermolecular interaction due to the different surrounding media.

In contrast to the enhanced redshifting of the absorption bands of the TPA derivatives with increasing conjugation, the fluorescence bands exhibit completely different behavior. An increase in the number of either MPE or DPE groups does not result in the redshift of fluorescence spectra. Conversely, it causes blueshifting of the fluorescence bands, which amounts to ~13 nm for the dilute solutions and neat films, and up to 7 nm for the in PS films. To explain this observation one has to take into account that compounds 2-MPE-mTPA and 2-DPE-mTPA bearing two phenylethenyl sidearms have one methoxy group, while compounds 1-MPE-dmTPA and 1-DPE-dmTPA having one phenylethenyl group contain two methoxy groups. The presence and the number of electron-donating methoxy moieties apparently play a decisive role in the electron charge redistribution in the excited state.[53] The importance of polar methoxy groups in the spectral shifts of fluorescence bands is evidenced by comparing the wavelengths of fluorescence band maxima of mTPA containing one methoxy group to dmTPA having two methoxy groups (Table 2).

The incorporation of phenylethenyl-substituted methoxy-TPA compounds into rigid PS matrixes at low concentration causes the fluorescence bands to appear at ~463 nm for compounds 1-DPE-dmTPA and 2-DPE-mTPA, and at ~433 nm for 1-MPE-dmTPA and 2-MPE-mTPA (Fig. 12a-d). The bands are blueshifted as compared to those observed for dilute solutions. This blueshift, or the corresponding redshift of the fluorescence bands observed for solutions, is likely to be caused by intramolecular twisting effects.[71] Possessing twisted geometry the TPA derivatives can exhibit geometry changes directed towards planarization upon excitation in a solution, which is suppressed in a rigid polymer matrix.

Fluorescence quantum yield of the monosubstituted methoxy-TPA derivative 1-MPE-dmTPA in dilute solution was estimated to be 41% (Fig. 12a). The replacement of methyl substituent by phenyl moiety in ethenyl group led to the drastic reduction of Φ_{FL} from 41% for 1-MPE-dmTPA down to 1% for 1-DPE-dmTPA, which can be attributed to the steric hindrance effect induced by the second phenyl group strongly activating phenyl vibrations/torsions, and thus, promoting radiationless decay.[72] The incorporation of the second MPE or DPE sidearm into methoxy-TPA core increased Φ_{FL} to 48% and 6%, respectively as compared to those of their single-sidearmed counterparts. The enhancement of Φ_{FL} is apparently caused by the increased number of the substituents impeding vibrations/ torsions of the phenyl groups constituting the TPA core, and thus, considerably reducing torsion

Table 2. Optical properties of methoxy-TPA derivatives.

	10^{-5} Toluene solution				0.1 wt% PS film				Neat film			
	λ_{abs}^{max}[a]	λ_{FL}^{max}[b]	Φ_{FL}	τ[c]	λ_{abs}^{max}[a]	λ_{FL}^{max}[b]	Φ_{FL}	τ[c]	λ_{abs}^{max}[a]	λ_{FL}^{max}[b]	Φ_{FL}	τ[c]
Comp.	nm, ($M^{-1}\times cm^{-1}$)	nm	%	ns, [%]	nm	nm	%	ns	nm	nm	%	ns
mTPA	299 (22300)	373	3	1.54 [84] 3.75 [16]	301	369 383	6	0.05 [8] 1.89 [41] 6.07 [51]	303	373	3	0.03 [23] 1.52 [60] 2.89 [17]
dmTPA	300 (26800)	387	3	1.54 [73] 4.23 [27]	300	386	7	0.01 [29] 1.82 [24] 5.79 [47]	302	393 417	3	1.07 [20] 2.66 [43] 6.48 [37]
1-MPE-dmTPA	347 (22890)	448	41	2.00	349	436	48	1.97 [87] 5.35 [13]	351	466	15	0.29 [36] 1.39 [51] 6.15 [13]
2-MPE-mTPA	364 (29625)	435	48	1.50	368	429	54	1.55 [89] 2.58 [11]	366	452	6	0.13 [58] 0.69 [33] 4.88 [9]
1-DPE-dmTPA	376 (27930)	489	1	0.03 [48] 0.13 [46] 3.01 [6]	378	464	57	1.47 [28] 2.94 [72]	377	499	14	0.27 [42] 1.16 [50] 5.71 [8]
2-DPE-mTPA	397 (37575)	477	6	0.02 [12] 0.22 [82] 2.89 [6]	402	462	58	2.02 [81] 2.66 [19]	399	487	7	0.18 [66] 0.97 [26] 6.02 [8]

[a] Absorption band maximum.

[b] Fluorescence band maximum; for compounds mTPA and dmTPA excitation wavelength of 305 nm was used; for the rest of compounds - 365 nm.

[c] Fluorescence lifetime measured at λ_{FL}^{max}. Fractional contribution to the total fluorescence intensity is given in the parentheses.

activated non-radiative relaxation pathway. These results are confirmed by high Φ_{FL} (48–58%) obtained for the TPA compounds dispersed in rigid PS matrixes, where intramolecular vibrational/torsional motions of the phenyl moieties are suppressed irrespectively of the substitution pattern (Fig. 12).

Fluorescence spectra of the neat films of phenylethenyl-substituted methoxy-TPA compounds are somewhat broadened and redshifted as compared to those of the dilute solutions, which is in correspondence with enhanced intermolecular interaction in a solid state (Fig. 12). Despite that a shape of the spectra remains unchanged and contains no traces of vibronic structure, thus verifying an amorphous character of the films formed. Φ_{FL} for the amorphous films of the compounds is found to range from 6% to 15% with ca. 2 times higher values for the monosubstituted compounds as compared to disubsituted counterparts (Table 2). Fluorescence transients of the dilute solutions of the MPE-substituted methoxy-TPA derivatives demonstrate single-exponential decay profiles with excited state decay time constants (τ) of 2.0 and 1.5 ns, respectively (Fig. 12e,f). In sharp contrast, the diphenylethenyl-substituted compounds 1-DPE-dmTPA and 2-DPE-mTPA demonstrate multi-exponential decay profiles with extremely fast (20–30 ps) initial relaxation (Fig. 12g,h). This dramatic reduction of initial τ is apparently caused by the presence of the second phenyl moiety in the substituents, which strongly activates intramolecular torsions, and thus, torsion-induced non-radiative decay channel. For a quantitative comparison of the decay rates of multi-exponential transients, the dominant τ component with the largest fractional intensity can be used (Table 2). Incorporation of the methoxy-TPA derivatives into the rigid PS matrixes suppressed torsional motions of the phenyl groups located both in the TPA core as well as in the substituents and caused a remarkable increase of τ (up to 2.0–2.9 ns) for the DPE-substituted compounds and

only a slight increase (up to 1.6–2.0 ns) for MPE-substituted compounds. The comparable τ estimated for the methoxy-TPA derivatives regardless of the number and type of the substituents used (Figure 12 and Table 2) again well correlates with the enhancement of Φ_{FL} observed upon the incorporation of the derivatives into PS matrixes and also with the independence of this enhancement on the type and number of phenylethenyl substituents (Fig. 12).

In the neat TPA films, likewise in low concentration (0.1 wt%) PS films, the phenyl vibrations/torsions are severely inhibited, however, unlike in the polymer matrix the condensed phase enables exciton migration, which facilitates exciton quenching at non-radiative decay sites. This is apparently the main reason of the fast initial excited state decay observed for the neat films of the compounds (Fig. 12e-h). Generally, highly non-exponential transients observed for the neat films are a signature of dispersive exciton hopping through the localized states in the disordered media.[76] The faster decay profiles observed for the disubstituted methoxy-TPA derivatives as compared to those of the monosubstituted derivatives (cf. transient of 2-MPE-mTPA with that of 1-MPE-dmTPA and transient of 2-DPE-mTPA with that of 1-DPE-dmTPA) indicate phenylethenyl sidearms assisted enhanced exciton migration (or diffusion) and migration induced quenching.

4.1.3 Photophysical properties of TPA dendrimers

In the previous sections (4.1.1 and 4.1.2) dependence of photophysical parameters on the number (1—>3) and different type (MPE, DPE or DMPE) of sidearms has been assessed. It has been demonstrated that photophysical properties such as Φ_{FL} and τ strongly depend on the number of sidearms, as well as on the intramolecular distance between the molecules in the solid films. The attachment of

different number of slightly different chemical structure possessing phenylethenyl sidearms results in altered intermolecular distance, however, simultaneously the conjugation of the compounds are also modified. To assess the influence only of intramolecular separation to the photophysical properties, the phenylethenyl-substituted TPA derivatives with different length of non-conjugated alkoxy chains were chosen and are presented in this section (Fig. 13).

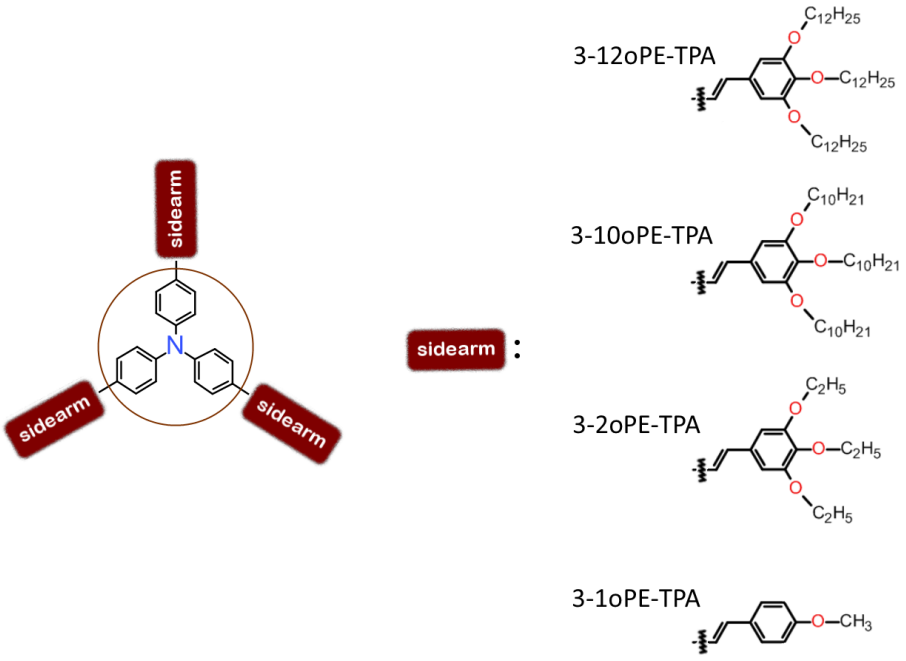

Fig. 13 Chemical structure of dendritic TPA compounds with different length of alkoxy chains of the phenylethenyl sidearms: 3-12oPE-TPA with dodecyloxy groups, 3-10oPE-TPA with decyloxy, 3-2oPE-TPA with ethoxy groups and 3-1oPE-TPA possessing single methoxy group at *para*-position.

Absorption and fluorescence spectra of dendritic TPA derivatives 3-12oPE-TPA, 3-10oPE-TPA, 3-2oPE-TPA and 3-1oPE-TPA are shown in Figure 14a-d. The obtained optical properties of the derivatives are summarized in Table 3.

All the studied compounds were found to exhibit similar absorption spectra in 10^{-5} M THF solutions, which are typical for phenylethenyl-substituted TPA derivatives (section 4.1.1 and 4.1.2)

(Fig. 14). Since the compounds have identical backbone and different (yet non-conjugated) alkoxy end-groups, the lowest energy absorption band maxima is located at 392-393 nm. Owing to highly twisted and labile molecular structure of the dendritic TPA compounds, they demonstrate unstructured fluorescence spectra in THF solutions with the band maxima peaked at ~455 nm. As it was expected, fluorescence quantum yield of the compounds in dilute solutions was estimated to be almost independent of the alkoxy end-groups and ranged from 49% to 52% (Table 3).

Table 3. Photophysical properties of compounds 3-12oPE-TPA, 3-10oPE-TPA, 3-2oPE-TPA and 3-1oPE-TPA.

	10^{-5} M THF Solution						Film					
	λ_{abs}^{max}[a]	λ_{FL}^{max}[b]	Φ_{FL}[c]	τ[d]	f_i[e]	$<\tau>$[f]	λ_{abs}^{max}[a]	λ_{FL}^{max}[b]	Φ_{FL}[c]	τ[d]	f_i[e]	$<\tau>$[f]
	nm	nm	%	ns	%	ns	nm	nm	%	ns	%	ns
3-12oPE-TPA	311 392	456	52	1.9	100	1.90	319 391	453	33	0.25 1.01 2.27	25 51 24	1.12
3-10oPE-TPA	311 392	456	50	0.54 1.78	4 96	1.73	316 394	456	20	0.20 0.79 2.45	36 48 16	0.84
3-2oPE-TPA	311 393	457	49	1.79	100	1.79	398	477	8	0.20 1.12 12.6	50 17 33	4.46
3-1oPE-TPA	302 393	453	49	0.55 1.74	6 94	1.67	396	555	4	0.02 1.05 3.93	74 14 12	0.63

[a] Absorption band maximum.
[b] Fluorescence band maximum.
[c] Fluorescence quantum yield.
[d] Fluorescence lifetime measured at λ_{FL}^{max}.
[e] Fractional contribution to the total fluorescence intensity.
[f] Average fluorescence lifetime calculated by $<\tau>=\sum \tau_i \cdot f_i$.

Unlike in dilute solutions the absorption spectra of the TPA derivatives in the neat films continuously redshifted and broadened with decreasing the size of alkoxy chains. For the compounds with long decyloxy and dodecyloxy chains (compounds 3-12oPE-TPA and 3-10oPE-TPA) absorption spectra closely resemble those of dilute solutions. Obviously, bunches of long alkoxy chains prevent close packing of the

molecules, thus weakening their intermolecular interactions in the solid state. On the other hand, short ethoxy groups (compound 3-2oPE-TPA) are unable to suppress this interaction resulting in broadened and redshifted (by ~5 nm) absorption spectrum with respect to that of solution. Upon replacement of the long tris(alkoxy) end-moieties with single methoxy group at the *para* positions of the phenyls (compound 3-1oPE-TPA) intermolecular interactions are enhanced even more causing much stronger broadening of the band (Fig. 14d).

Similar to the absorption spectra of neat films of compounds 3-12oPE-TPA, 3-10oPE-TPA, 3-2oPE-TPA and 3-1oPE-TPA, fluorescence spectra also showed constant redshift as the size of alkoxy chains is being reduced. Due to the weak intermolecular interaction caused by sufficiently long alkoxy end-groups fluorescence spectra of the neat films of compounds 3-12oPE-TPA and 3-10oPE-TPA demonstrate negligible redshift as compared to those of solutions. Interestingly, vibronic structure in the spectra of 3-12oPE-TPA and 3-10oPE-TPA can be noticed, which might suggest molecular ordering in the films caused by the formation of liquid-crystalline phase at room temperature.[51] The relatively short ethoxy groups (compound 3-2oPE-TPA) already cause noticeable redshift of the fluorescence spectrum (by 20 nm) as compared to that in solution. Since the fluorescence spectrum of neat film of 3-2oPE-TPA contains no traces of vibronic replica and maintains the shape like in solutions, it is likely dominated by amorphous character. Fluorescence spectrum of the neat film of compound 3-1oPE-TPA is found to be radically different in respect to those of the rest TPA derivatives. The methoxy groups are too small to impede tight molecule packing inducing dimer state formation *via* enhanced molecular interactions. Thus, a new significantly redshifted (by 74 nm) and unstructured band at 555 nm is formed due to the dimer states. Interestingly, a small band at the shorter wavelengths (~460 nm) of compound 3-1oPE-TPA similar to those

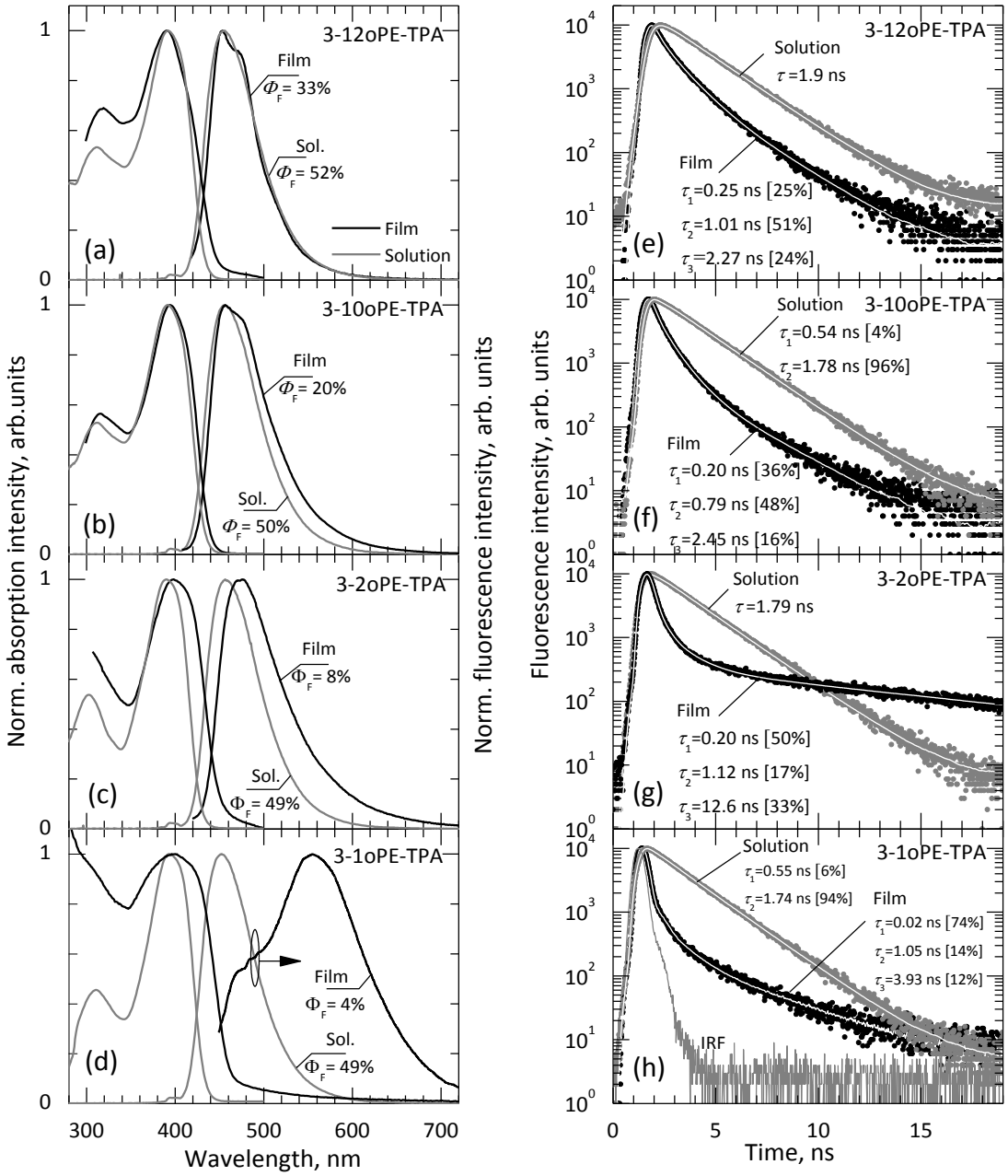

Fig. 14. Absorption and fluorescence spectra (a-d) and fluorescence transients (e-h) of the TPA derivatives 3-12oPE-TPA (a, e), 3-10oPE-TPA (b, f) 3-2oPE-TPA (c, g) and 3-1oPE-TPA (d, h) in 10^{-5} M THF solutions (grey lines and points) and neat films (black lines and points). Fluorescence quantum yield values are indicated. Lines at fluorescence transients mark exponential fits to the experimental data. Instrument response function (IRF) and fluorescence lifetimes are indicated.

observed in the neat films of compounds 3-12oPE-TPA, 3-10oPE-TPA and 3-2oPE-TPA can be also detected, which likely originates from the areas featuring weakly interacting molecular species.

Φ_{FL} of the neat films of the compounds was found to be considerably reduced (down to an order of magnitude) as compared to those of solutions. Φ_{FL} of 33%, 20%, 8% and 4% were obtained for the compounds 3-12oPE-TPA, 3-10oPE-TPA, 3-2oPE-TPA and 3-1oPE-TPA, respectively. The most pronounced reduction of Φ_{FL} occurred for the TPA compounds with shorter alkoxy end-groups, and this corresponded well to the stronger redshift of absorption and fluorescence spectra in the neat solid films. This reduction in Φ_{FL} confirmed enhanced intermolecular interactions, and moreover, suggested migration-induced exciton quenching at non-radiative decay sites to be the main excited-state deactivation channel. Additionally, the significant reduction of Φ_{FL}, which is particularly well pronounced in compound 3-1oPE-TPA and partly also in compound 3-2oPE-TPA, can be attributed to the appearance of long-lived dimer states. This is because long-lived states are naturally more susceptible to trapping by quenching sites such as lattice distortions, impurity traps and other defects.

Fluorescence transients of these methoxy-TPA derivatives in dilute solutions demonstrate single exponential decay profiles with fluorescence lifetime varying from 1.7 ns to 1.9 ns (Fig. 14e-h). Very similar τ of the compounds perfectly correlates with the similar fluorescence quantum yield data. Unlike in solutions, fluorescence transients in the compound neat films are clearly non-exponential indicating dispersive exciton hopping through the localized states in the disordered media.[76] Each transient consists of the very fast (sub-nanosecond) and slower nanosecond-time-scale components, which contribute unequally to the overall excited state decay. The slower component ($\tau \geq 1$ ns) dominates in compounds 3-12oPE-TPA and 3-

10oPE-TPA featuring long alkoxy end-groups, whereas the fast one prevails in compounds 3-2oPE-TPA and 3-1oPE-TPA with much shorter end-moieties. Since the latter two compounds suffer from strong emission quenching in the neat films (stronger than observed in compounds 3-12oPE-TPA and 3-10oPE-TPA) due to exciton migration facilitated non-radiative decay, it is natural to associate the initial fast decay in the transients to migration induced exciton quenching.[71,77] Thus, the transients of the neat films directly support Φ_{FL} data and unambiguously indicate the importance of the long alkoxy chains for suppressing exciton migration to non-radiative decay sites. The long peripheral moieties are assumed to prevent molecule agglomeration in the solid state due to steric hindrance effects. Much slower decay components (τ > 4 ns) present only in the transients of compounds 3-2oPE-TPA and 3-1oPE-TPA can be explained by long-lived dimer states revealed in the fluorescence spectra of the compounds neat films.

4.1.4 Exciton diffusion in phenylethenyl-substituted TPAs

4.1.4.1 Monte Carlo simulations

Exciton diffusion of the TPA derivatives possessing different number (one, two and three) and different type MPE, DPE and DMPE of sidearms (Fig. 2; Section 4.1.1) was investigated by employing the volume quenching method with combination of Monte Carlo simulation.

For the determination of singlet exciton diffusion length the series of TPA derivatives with different PCBM concentrations were fabricated and fluorescence decays were measured. Typical measured fluorescence transients for 3-DPE-TPA:PCBM blends with various PCBM concentrations are shown in Figure 15. An increase in PCBM concentration obviously shortens fluorescence decay time, which is a result of the diffusion limited exciton quenching at the TPA:PCBM

interface. Considerable quenching sets in as the average distance betweenPCBM molecules becomes comparable to the exciton diffusion length in the investigated compound. The fluorescence decay time also depends on the nanocomposition of the blend. At a certain PCBM concentration the largest quenching surface and consequently the shortest

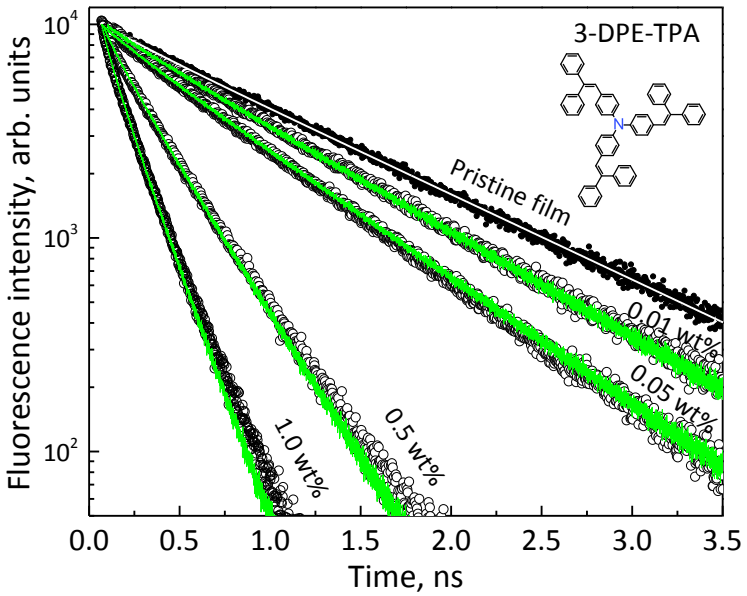

Fig. 15. Fluorescence transients of pristine 3-DPE-TPA film and the films doped with PCBM at different concentrations (indicated). Experimental data – points, Monte Carlo simulations – green lines, exponential fit – white line.

fluorescence decay time is achieved for PCBM molecularly dispersed in the investigated material. In the case of clusterization of the quencher molecules, fluorescence transients should show a slower decay due to the reduced quenching surface. Thus knowledge about the distribution of PCBM in the blend is important and has to be taken into account while simulating exciton diffusion. In Figure 15 simulated fluorescence transients assuming no PCBM clusterization in the 3-DPE-TPA:PCBM blends are shown. Evidently, the modeling gives good agreement with the experimental data, thereby enabling quantitative evaluation of exciton diffusion parameters. For the estimation of PCBM concentration in the

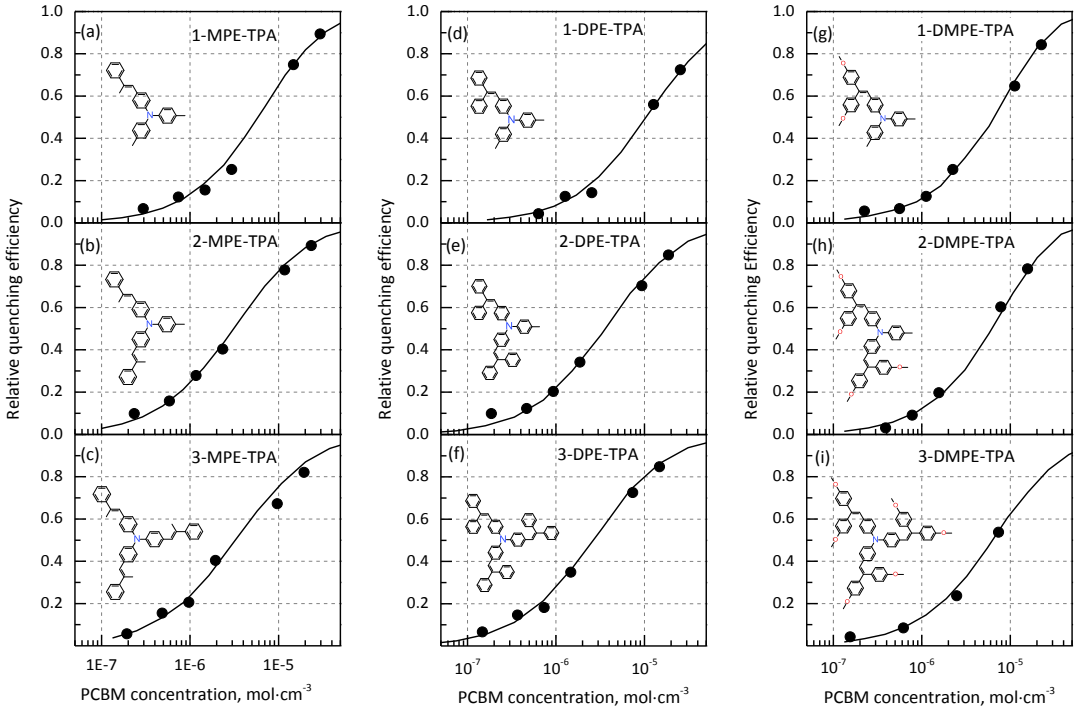

Fig. 16. Relative quenching efficiency *vs* molar PCBM concentration in the blends with mono-substituted TPA (a, d, g), di-substituted TPA (b, e, h) and tri-substituted TPA (c, f, i) with different sidearms: MPE (a, b, c), DPE (d, e, f) and DMPE (g, h, i). Points and lines depict experimental and modelled results, respectively.

TPA:PCBM blends, which is required for the evaluation of D, density of the TPA derivatives was assumed to be equal to 1.15 g/cm^3 in accordance with the densities of arylamine compounds possessing similar chemical structure.[78] The densities of the structurally similar arylamines differed by no more than ±0.1 g/cm^3 implying variation in L_D up to ±0.8 nm, which is below 10% of the determined L_D value. The exciton diffusion coefficient of 4×10^{-4} cm^2/s corresponding to the diffusion length of 11.1±0.9 nm was obtained for 3-DPE-TPA film from Monte Carlo simulations. The obtained L_D value compares well with those found in most small-molecule[55,59,32,79] or polymer[55–57,80,81] compounds exhibiting excellent performance in OSCs.

To elucidate the morphology of the TPA:PCBM blends at the nanoscale, relative quenching efficiency (Q) was estimated for all the

investigated TPA derivatives as a function of PCBM fraction. Close to zero Q values indicate that the exciton quenching is insignificant, which is typical for low concentrations of quenchers, whereas nearly unity values of Q at high PCBM concentrations accompanied by considerable lifetime shortening signify very effective quenching.

Figure 16 displays the measured and modeled quenching efficiencies of the DPE-TPA:PCBM blends with increasing PCBM concentration. The solid lines were modeled using Monte Carlo simulations by setting previously calculated exciton diffusion coefficient for each TPA film and assuming the blend morphology as an intimate mixture. Evidently, the simulated curves perfectly fit the measured data in all the studied range of PCBM concentration (0.01 - 1 wt%), which shows that the aggregation of the quenching molecules is unlikely. Good agreement between experimental and simulated Q dependences was also obtained for the MPE-TPA:PCBM and DMPE-TPA:PCBM blends (Fig. 16) indicating the absence of PCBM clusters. Otherwise, in the case of formation of phase separated domains reduced quenching efficiency as compared to the simulation results should immediately manifest at higher PCBM concentrations.[18] Additionally, the studied TPA compounds are known to form glassy state implying intimate mixture of PCBM and TPA molecules indeed very probable.[49]

It is worth mentioning that energy transfer rate, i.e. diffusion, strongly depends on the distribution of energy states of the material. Non-coherent exciton diffusion proceeds as series of hops from one molecule to another. In a material with a broad distribution of energy states an exciton that is created on a high energy site at first will be able to hop to any of its neighboring molecules. Over time, excitons are likely to hop to more favorable lower energy sites and consequently the exciton hopping rate to slightly higher states eventually slows down. This is known as dispersive diffusion, which can be described with time-dependent diffusion

coefficient.[82–84] In materials such as amorphous TPA derivatives, the exciton diffusion coefficient measured using measurement techniques that do not allow to estimate the time-depended diffusion mostly represents time-averaged exciton diffusion.[85]

Estimated exciton diffusion coefficient of the TPA compounds featuring the different type (MPE, DPE and DMPE) and different number of the sidearms is shown in Figure 17a. A clear tendency of increasing *D* with increasing the number and decreasing the size of the sidearms is observed. Experimentally obtained $<\tau>$ as a function of the number of sidearms is depicted in Figure 17b. Interestingly, $<\tau>$ shows different behavior for the compounds with the different type of the sidearms. For compounds with MPE and DMPE sidearms it decreases down to 3 times, whereas for DPE-TPA compounds it slightly increases from 0.70 ns to 1.04 ns as the number of sidearms increases from 1 to 3. Although $<\tau>$ decreases with increasing the number of MPE and DMPE sidearms (Fig. 17b), the concomitant enhancement of diffusion coefficient is stronger resulting in an overall increase of the diffusion length (Fig. 17c). The greatest increase of L_D is observed for the DPE sidearms containing compounds, L_D increases from 4.8 nm up to 11.1 nm. The 2-fold and 1.4-fold increase is also observed as the number of MPE and DMPE sidearms increases from 1 to 3, respectively (Fig. 17c). This result clearly demonstrates importance of phenylethenyl sidearms in facilitating exciton diffusion. The largest *D* is obtained for the smallest sidearms containing MPE-TPA compounds, meanwhile attachment of additional phenyl ring in the DPE or methoxyphenyl in DMPE sidearms considerably reduces diffusion coefficient. Methoxyphenyl groups were found to have the most profound effect in the suppression of exciton diffusion (Fig. 17a). One of the plausible reasons for the diminished *D* in the DPE-TPA, and especially, DMPE-TPA compounds could be less dense molecular packing in the solid state caused by the additional out-of-plane twisted phenyl ring

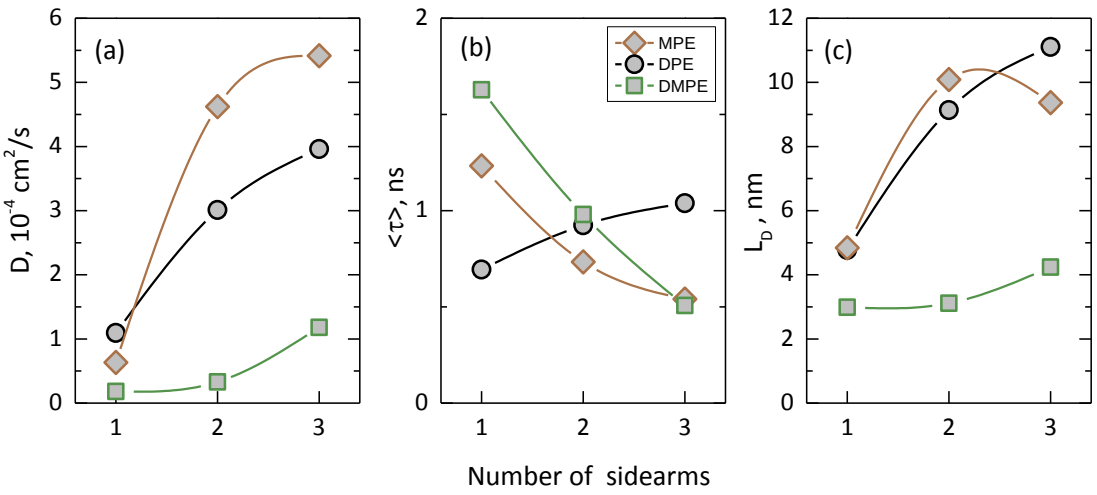

Fig. 17. Exciton diffusion coefficient (a), average fluorescence lifetime (b) and exciton diffusion length (c) as a function of the number of TPA sidearms.

and methoxy group in their sidearms. Since energy transfer is very sensitive to the intermolecular distance ($\sim 1/d^6$), more bulky sidearms are likely to lower exciton diffusion in the TPA films.[29]

4.1.4.2 Förster energy transfer calculations

Intuitively, incorporation of the larger number of the sidearms into the core, and thus making TPA molecular structures branchier should also cause a decrease in exciton diffusion coefficient. However, an opposite effect was observed, *i.e.* exciton diffusion was actually enhanced with increasing the number of the sidearms irrespectively of their type. To determine the origin of the enhancement, Förster energy transfer rates for the series of MPE-TPA, DPE-TPA and DMPE-TPA derivatives were calculated.[29]

In contrast to the study carried out on phthalocyanine and rubrene derivatives by R.J. Holmes group,[25] where significant gains in D and L_D were revealed to originate from increased R_0 (*via* enhanced Φ_{FL}) as a result of the optimized intermolecular distance, no Φ_{FL} enhancement in the pristine TPA films with increasing the number of

Table 4. Optical properties of the TPA compounds.

	10^{-5} M THF solution		Encapsulated pristine film					
	λ_{abs}^{max} [a]	σ_A [b]	λ_{abs}^{max} [a]	λ_{FL}^{max} [c]	Φ_{FL}	τ [d]	Stokes shift	d [e]
Compound	nm	cm^2	nm	nm	%	ps	cm^{-1}	nm
1-MPE-TPA	348	1.00×10^{-16}	353	435	23	449 [12%] 1340 [88%]	5340	1.02
2-MPE-TPA	358	1.25×10^{-16}	362	449	34	467 [42%] 927 [58%]	5353	0.88
3-MPE-TPA	364	1.89×10^{-16}	370	462	22	328 [63%] 902 [37%]	5382	0.82
1-DPE-TPA	374	1.62×10^{-16}	379	482	21	327 [35%] 892 [65%]	5638	1.08
2-DPE-TPA	393	1.70×10^{-16}	397	480	18	541 [29%] 1071 [71%]	4356	0.95
3-DPE-TPA	396	2.67×10^{-16}	401	483	21	264 [6%] 1088 [94%]	4234	0.90
1-DMPE-TPA	371	1.54×10^{-16}	374	477	33	573 [15%] 1814 [85%]	5774	1.12
2-DMPE-TPA	384	1.52×10^{-16}	384	478	23	327 [24%] 1056 [76%]	5121	1.01
3-DMPE-TPA	382	2.21×10^{-16}	383	481	19	233 [52%] 804 [48%]	5320	0.96

[a] Absorption band maximum.
[b] Absorption cross-section at λ_{abs}^{max}.
[c] Fluorescence band maximum.
[d] Fluorescence lifetime measured at λ_{FL}^{max}. Fractional contribution to the total fluorescence intensity is given in the parentheses.
[e] Intermolecular distance between the sidearms.

phenyletehenyl sidearms was observed (Table 4). Conversely, Φ_{FL} had either remained almost unchanged (in the case of MPE-TPA and DPE-TPA) or even decreased slightly (in the case of DMPE-TPA) with the increasing number of the sidearms. This confirms that phenyletehenyl sidearms act not as some kind of spacers increasing molecular separation, but rather as exciton migration promoters, which can even cause fluorescence quenching. Spectral overlap integral $J(\lambda)$ (Fig. 18 inset) in equation (12) was determined by measuring fluorescence spectrum and absorption cross-section (Table 4, Fig. 19). $J(\lambda)$ is observed to increase with the larger number of sidearms reflecting a corresponding increase in absorbance and

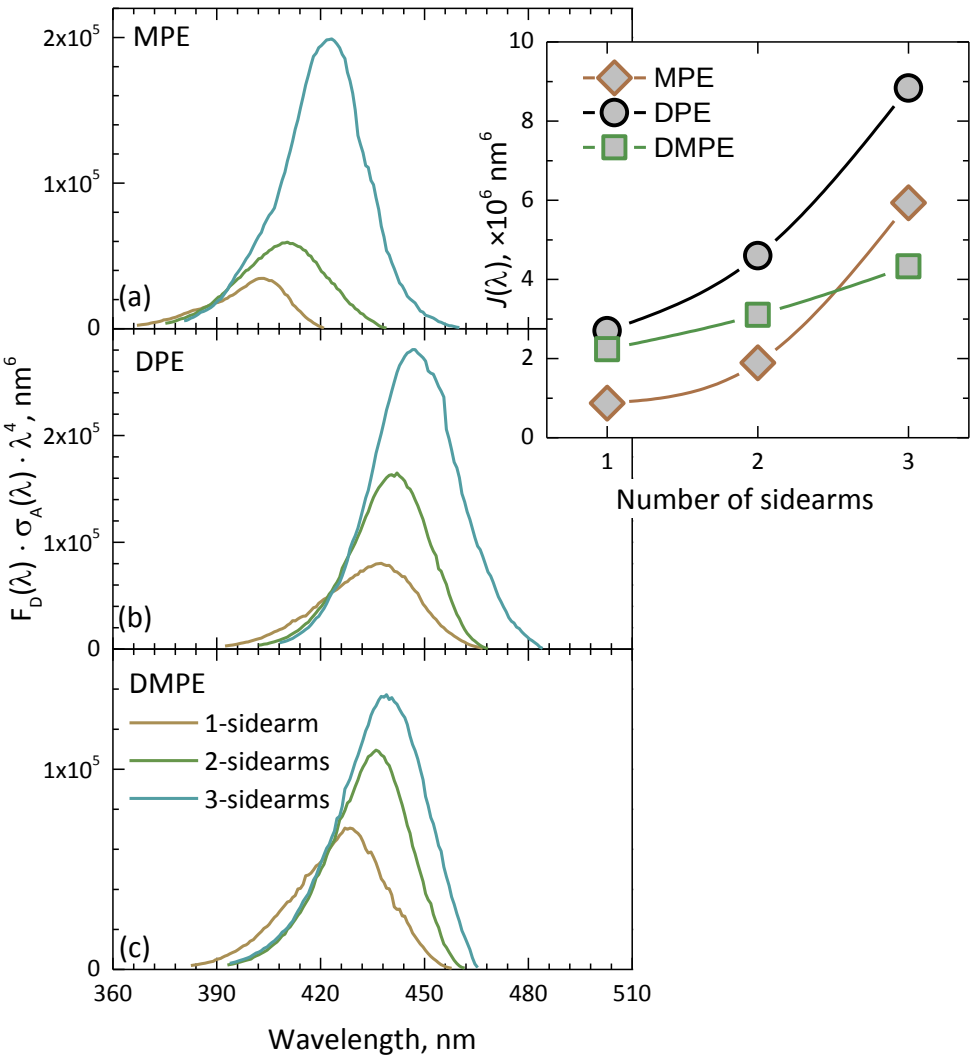

Fig. 18. Spectral overlap of absorption and fluorescence spectra of the neat films of TPA compounds MPE-TPA (a), DPE-TPA (b) and DMPE-TPA (c). Inset shows spectral overlap integral as a function of the number of phenylethenyl sidearms.

reduced Stokes shift of the neat films of TPA compounds (Fig. 18).[49] The reduced Stokes shift to a greater extent can be accounted for by the redshifting absorption band as opposed to the fluorescence band, which is almost independent of the number of sidearms (Fig. 19). An exception is pristine MPE-TPA films, for which noticeable fluorescence redshift of 17 nm is observed due to the formation of dimer states. Intermolecular distance, entering the equation (12) for L_D, was used as an average distance between the sidearms of two

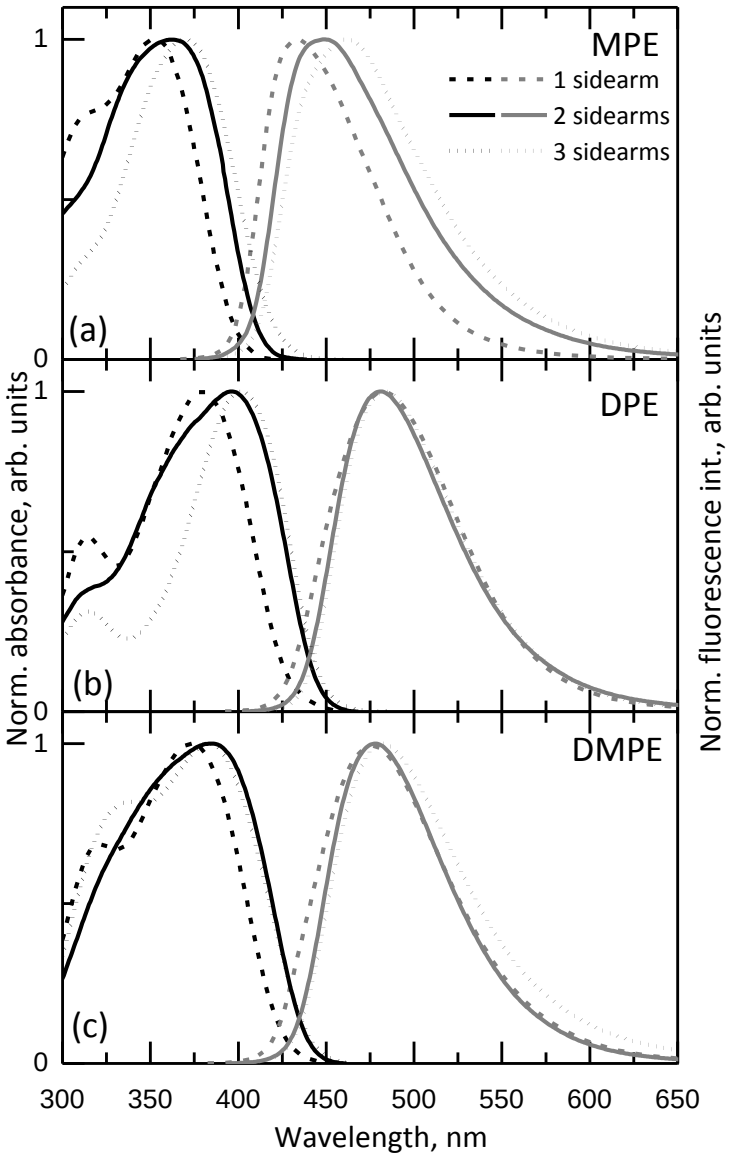

Fig. 19. Normalized absorption and fluorescence spectra of the neat films of TPA compounds bearing MPE (a), DPE (b) and DMPE (c) sidearms.

neighboring molecules, since it was shown before that in these compounds exciton is localized on one of the sidearms (section 4.1.1). The intermolecular distance estimated from the volume averaged molecular radius evidently decreases with increasing the number (or the density) of the sidearms (Table 4). The distance also decreases for the TPA compounds bearing smaller sidearms such as MPE. Index of refraction for the studied TPA compounds was set to 1.7, *i.e.* to an average value obtained by averaging over refractive

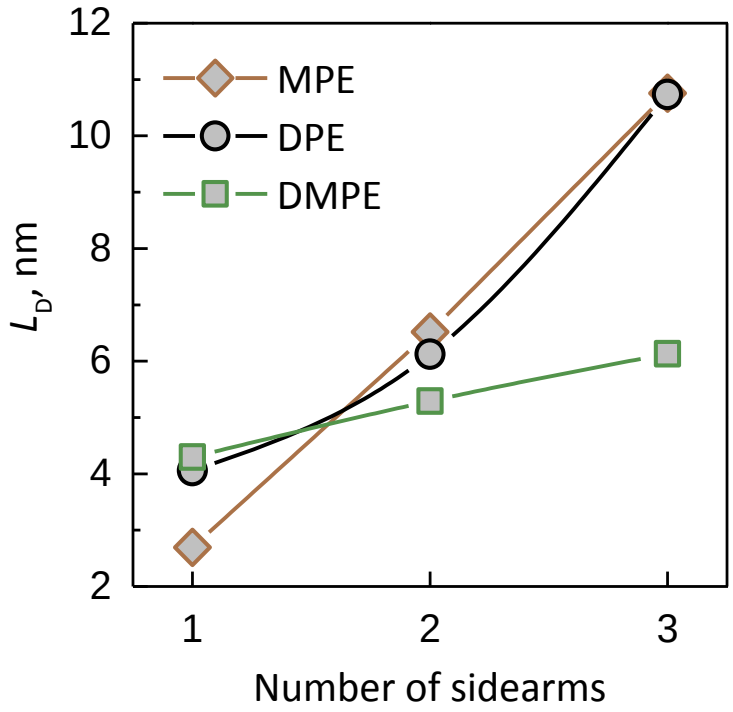

Fig. 20. Exciton diffusion length in MPE-TPA (a), DPE-TPA (b) and DMPE-TPA (c) films as a function of the number of sidearms attached calculated by Förster theory, lines serve as the guides for the eyes.

indices of various similar TPA derivatives.[87] The value of A=1, comparable to those reported previously was utilized.[25,88,89]

In Figure 20, exciton diffusion lengths calculated using Förster's theory are displayed. The results clearly demonstrate that L_D can be roughly tripled by increasing the number (from one to three) of MPE or DPE sidearms linked to the TPA core. The maximal attainable L_D value is around 11 nm, which is rather high and compares well with that of the well-known small-molecule (CuPc,[59,79] Alq_3,[55] NPD,[55] CBP,[55] PTCDA[32]) or polymer (P3HT,[20,80] PPV,[56,81] PCPDTBT[18]) compounds widely used for fabrication of OSCs. Although attachment of more DMPE sidearms increases L_D as well, the enhancement is less obvious (Fig. 17c, Fig. 20). A fairly good agreement between the diffusion lengths determined by both models supports the idea that the incorporation of the larger number of

phenylethenyl sidearms improves exciton diffusion in the TPA compounds. According to the Förster's theory this improvement occurs as a result of the enhanced overlap of the emission and absorption spectra (reduced Stokes shift), increased extinction coefficient, and also increased density of the sidearms in the TPA films allowing for more efficient exciton hopping through the neighboring molecules. In other words, increasing number of phenylethenyl sidearms forms a dense network of exciton hopping sites in the amorphous TPA films that facilitate exciton diffusion. Such control of exciton diffusion in the TPA films achieved *via* incorporation of the phenylethenyl sidearms acting as hopping sites is an alternative approach as that proposed by R. J. Holmes group,[25,86] where covalently-linked peripheral groups or wide bandgap host were utilized to increase intermolecular separation in order to avoid fluorescence quenching, and thus, to keep Förster transfer rates high.

4.1.5 Exciton diffusion in diphenylethenyl-substituted TPA dimers

In the previous section exciton diffusion enhancement has been demonstrated in the films of TPA derivatives with increasing number of phenylethenyl sidearms. Since molecular structure of the TPA features C3 radial symmetry the effect for the TPA-cored compounds containing only up to three sidearms could be tested. To verify the reported diffusion enhancement for a larger number of sidearms, TPA dimer (TPD) featuring four sidearms was studied. TPD and its structurally modified counterparts are well known compounds and are frequently exploited in various optoelectronic devices.[39,40] However, exciton diffusion length in these compounds is rarely studied. Therefore, the two TPD compounds substituted with DPE sidearms, exhibiting the most prominent L_D enlargement (section 4.1.4), were chosen for evaluation and verification of

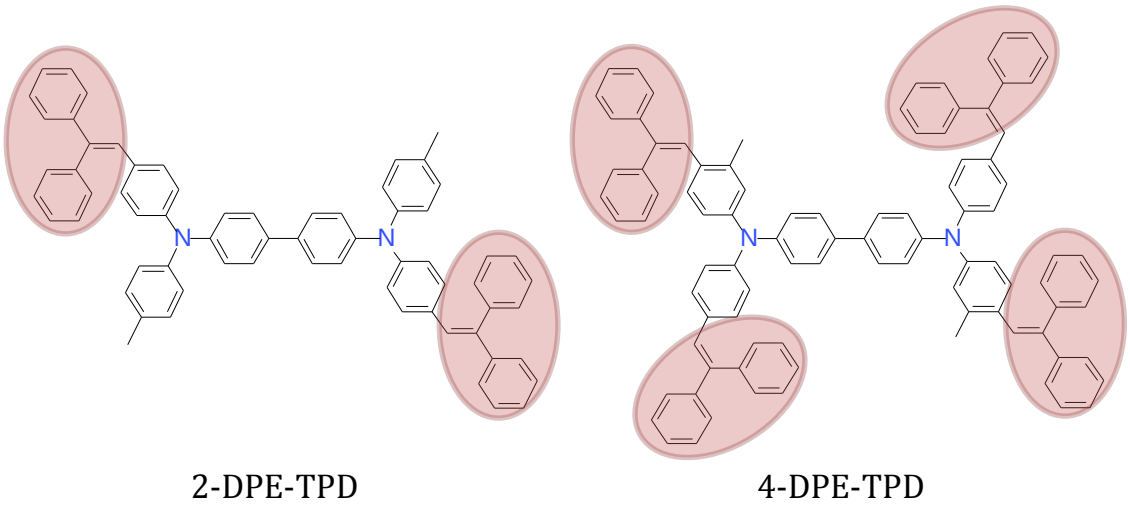

Fig. 21. Chemical structure of the TPA dimers with two and four DPE sidearms.

the importance of phenylethenyl sidearms to singlet exciton diffusion. The chemical structure of TPD derivatives possessing two and four DPE sidearms is shown in Figure 21.

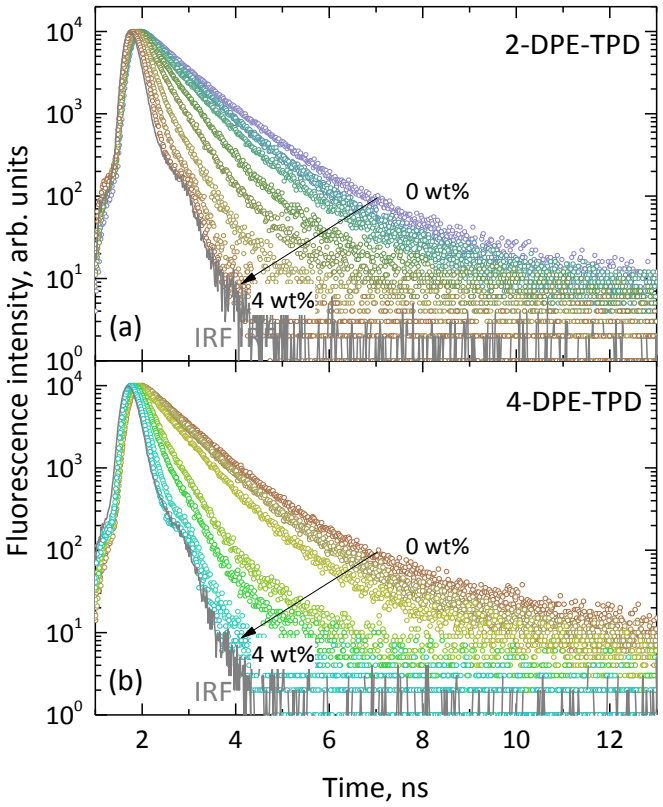

Fig. 22. Fluorescence transients of 2-DPE-TPD (a) and 4-DPE-TPD (b) films doped with PCBM quencher at different concentrations (0 – 4 wt%). IRF – instrumental response function.

For the determination of L_D, 2-DPE-TPD and 4-DPE-TPD films containing different PCBM quencher concentration have been fabricated. The measured fluorescence transients are displayed in Figure 22. The top curves in Figure 22 represent transient of the neat films of 2-DPE-TPD and 4-DPE-TPD without PCBM quencher and feature multi-exponential decays with the average decay time of 0.91 and 0.92 ns, respectively. Obviously, the presence of the quencher significantly accelerates fluorescence decay and the films with 4 wt% of PCBM exhibit very fast transients, which practically echoes IRF suggesting very efficient fluorescence quenching by PCBM. From the fluorescence transients relative quenching efficiency was

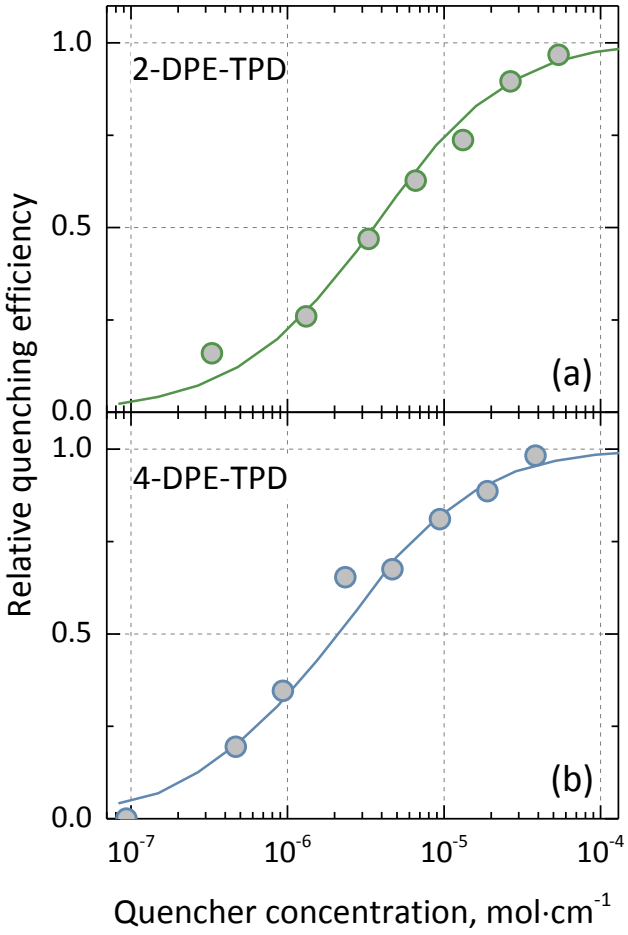

Fig. 23. Relative quenching efficiency *vs* PCBM molar concentration in 2-DPE-TPD (a) and 4-DPE-TPD blends. Points and lines depict experimental and modelled data, respectively.

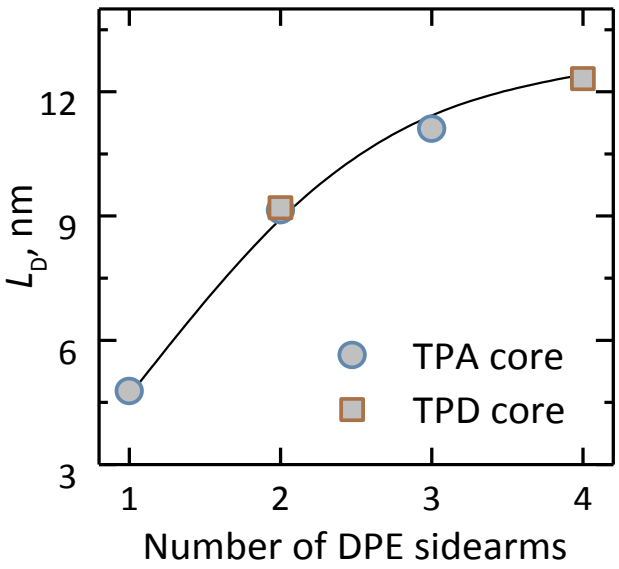

Fig. 24. Exciton diffusion length as a function of the number of DPE sidearms in TPA and TPD compounds.

calculated according to equation (5) and is depicted in Figure 23. The best agreement between Monte Carlo simulated and experimentally determined Q values *vs* quencher concentration was found in the case when exciton diffusion coefficient was set to 3.1×10^{-4} cm^2/s and 5.5×10^{-4} cm^2/s for 2-DPE-TPD and 4-DPE-TPD compounds, respectively (Fig. 23). All the necessary parameters for the exciton diffusion simulation e.g. density of the material, exciton radius, was used the same as described in previous section 4.1.5. The simulated D then can be used for the calculation of three-dimensional exciton diffusion length in DPE-substituted TPD derivatives and is shown in Figure 24. Here, L_D of the same DPE sidearms possessing TPA and TPD compounds is compared. Both TPA and TPD compounds with two DPE sidearms demonstrate very similar L_D of 9.2 nm. Importantly, the incorporation of four DPE sidearms into TPD enlarges L_D up to 12.3 nm. This finding confirms that the increased number of DPE sidearms is capable of forming the dense network of hopping sites with enhanced singlet exciton diffusion.

Interesting, that intermolecular distance between sidearms in the neat films of 2-DPE-TPD and 4-DPE-TPD is 1.06 and 0.95 nm, which is very close to intermolecular distance for TPA compounds 1-DPE-TPA and 2-DPE-TPA (Table 4). Identical intermolecular distance signifies that the density of sidearms in the TPD films is also the same as compared with one and two sidearm-substituted TPA derivatives. However, higher L_D measured in the TPD derivatives unambiguously suggests the importance of the core. One possible explanation might be that enhancement of exciton diffusion in TPD derivatives as compared to TPA, is achieved as a result of intramolecular exciton transfer. Due to prolonged molecular structure, the packing in the neat film might be organized in more favorable fashion for exciton diffusion, e.g. induced twisting at the TPA units might improve dipole orientation factor.

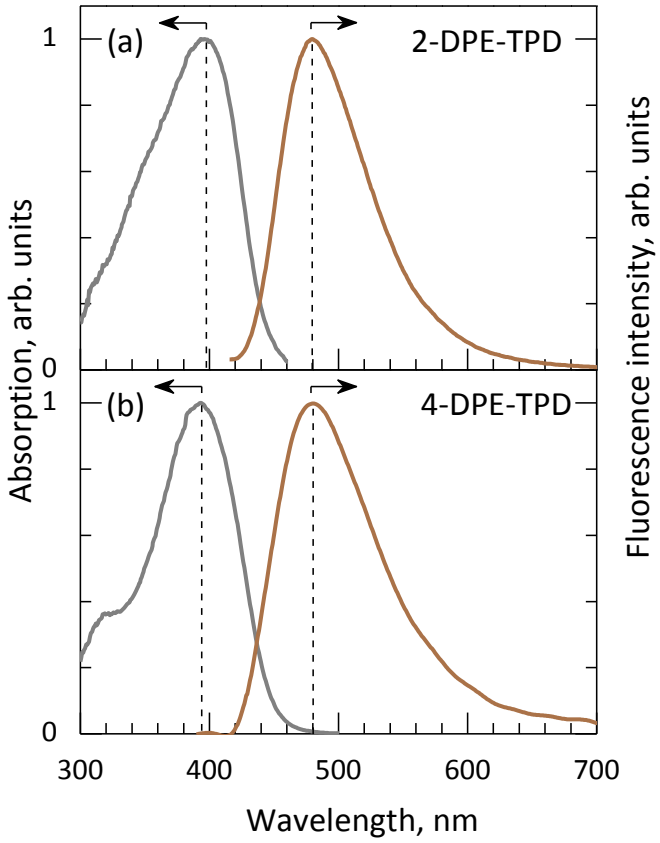

Fig. 25. Normalized absorption and fluorescence spectra of the TPD compounds with two (a) and four (b) DPE sidearms.

Measured absorption and fluorescence spectra of encapsulated neat films of 2-DPE-TPD and 4-DPE-TPD are shown in Figure 25. 2-DPE-TPD and 4-DPE-TPD feature absorption with the maximum at 396 and 394 nm, respectively, and fluorescence with the maximum at 480 nm of both compounds. The spectral positions of these TPD compounds are very similar to those of TPA monomers with the same DPE sidearms (4.1.1). The absence of spectral shifts in absorption and fluorescence bands after significant enlargement of molecular structure by additional DPE units in TPD derivatives suggest that in these compounds the exciton localization on one of the sidearms is also taking place.

4.1.6 Exciton diffusion in 1,8-naphthalimide-substituted TPAs

Singlet exciton diffusion in the neat films of phenylethenyl-substituted triphenylamines and even triphenylamine dimers is

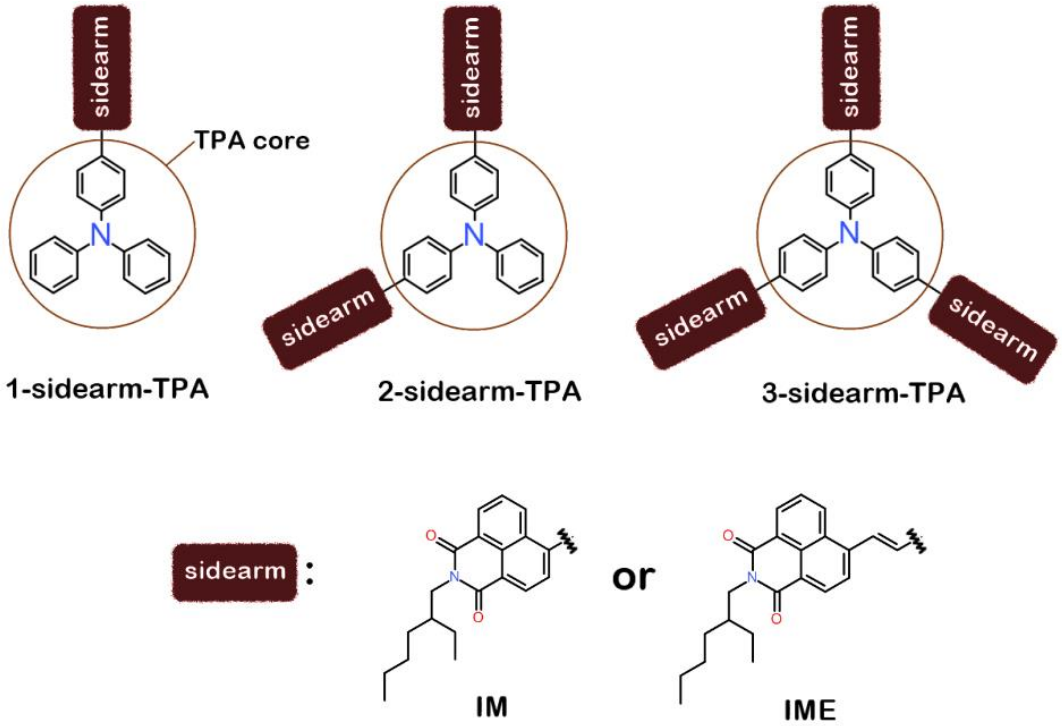

Fig. 26. Chemical structure TPA compounds with different number (one, two and three) and different type of sidearms: *N*-(2-ethylhexyl)-1,8-naphthalimide (IM) and (*N*-(2-ethylhexyl)-1,8-naphthalimid-4-yl)-ethenyl (IME).

significantly enhanced when higher number of phenylethenyl sidearms is attached to TPA or TPD core. However, it is still unclear whether the attachment of other than phenylethenyl sidearms would still results in enhancement of L_D. For this reason, the measurements of L_D in the neat films of TPA derivatives possessing different number (from one to three) of naphthalimide (IM) sidearms were conducted. One series of naphthalimide substituted TPA derivatives consisted of single-bonded IM sidearms (IM-TPA compounds), whereas in another series ethenyl linking

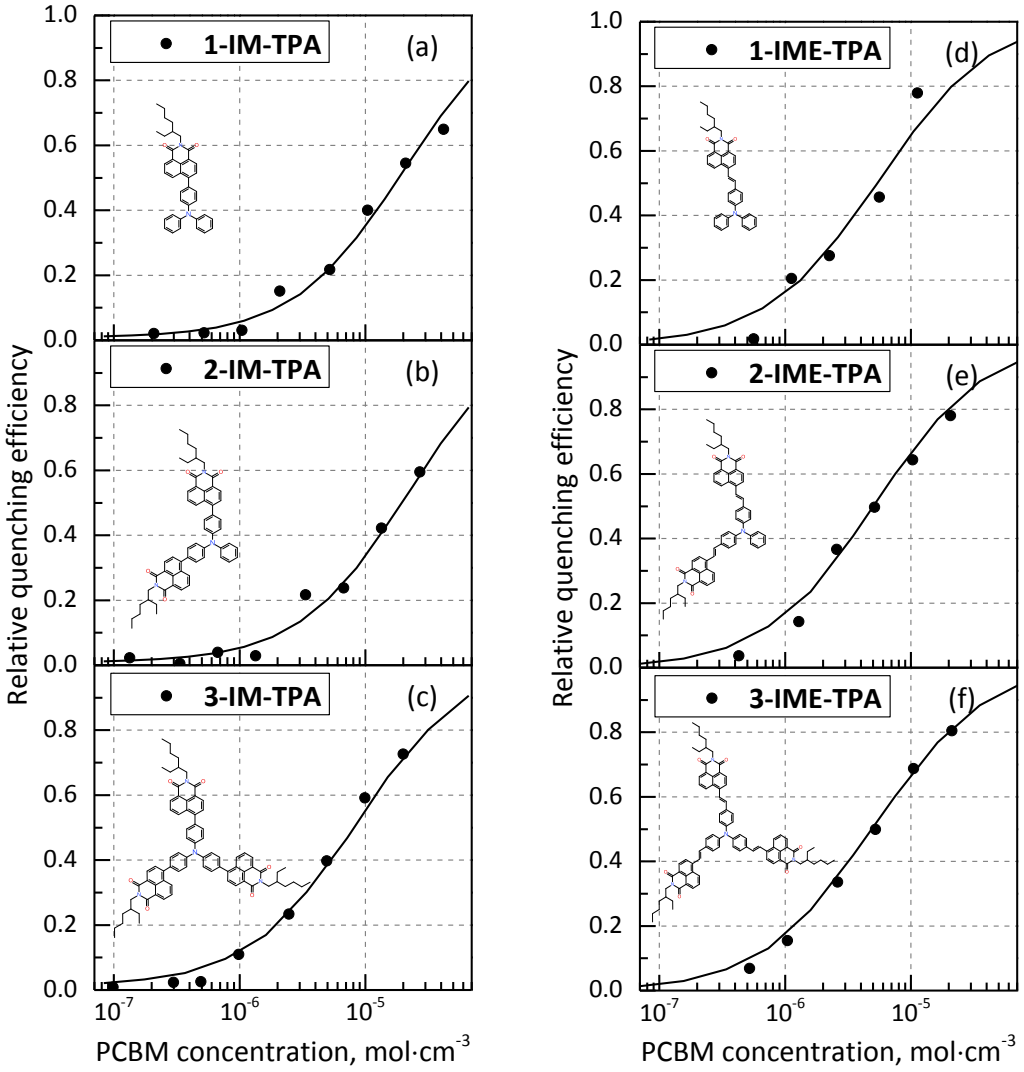

Fig. 27. Relative quenching efficiency *vs* PCBM molar concentration in TPA:PCBM blends of IM-TPA derivatives with one (a), two (b) and three (c) IM sidearms and IME-TPA derivatives with one (d), two (e) and three (f) IME sidearms. Points and lines depict experimental and modelled results, respectively.

groups (IME-TPA compounds) were employed (Fig. 26). For the determination of L_D, films containing IM-TPD and IME-TPD compounds with variable concentration of PCBM were fabricated under nitrogen atmosphere and fluorescence transients were measured. From the obtained data relative quenching efficiency was calculated and its dependence on molar quencher concentration is depicted in Figure 27.

Monte Carlo simulations allowed evaluating exciton diffusion coefficient, which is shown in Figure 28. Additionally, relative quenching efficiency versus PCBM quencher concentration was modeled using previously determined *D* (Fig. 27). Fairly good agreement between simulations and experimental data again demonstrates intimate mixture of naphthalimide-substituted TPA derivatives and PCBM quencher, and thus, hints on reliable determination of exciton diffusion coefficient. Homogenous quencher distribution in these IM-TPA and IME-TPA compounds is rather probable as compounds form molecular glasses with glass transition temperature between 45 and 107°C.[52,53] Similarly to the phenylethnely sidearms, increasing number of IM sidearms also increased *D* for both IM-TPA and IME-TPA compounds. Interestingly, that *D* for IME-TPA compounds was found to be almost one order of magnitude to that of

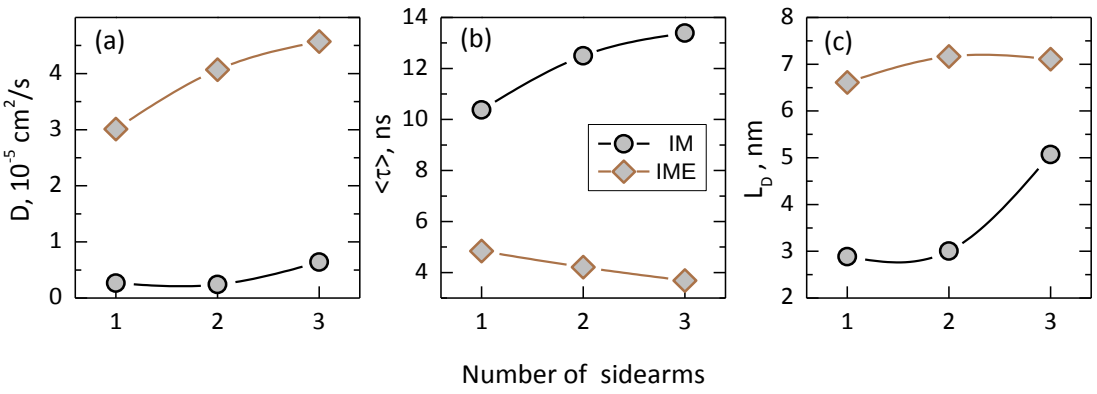

Fig. 28. Exciton diffusion coefficient (a), average fluorescence lifetime (b) and exciton diffusion length (c) as a function of the number of IM and IME sidearms of TPA derivatives.

IM-TPA, despite the fact that the molecular structure of the IM-TPA compounds is smaller as compared to IME-TPAs featuring additional ethenyl linkers. To understand such a large difference of *D*, it is necessary to analyze photophysical properties of these compounds.

Fluorescence transients of the encapsulated films of IM-TPAs were found to express multi-exponential transients with average decay time ranging from 10.4 ns to 13.4 ns, which slightly increased with the number of IM sidearms. Whereas, IME-TPAs showed opposite trend with increasing number of IME sidearms. $<\tau>$ of 4.8 ns for 1-IME-TPA was determined, which is more than 2 times shorter as compared to 1-IM-TPA. 2-IME-TPA and 3-IME-TPA exhibited fluorescence lifetime of 4.2 and 3.7 ns, respectively (Fig. 29). These differences might be related to different extension of charge transfer states. Earlier reports showed that dihedral angle between naphthalimide and TPA core for IM-TPAs is ~53°, whereas for IME-TPA compounds this angle is significantly smaller ~29°.[52,53] Generally, higher dihedral angle between the donor and acceptor in such type of molecules facilitates CT character. Moreover it was demonstrated that HOMO (highest occupied molecular orbital) and LUMO (lowest unoccupied molecular orbital) orbitals are localized predominantly on the donor and acceptor moieties for both IM-TPA and IME-TPA compounds, respectively. However, it is likely that for IM-TPA compounds the separation of HOMO and LUMO orbitals due to larger dihedral angle is higher.[52,53] Effective separation of HOMO and LUMO orbitals forms CT states, which typically have lower oscillator strength. Again, for IM-TPAs oscillator strength (*f*) was found to range from 0.15 to 0.30, whereas for IME-TPA compound it was significantly higher – from 0.6 to 1.1, depending on the number of sidearms attached.[52,53] Increased *f* well correlated with the increased absorption intensity, which for IM-TPAs is 1.4×10^4 – 3.2×10^4 $L\times mol^{-1}\times cm^{-1}$ and is roughly 2 times smaller as compared to IME-TPAs (3.5×10^4 – 7.1×10^4 $L\times mol^{-1}\times cm^{-1}$).[52,53]

Furthermore, stronger character of charge transfer confirms that the Stokes shift in the neat films of IM-TPAs is ~100 meV larger as compared to that of IME-TPAs, which is 0.72 eV and 0.63 eV for IM-TPA and IME-TPA compounds, respectively. Very likely that stronger nature of CT in IM-TPA compounds is responsible for the 10-fold lower exciton diffusion coefficient as compared with IME-TPA compounds (Fig. 28a).

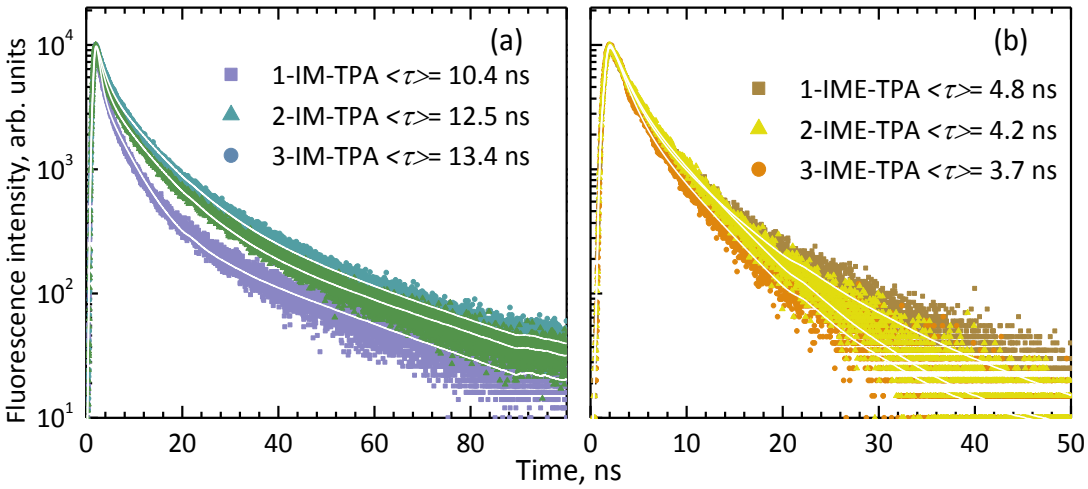

Fig. 29. Fluorescence transients of the neat films of IM-TPA (a) and IME-TPA (b) derivatives. White lines – exponential fit; average fluorescence lifetimes are indicated.

Nevertheless, the increase in exciton diffusion coefficient is still observed for both IM-TPA and IME-TPA compounds with maximum values of 6.5×10^{-6} and 4.6×10^{-5} cm^2/s for three IM sidearms possessing 3-IM-TPA and 3-IME-TPA compounds, respectively (Fig. 28a). The L_D with higher number of sidearms increases from 2.9 to 5.1 nm and from 6.6 to 7.1 nm, for IM-TPA and IME-TPA compounds, respectively (Fig. 28c). Generally, the incorporation of higher number of naphthalimide sidearms into TPA core improves exciton diffusion in the films of IM-TPA and IME-TPA compounds, however, due to donor-acceptor type of the molecules the increase in absolute value of L_D is small, not exceeding 7.1 nm.

4.1.7 Summary

Photophysical measurements revealed that increase in the number of 2-methyl-2-phenylethenyl, 2,2-diphenylethenyl and 2,2-di(4-methoxyphenyl)ethenyl of sidearms effectively suppresses intramolecular motions of the TPA core and causes significant enhancement (up to 10 times) of fluorescence quantum yield of the TPA compounds in dilute solutions. Almost complete suppression of intramolecular motions achieved by dispersing triphenylamine derivatives in a rigid polymer matrix at low concentration resulted in increased fluorescence quantum yield 47 – 63% and fluorescence lifetimes of about 2 ns, which were found to be roughly independent of the number and type of phenylethenyl sidearms attached.

It has been shown that spectral shifts of absorption spectra and almost independent fluorescence spectra of phenylethenyl-substituted TPA derivatives can be explained in terms of exciton localization onto one of the sidearm.

Although, in the solid state intramolecular torsions of the TPA core are also effectively suppressed, however the dense network of the sidearms formed facilitates exciton migration and migration induced fluorescence quenching at the non-radiative sites. In turn, enhanced exciton migration reduces fluorescence quantum yield up to 5 times in the neat films followed by accelerated fluorescence lifetime.

Phenylethenyl-substituted TPA derivatives containing flexible alkoxy chains showed virtually identical photophysical properties in dilute solutions, whereas in the neat films shortening of alkoxy chains resulted in prominently enhanced intermolecular interactions, which was evident by redshifted emission. Moreover, shortening of the alkoxy chains reduced fluorescence quantum yield by a factor of 8, what indicates migration-induced exciton quenching at non-radiative decay sites.

For the determination of exciton diffusion length fluorescence quenching efficiency in the neat films of TPA derivatives with randomly distributed exciton quenchers were estimated. Monte Carlo simulations of the fluorescence transients in TPA:quencher blends with different quencher concentration (0 – 1 wt%) were performed for the evaluation of L_D. An increase of the number of phenylethenyl sidearms from one to three, irrespectively of their type, was shown to cause the considerable enhancement of the exciton diffusivity accompanied with the 3-fold increase of L_D for MPE and DPE sidearms. The largest exciton diffusion coefficient $D = 5.4 \times 10^{-4}$ cm^2/s and diffusion length $L_D = 11$ nm were obtained for the TPA compounds bearing three MPE and DPE sidearms, respectively. Exciton diffusion measurements performed for TPA dimers possessing two and four DPE sidearms revealed that incorporation of four DPE sidearms allows enlarging L_D from 9 nm to 12 nm. The exciton diffusion enhancement with increasing the number of sidearms was attributed to the increased Förster energy transfer rate caused by the enhanced overlap of the emission and absorption spectra (reduced Stokes shift), increased extinction coefficient, and also increased density of the sidearms in the TPA films allowing for more efficient exciton hopping through the neighboring molecules.

The attachment of higher number of naphthalimide sidearms into TPA core also resulted in up to 2-fold enhanced exciton diffusion coefficient. It was found that incorporation of ethenyl linker between the sidearm and TPA core slightly reduced charge transfer character in these donor – acceptor type molecules what stimulated 10-fold increase in exciton diffusion coefficient. The higher exciton diffusion coefficient of 4.6×10^{-5} cm^2/s and diffusion length of 7 nm was obtained for the TPA compounds with three IME sidearms. Unfortunately, donor – acceptor molecular structure determines small absolute value of the diffusion coefficient and therefore exciton diffusion length does not exceed 7 nm.

4.2 Light upconversion in sensitized DPA/PMMA films

Fueled by the many opportunities that it offers in terms of enhancement of solar harvesting,[90,91] photocatalysis,[92] light emission[93,94] or bioimaging[95,96] for instance, sensitized light upconversion (UC) mediated by triplet-triplet annihilation (TTA) has attracted increasing attention in the past decade.[97,98] TTA-UC presents two obvious advantages over alternative UC schemes, namely the abilities to operate at subsolar irradiance power densities (~10 mW/cm^2) and with noncoherent light.[14] For comparison, widely used UC *via* generation of high harmonics requires not only coherent excitation, but also needs to fulfill stringent constraint of phase matching. Briefly, TTA-UC relies on a cascade of photophysical events whereby lower-energy photons are harvested by a sensitizer molecules, followed by intersystem crossing and triplet-triplet energy transfer (TTET) to emitter molecules. These triplet excitons then diffuse until they encounter each other such that a singlet excited emitter is formed by means of TTA and blueshifted light is eventually emitted (Fig. 30). Such TTA-UC scheme, exploiting strong oscillator strength of singlet manifold for absorption and emission with long-lived triplet state for intermediate energy storage, also surpasses lanthanoid-based UC scheme in terms of efficiency. Lanthanoid-based upconverting phosphors use the same electronic manifold for all the processes leading to low absorptivity and inherent competition of non-radiative losses with the UC emission.[13,98]

There have been numerous reports demonstrating TTA-UC in conjugated oligomeric thin-films,[99,100] elastomeric (rubbery) doped-matrices,[101–103] gels,[104,105] composites[106], nanoparticles[107] or glassy materials such as polymer films.[108–113] Undoubtedly the latter offer multiple advantages in terms of transparency, mechanical stability and are much more attractive from a device point of view, however, maximum

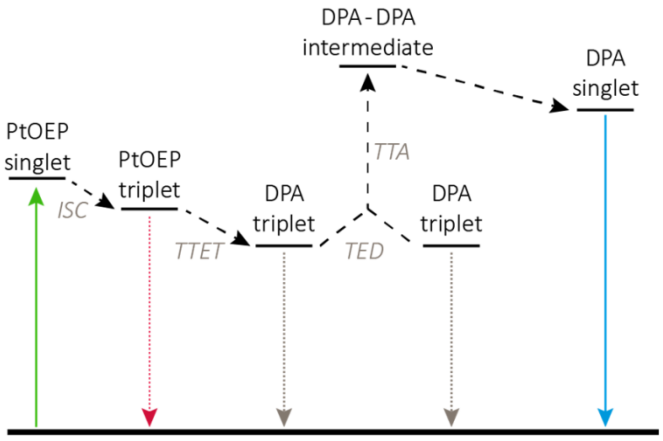

Fig. 30. TTA-UC energy diagram showing the various energy transfers between the platinum octaethylporphyrin and the 9,10-diphenylanthracene: intersystem crossing (ISC), triplet-triplet energy transfer (TTET), triplet exciton diffusion (TED) and triplet-triplet annihilation (TTA).

quantum efficiency of TTA-UC achieved is an order of magnitude lower as compared to that found in solution or liquid medium (~26%).[15] The main factors limiting upconversion efficiency in disordered glassy films are not fully understood,[111] still they are believed to be mainly related to aggregation of the emitter molecules, inefficient diffusion of the triplet excitons and their non-radiative relaxation in emitter molecules.

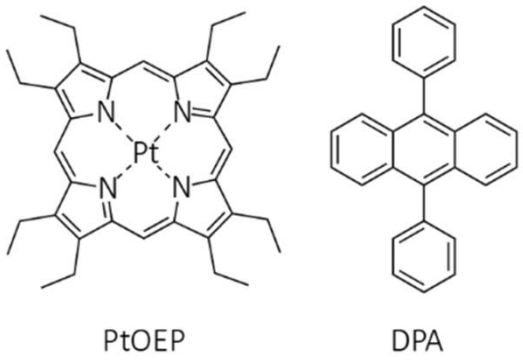

Fig. 31. Molecular structures of PtOEP sensitizer and DPA emitter.

A dye pair (Fig. 31) consisting of 9,10-diphenylanthracene (DPA) as an emitter and platinum octaethylporphyrin (PtOEP) as a triplet sensitizer was chosen due to its high reported solution upconversion

efficiency and widespread use, making it an excellent model system. The absorption and emission spectra of these dyes are shown in Figure 32. Poly(methyl methacrylate) (PMMA) polymer was used as a matrix to attain homogeneous glassy films with high DPA concentration.

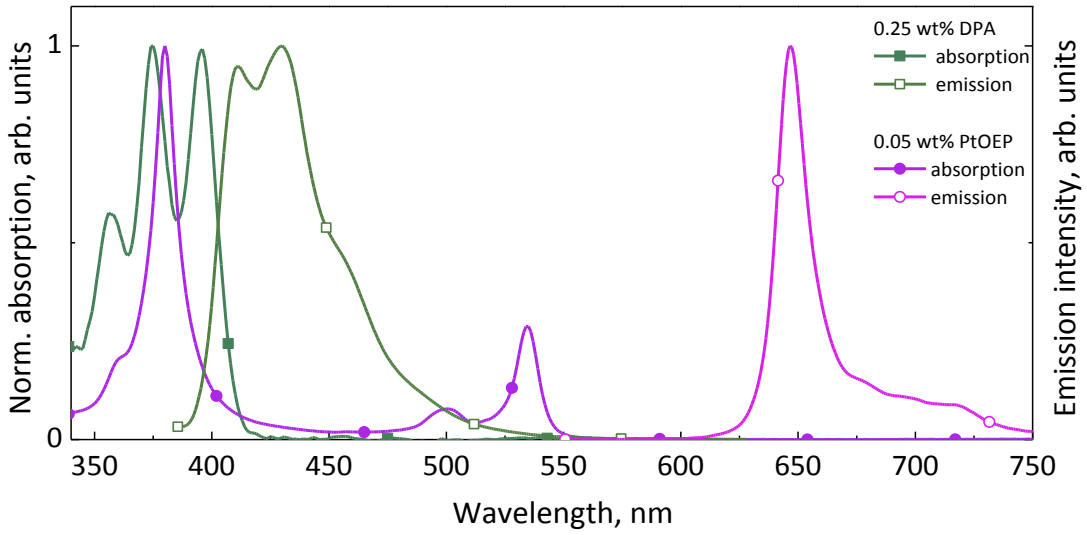

Fig. 32. Normalized absorption and emission spectra of melt-processed PtOEP/PMMA (c_{PtOEP} = 0.05 wt%) and DPA/PMMA (c_{DPA} = 0.25 wt%) films.

The photophysical processes ongoing in these solid DPA/PtOEP/PMMA films were investigated in great detail to evaluate the limiting factors of upconversion efficiency. Identification of such factors is essential to understand the loss mechanisms and reduce their impact to overall upconversion quantum efficiency.

4.2.1 Fluorescence concentration quenching in DPA/PMMA films

Concentration effects that could originate from inhomogeneous DPA distribution in upconverting PMMA films due to high DPA loadings were assessed from fluorescence spectra and fluorescence quantum yield measurements. Figure 33a depicts fluorescence spectra of DPA/PMMA films with different DPA content measured after excitation with 365 nm.

No noticeable emission shift was observed, just a clear tendency of decreasing 0th vibronic peak of DPA emission with higher DPA load which is attributed to reabsorption effect. Measured emission Φ_{FL} showed monotonous decrease from 87% to 57% with increasing DPA concentration from 15 wt% to 40 wt% (Fig. 33b). 1.5-fold decrease of Φ_{FL} indicates moderate fluorescence quenching and even distribution of DPA throughout the polymer matrix at such high DPA concentrations.

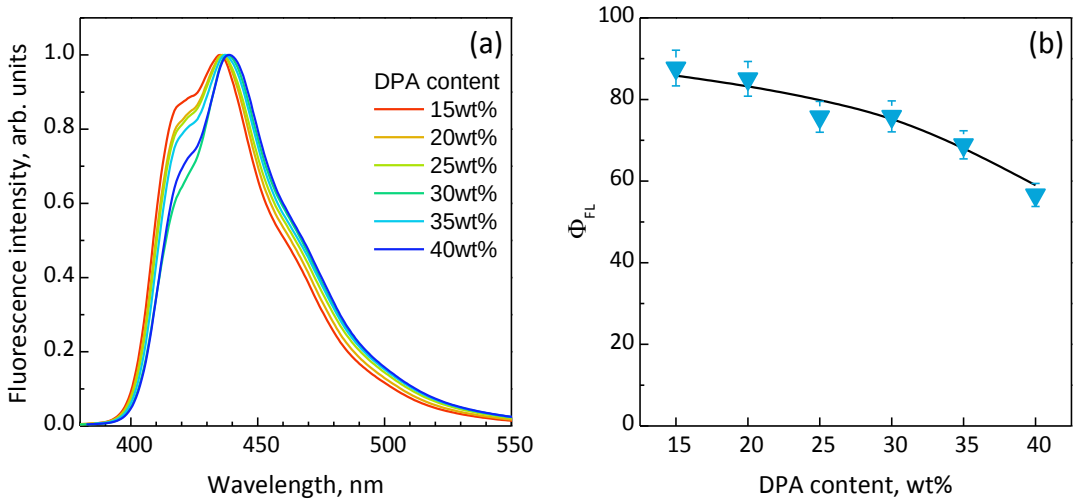

Fig. 33. Fluorescence spectra (a) (λ_{ex} = 365 nm) and fluorescence quantum yield (b) of melt-processed DPA/PMMA films at different DPA content (λ_{ex} = 405 nm).

This is attributed to the melt-processing route followed by rapid cooling, which were used for the preparation of polymer films. Massive aggregation would have otherwise resulted in significantly higher concentration quenching which was not observed in this sample set.[115]

4.2.2 Triplet energy transfer in DPA/PtOEP/PMMA films

Since triplet energy transfer from the photoexcited PtOEP to DPA is one of the first events in the cascade processes of UC, it must have

high enough rate to ensure efficient overall TTA-UC process. The TTET efficiency was evaluated by analyzing phosphorescence intensity decays at different DPA concentrations. Figure 34a shows an emission of DPA/PtOEP/PMMA films in a semi-logarithmic plot as a function of emitter concentration with 0.05 wt% of PtOEP excited at the Q band of the sensitizer (532 nm) with a 30 mW power green laser diode. At each concentration two distinct signals can be observed on either side of the excitation band: a blueshifted emission at ~440 nm, corresponding to the

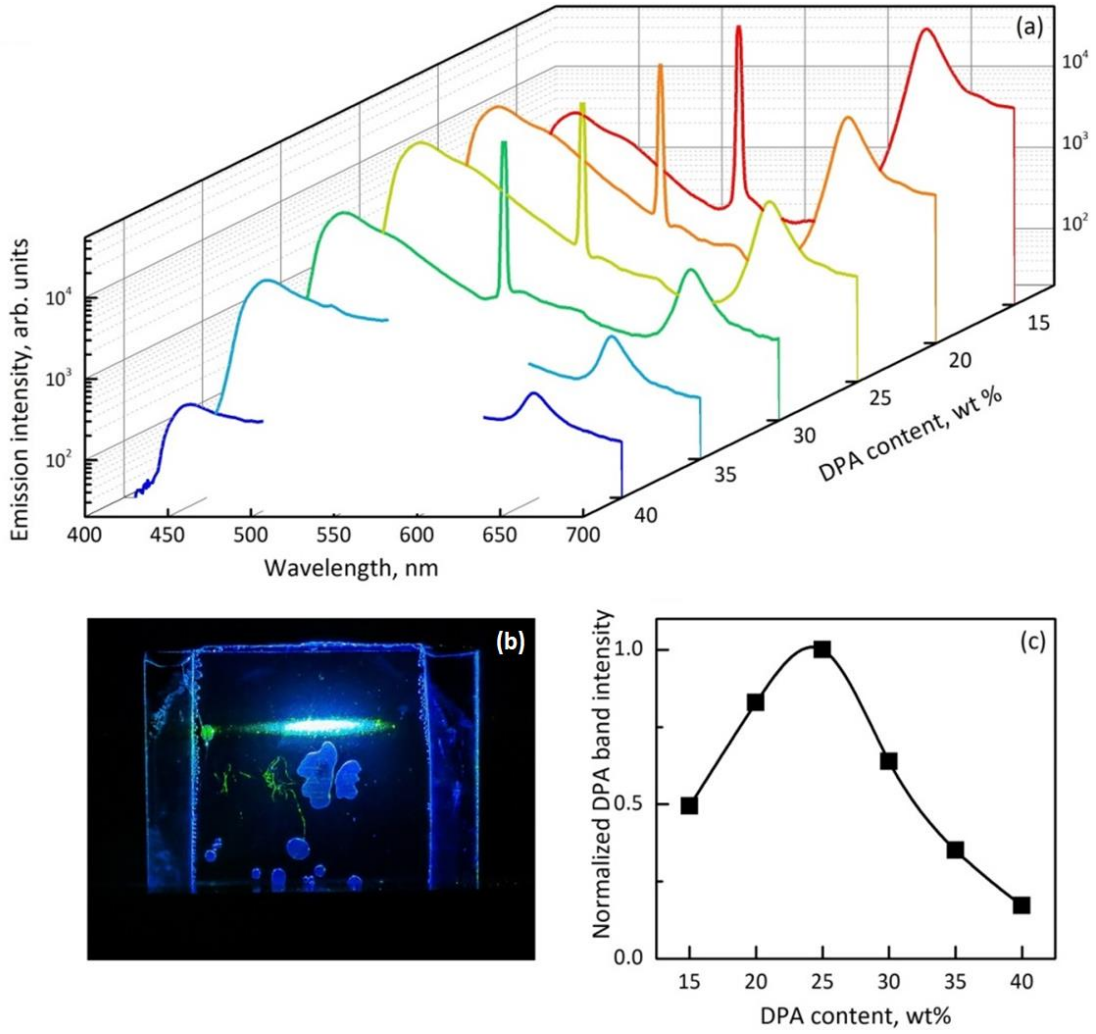

Fig. 34. (a) Emission spectra of DPA/PtOEP/PMMA films excited at 532 nm as a function of DPA concentration. Note that the vertical axis has a logarithmic scale. (b) A picture of green-to-blue upconversion in the polymer film. (c) Emission intensity of DPA band.

upconverted light and a red-shifted peak at 647 nm, corresponding to residual phosphorescence from the triplet exciton sensitizer (Fig. 34a). The spectra region in the vicinity of excitation wavelength (532 nm) was cut off for the films with 35 wt% and 40 wt% of DPA due to immense signal caused by enhanced scattering of excitation light (Fig. 34a). A bright blue UC signal could be observed readily with the naked eye by irradiating the film containing 25 wt% of DPA under the same experimental conditions (Fig. 34b). As expected, a monotonous decrease of PtOEP phosphorescence intensity is observed with increasing DPA concentration (Fig. 34a), which is consistent with enhanced TTET to DPA. The UC intensity increases with DPA concentration up to 25 wt% of DPA, and then decreases as the DPA concentration further increases. The non-monotonous behavior of UC can be clearly observed from Figure 34c, where the peak maximum intensity of DPA emission band is displayed as a function of DPA concentration. While this is not an absolute measurement of the quantum yield of the process, it provides a good qualitative indication of the overall UC efficiency at each concentration given the identical processing conditions and PtOEP concentration. The initial increase of UC intensity with the DPA load could be attributed to the increased triplet exciton concentration in the DPA due to the enhanced triplet energy transfer from PtOEP. The reduction of UC intensity to a small extent could potentially be ascribed to the concentration quenching of singlet excitons in DPA (Fig. 33b). However, as will be described further, additional non-radiative decay phenomena of the DPA triplet excitons must be at play to account for the significant UC intensity decrease at higher DPA contents.

Figure 35a shows the accelerated decay in PtOEP phosphorescence transients with increasing DPA loadings, which further supports the fact that TTET from sensitizer to emitter is in fact quite efficient. These transients were obtained using a variable optical window

method, which allowed at different delays and exposure times to measure optical signal,[116] thus enabling to probe time evolutions ranging from 100 ns to 10 ms. A reference film of PtOEP embedded in a PMMA matrix was shown to possess an intrinsic phosphorescent decay time constant of ca. 100 μs (Fig. 35a). Several orders of magnitude lower intensity long-lived decay component observed in the transients on a

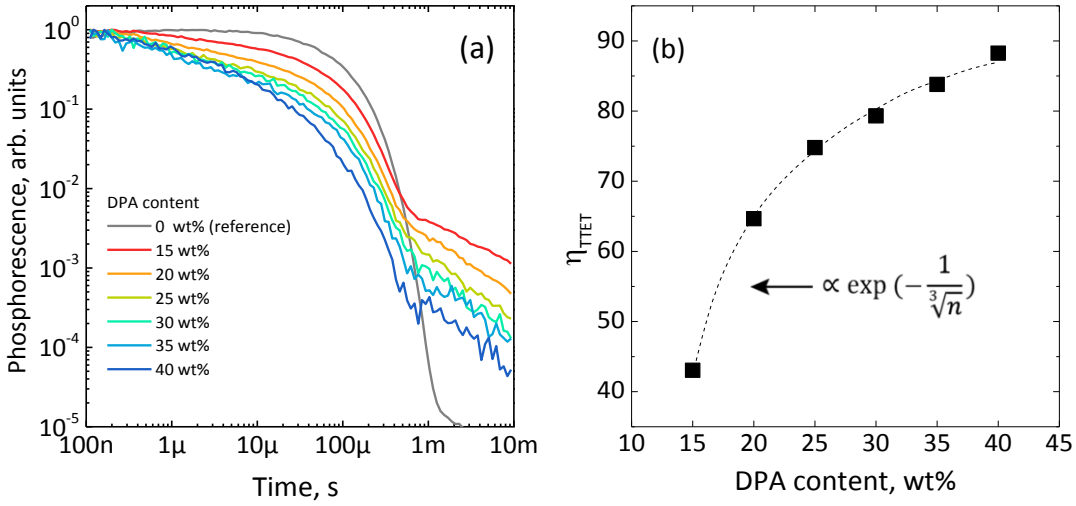

Fig. 35. (a) Phosphorescence transients of DPA/PtOEP/PMMA (C_{PtOEP} = 0.05 wt%) films with different DPA loadings (λ_{ex} = 532 nm). (b) Triplet energy transfer rate from PtOEP to DPA. The dashed line corresponds to Dexter-type energy transfer fit of experimental data, where *n* is the DPA concentration.

millisecond time-scale (Fig. 35a), and which is missing in the transient of the reference sample, is attributed to the back-energy-transfer from DPA to PtOEP triplet. Similar observations were previously reported for blue phosphorescence materials.[117] The intrinsic phosphorescence lifetime of PtOEP evidently shortens rapidly with the introduction of additional DPA into the polymeric matrix. In order to estimate the efficiency of the TTET step (η_{TTET}), the following relation was used:

$$\eta_{TTET} = \frac{\int I_{0\%DPA}(t)dt - \int I_{X\%DPA}(t)dt}{\int I_{0\%DPA}(t)dt}, \qquad (23)$$

where $I_{X\%DPA}(t)$ corresponds to the transient obtained at X wt% of DPA. As expected, η_{TTET} increases monotonously with increasing DPA concentration and exceeds 75% for DPA content above 25 wt% implying TTET process to be highly efficient (Fig. 35b).

4.2.3 TTA-UC quantum yield *vs* DPA concentration

Light upconversion mediated by TTA is a bimolecular process (eq. 19) and its efficiency depends on the excitation power density. Therefore, prior to estimating TTA-UC quantum yield (Φ_{UC}) in DPA/PtOEP/PMMA films proper excitation conditions need to be found. To this end, UC emission and sensitizer phosphorescence intensity was measured as a function of incident power density for all DPA concentrations (15 – 40 wt%) (Fig. 36).

Since the emission spectral shape did not change with increasing excitation power the UC peak intensity could be used instead of the integral value. As expected, the phosphorescence intensity increases linearly with increasing excitation power density, i.e., increasing number of excited PtOEP molecules. Conversely, the UC emission exhibits a dual behavior: i) a quadratic dependence at low excitation densities and ii) a linear at higher excitation densities. Such behavior is characteristic of the TTA-UC process and has been previously examined in detail.[118,119] Briefly, the linear behavior corresponds to a regime where triplet emitters decay preferentially *via* TTA, whereas the quadratic regime is consistent with spontaneous decay of the DPA triplet excited states. Consequently, the intensity threshold (I_{th}),[119] whereby the kinetics of UC switches from quadratic to linear is a critical figure of merit as it characterizes the performance of a certain TTA-UC system. The lower this value is, the more performant the system. This threshold value was also determined at different emitter concentrations (Fig. 36) and plotted as a function of DPA

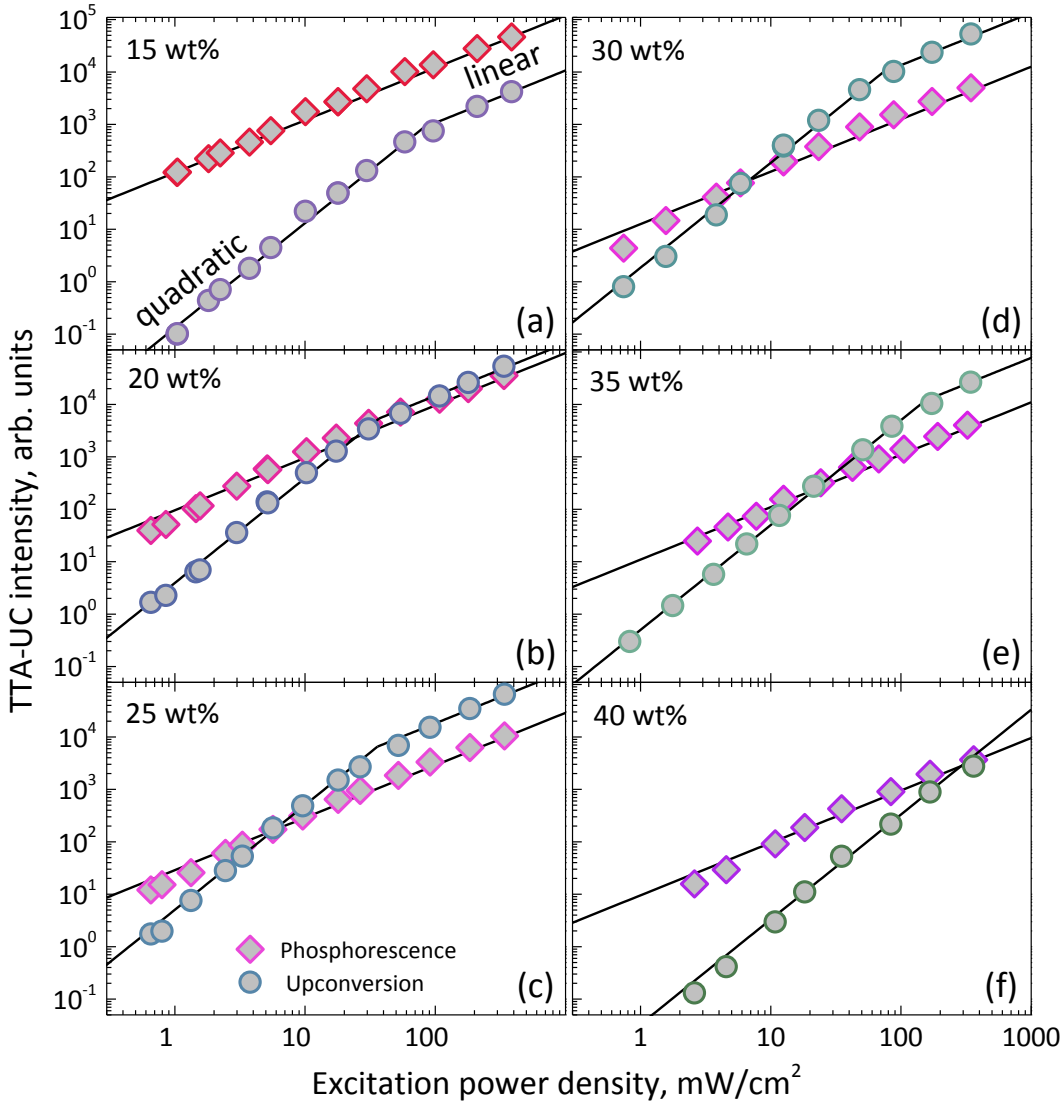

Fig. 36. TTA-UC intensity as a function of excitation power density (λ_{ex} = 532 nm) at different emitter concentrations (a) 20 wt%, (b) 25 wt%, (c) 30 wt%, (d) 35 wt% in DPA/PtOEP/PMMA films (C_{PtOEP} = 0.05 wt%).

content (Fig. 37). It is obvious that the lowest I_{th} is obtained for the sample with 25 wt% of DPA.

Obtaining I_{th} is essential for correct determination of TTA-UC quantum yields. Indeed, the measurements must be accomplished in a regime where the upconversion depends linearly upon the incident light (i.e., where $I > I_{th}$), meaning that the estimated quantum yield value of UC must not depend upon the excitation power density. Consequently, all of

the quantum yield measurements were performed at an excitation power density of 155 mW/cm², which is in the linear regime for most of concentrations except for the highest one (40 wt%) used in the experiments (Fig. 36 and Fig. 37).

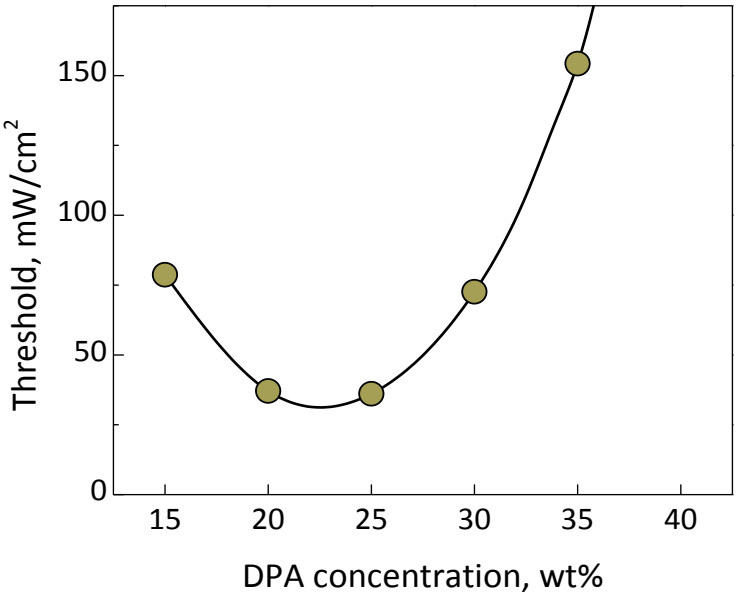

Fig. 37. TTA-UC intensity threshold at different DPA concentrations.

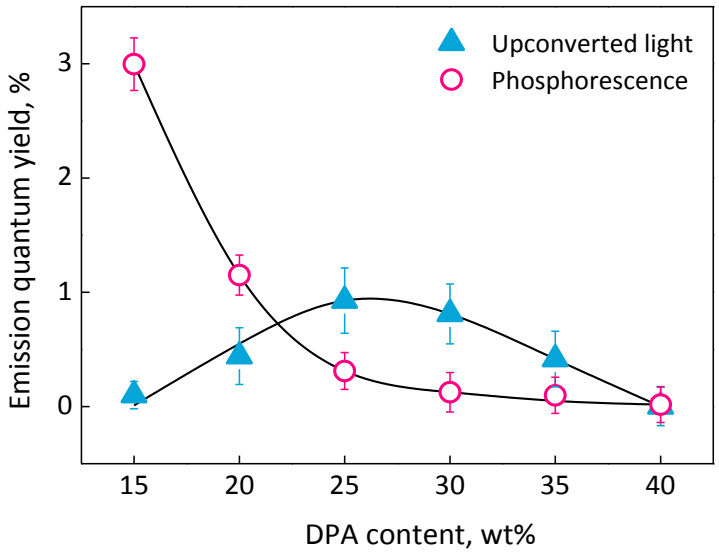

Fig. 38. Phosphorescence and TTA-UC quantum yield in DPA/PtOEP/PMMA (C_{PtOEP} = 0.05 wt%) films as a function of DPA concentration. Note that maximum theoretical TTA-UC efficiency is 50%. Lines are guides for the eyes.

The absolute measurements of Φ_{UC} and the phosphorescence quantum yield (Φ_{Ph}) in the upconverting polymer films were carried out by using an integrating sphere (Fig. 38). Again, the decrease of Φ_{Ph} with increasing DPA concentration confirms enhanced TTET from the sensitizer to the emitter molecules. The evolution of Φ_{UC} is somewhat more intricate. The initial increase in TTA-UC quantum yield is in agreement with enhanced TTET to DPA. However, the later dramatic decrease of TTA-UC quantum yield from 0.9% to 0.0006% cannot solely be accounted by the concentration quenching of singlet emission in DPA (Fig. 33b). For the sake of clarity, it is important to mention that TTA-UC quantum yield (with the maximum Φ_{UC} of 50%) scales by a factor of 2 as compared to TTA-UC quantum efficiency, which maximum value is normalized to 100%).[98] The decrease of Φ_{UC} by ca. three orders of magnitude is indeed inconsistent with the previously described 4/5 decrease in DPA emission upon excitation at 405 nm. This decrease can presumably be ascribed to triplet exciton quenching due to enhanced triplet exciton diffusion, and thus increased probability to reach

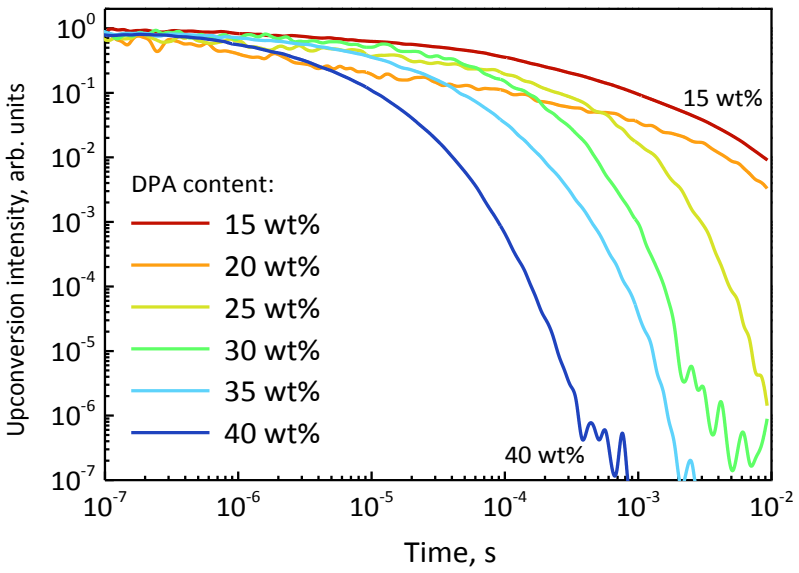

Fig. 39. UC emission transients of the DPA/PtOEP/PMMA (C_{PtOEP} = 0.05 wt%) films at different DPA loadings.

non-radiative decay sites. Unlike pre-organized systems, amorphous glasses bear high number of defects which could potentially serve as non-radiative sites for long-lived triplet excitons.

The essential role of the triplet exciton quenching is confirmed by the accelerated decay of UC intensity with increasing DPA content in UC transients (Fig. 39). The changes in the UC decay rate occurring on a millisecond time-scale indicate that the dominant quenching mechanism is governed by the triplet excitons and not by the singlets.

4.2.4 Triplet exciton diffusion length in DPA/PtOEP/PMMA films

Triplet excitons are very important in upconversion process since for the triplet-triplet annihilation two triplets located at neighboring molecules are necessary to generate one singlet exciton. Generally, triplets are generated at different locations in the upconverting system, therefore they have to diffuse towards one another to be able to encounter. For this reason, effective long-range diffusion of triplet excitons is essential for the efficient TTA-UC process. Therefore, to clarify the role of triplet exciton diffusion in upconverting polymer glasses, the triplet exciton diffusion coefficient (D) and diffusion length (L_D) were evaluated as a function of emitter concentration. For this evaluation time-resolved photoluminescence bulk-quenching technique[26] was employed with PCBM (Fig. 1) serving as appropriate triplet exciton quencher.[19,120] Experimentally obtained excited state relaxation dynamics (Fig. 40) enabled to evaluate relative quenching efficiency (eq. 20, Fig. 41) followed by Stern-Volmer modeling (section 2.3),[19] which recently has been proved to be the accurate tool for exciton diffusion length evaluation.[26]

Table 5 summarizes main Stern-Volmer fitting parameters along with the reaction radius, average UC emission lifetime $<\tau>$ and estimated triplet exciton diffusion length. The reaction radius in these calculations

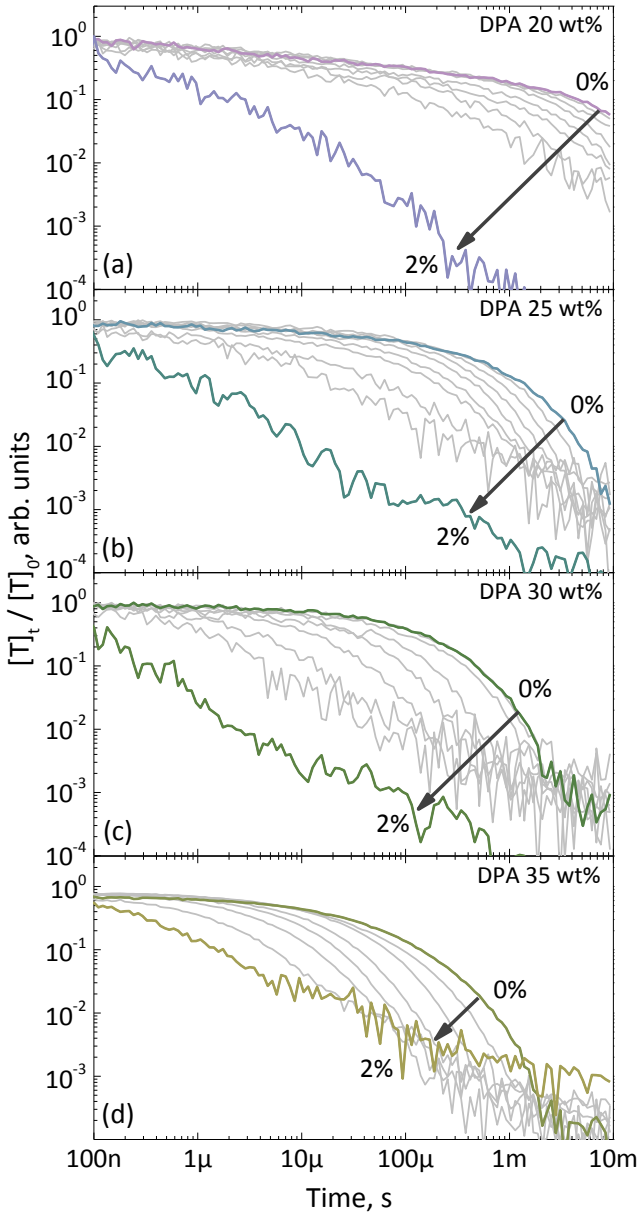

Fig. 40. Triplet exciton concentration dynamics of the DPA/PtOEP/PMMA (C_{PtOEP} = 0.05 wt%) films at different triplet quencher concentrations from 0 to 2 wt%.

was assumed to be equal to the average intermolecular distance of DPA molecules. The application of the time-resolved photoluminescence bulk-quenching technique for the evaluation of diffusion parameters at DPA loadings of 15 and 40 wt% was impossible due to insufficient UC signal (Fig. 34a). From the Table 5, it is obvious that D increases while the average lifetime of triplets shortens with emitter concentration.

Table 5. Main Stern-Volmer fitting parameters.

DPA loading	K_{SV} $cm^3 \times mol^{-1}$	D $cm^2 \times s^{-1}$	f_a	r nm	$<\tau>$	L_D nm
20 wt%	1.6×10^6	3.1×10^{-10}	1.0	1.32	5.3 ms	22.2
25 wt%	2.1×10^6	2.2×10^{-9}	0.97	1.23	1.0 ms	25.8
30 wt%	3.7×10^6	1.7×10^{-8}	0.97	1.15	240 µs	35.6
35 wt%	9.9×10^6	5.8×10^{-8}	0.86	1.10	210 µs	60.1

However, the increase of D prevails resulting in the final enhancement of L_D with increasing DPA content (Fig. 42).

L_D of the triplets was reported to depend very sensitively on the material and its morphology and therefore to range from several nanometers to hundreds of microns.[121] Mostly for purely amorphous films, L_D was found to be less than 100 nm, e.g., 54 nm for 4P-NPD,[122] 22 nm for platinum polyyne polymer (Ph100),[19] 30 nm for PtOEP film,[123] 9 nm for SY-PPV,[124] 28 nm for PdTPPC,[125] 87 nm for NPD[126]. In the case of highly-ordered organic crystals L_D values well beyond several microns could be obtained, e.g., 20 µm for anthracene crystals,[127] 8 µm for rubrene,[58] and up to 13 µm in anthracene-based metal-organic frameworks.[128] Exciton diffusion based on the energy transfer rate formalism can be applied. However, much more complex treatment of exciton diffusion is required for inherently disordered systems,[129] such as polymers or as in this case amorphous DPA/PtOEP/PMMA films. In contrast to the singlet excitons capable to migrate *via* long-range (1-10 nm) Förster energy transfer mechanism, triplet exciton diffusion is governed by Dexter energy transfer with a typical length scale of up to 1 nm (typical intermolecular distance). Therefore, Dexter mechanism is known as short-range energy transfer, which utilizes physical exchange of electrons, and thus requires spatial overlap of wave functions of the donor and acceptor. Taking this into account, local intermolecular arrangements/interactions play critical role for triplet excitons and defines their diffusion pathways.[130] The increase of triplet exciton diffusivity (parameter D) with DPA loading (Table 5) can be

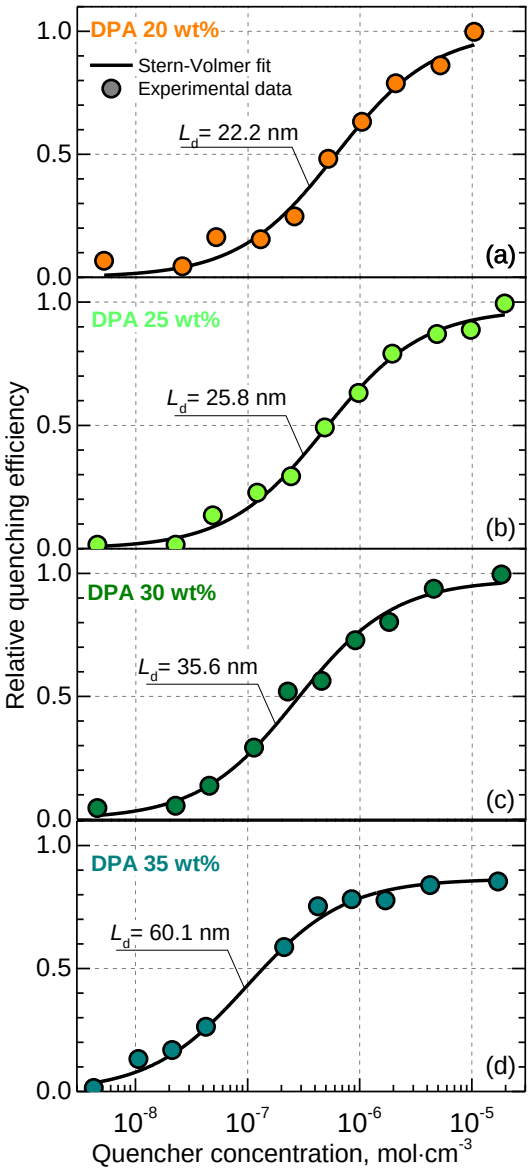

Fig. 41. Relative quenching efficiency as a function of quencher concentration for different DPA concentrations (a) 20 wt%, (b) 25 wt%, (c) 30 wt%, (d) 35 wt% in the DPA/PtOEP/PMMA (C_{PtOEP} = 0.05 wt%) films. Triplet exciton diffusion lengths are indicated. Lines are Stern-Volmer fits.

intuitively understood to occur as a result of reduced intermolecular separation, i.e. increase of the concentration of nearest-neighbor hopping sites. On the other hand, enhanced exciton mobility ensures access of a larger number of distant sites including those acting as non-radiative decay sites. This explains apparent shortening of the intrinsic lifetime of

triplet excitons with increasing DPA loading in the DPA/PtOEP/PMMA films (Table 5).

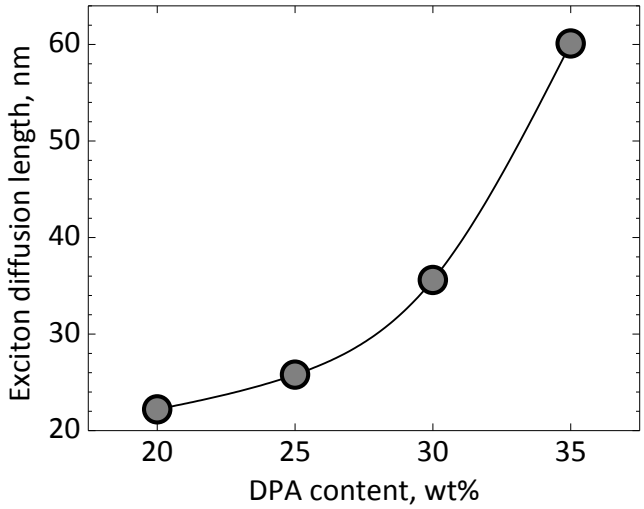

Fig. 42. Triplet exciton diffusion length as a function of emitter concentration in PMMA.

In the studied disordered DPA/PtOEP/PMMA films, L_D increased by a factor of 3 (from 22 to 60 nm) as the emitter concentration increased from 20 to 35 wt%. Unfortunately, enhanced triplet exciton diffusion in sensitized polymer glasses with increasing emitter concentration did not result in enhanced TTA-UC quantum yield (Fig. 38) suggesting that L_D is not a limiting factor in the amorphous polymer glasses. Evidently, the triplet exciton diffusion in the polymer glasses is found to be sufficiently efficient to not degrade TTA-UC efficiency. As it was discussed above, most likely the main limiting factor is related to non-radiative decay of triplet excitons in emitter molecules. In support of this statement a comparison of the estimated L_D values with the average distance between the sensitizer molecules, which is ~14 nm at PtOEP loading of 0.05 wt%, can be made. For the calculations of average distance the densities of ρ_{PMMA}=1.18 g/cm^3, ρ_{DPA}=1.22 g/cm^3,[131] ρ_{PtOEP}=1.5 g/cm^3 of materials were used. A significantly larger L_D than the intermolecular distance of sensitizer in PMMA implies a high probability for the triplet excitons

generated on the neighboring sensitizer molecules to encounter by diffusion process and promote TTA. This observation again confirms that triplet exciton diffusion plays a non-decisive role in limiting TTA-UC efficiency in the disordered DPA/PtOEP/PMMA films. In general, triplet exciton diffusion length might depend on the particular quencher chosen, as different triplet exciton quenchers might have slightly different quenching ability. Choosing a quencher with worse quenching ability will result in quantitatively different estimates for diffusion coefficient and diffusion length. Explicitly, applying Stern-Volmer model for quenching analysis worse quencher will yield underestimated diffusion coefficient, and correspondingly shorter diffusion length. However, in this scenario, general tendency still will not be affected.

4.2.5 TTA-UC quenching by PtOEP

In the previous section it was demonstrated that triplet excitons in heavily doped DPA/PMMA films are rather mobile and the triplet exciton diffusion is not the main limiting factor of TTA-UC efficiency. However the absolute value of TTA-UC quantum yield in amorphous films is still very low and does not exceed 1%. It was reported earlier for other TTA-UC systems that some of the singlet excitons generated through the TTA might be quenched *via* singlet-singlet energy transfer back to the triplet exciton sensitizer.[132,133] In this case, even if TTA process would be 100% efficient, the demand of two triplets to form one singlet exciton would still significantly reduce overall efficiency of TTA-UC depending on the singlet-singlet energy transfer rate. The mechanisms by which PtOEP might quench DPA singlets consist of possible exciplex formation between PtOEP and DPA or direct energy transfer from DPA to PtOEP by FRET.[111,132] To clarify the mechanism, fluorescence quantum yield of DPA/PtOEP/PMMA films was measured by directly exciting DPA emitter.

For the minimization of direct excitation of PtOEP the 405 nm excitation wavelength was chosen (Fig. 32). Φ_{FL} as a function of DPA concentration is presented in Figure 43a. Moreover for the comparison, the Φ_{FL} of DPA/PMMA films are shown in the same graph. The Φ_{FL} measurements indicate that in contrast to DPA/PMMA films, the Φ_{FL} of DPA/PtEOP/PMMA films (C_{PtOEP} = 0.05 wt%) negligibly depends on DPA concentration. However, their Φ_{FL} is approximately 4 to 8 times lower as compared to that of DPA/PMMA films. Up to 8-fold reduced Φ_{FL} of DPA in

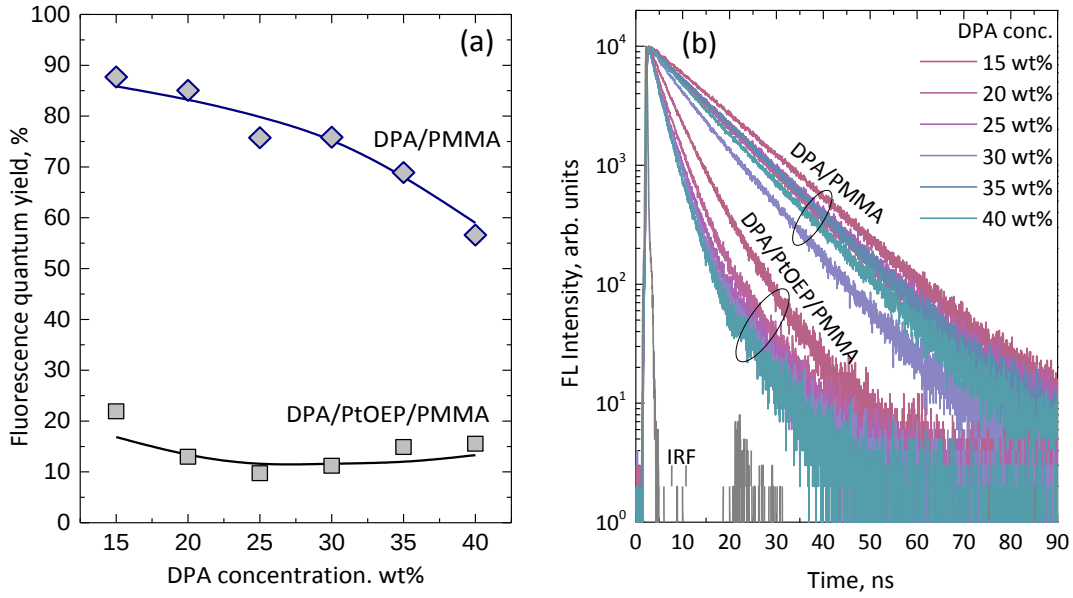

Fig. 43. Fluorescence quantum yield (a) and fluorescence transients (b) of DPA/PMMA and DPA/PtOEP/PMMA (C_{PtOEP}=0.05 wt%) films *vs* DPA concentration. For Φ_{FL} measurements 405 nm excitations was used, whereas for fluorescence transients- 375 nm.

a presence of PtOEP clearly demonstrates significant fluorescence quenching by the sensitizer, even for a very small amount (C_{PtOEP}=0.05 wt%), which is 300-800 times smaller than DPA (15-40 wt%). The fluorescence quenching by the sensitizer is also observed from fluorescence transients, which are depicted in Figure 43b. The incorporation of PtOEP into DPA/PMMA films considerably accelerates

fluorescence decay resulting in fluorescence lifetime drop from approximately 9 to 3 ns.

Strongly decreased Φ_{FL} suggests that PtOEP plays a dual role in these upconverting films, one of which is not as beneficial as populating triplet manifold. Therefore, to unravel the origin of the quenching, the series of UC films with different sensitizer concentration have been fabricated followed by detailed spectroscopic characterization.

The photographs of the series of PMMA samples with 25 wt% of DPA and increasing PtOEP concentration from 0.01 wt% to 0.8 wt% are shown in Figure 44. Under excitation of 532 nm samples showed apparent color change from bright blue to pale purple with increasing PtOEP concentration. This color change corresponds to spectral change of DPA and PtOEP bands (Fig. 45). The increasing amount of PtOEP concentration in DPA/PMMA films, first, resulted in increasing intensity of DPA band, however, at 0.05 wt% maximum intensity was reached and then started to degrade. Whereas, PtOEP band intensity at 647 nm varied just in moderate intensity range.

To assess sensitizer aggregation and related TTA-UC emission quenching, which was essential for poly(para-phenylene vinylene) copolymer doped with palladium (meso - tetraphenyl-tetrabenzo porphyrin) sensitizer,[134] the phosphorescence quantum yield (Φ_{Ph}) measurements were performed. Φ_{Ph} of the PMMA films with PtOEP

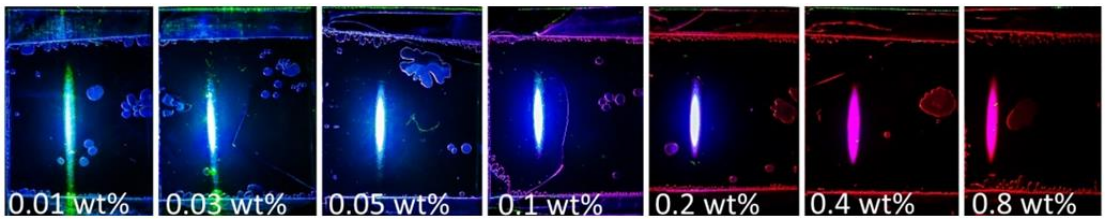

Fig. 44. Photographs of the upconverting films of 25 wt% of DPA and at different PtOEP concentrations (indicated).

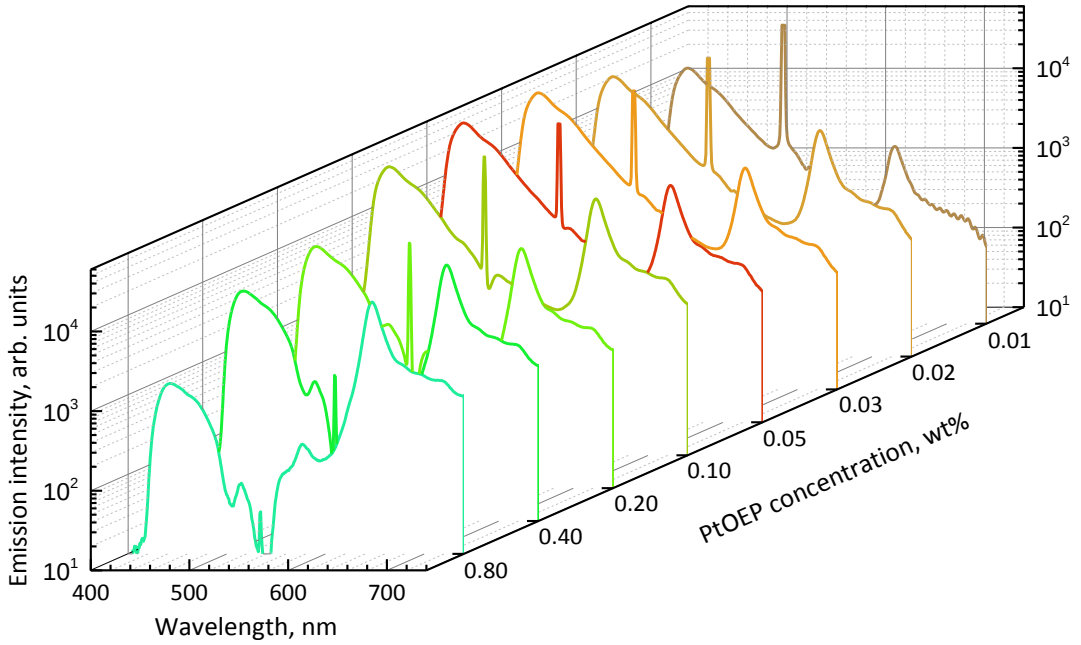

Fig. 45. Emission spectra of the DPA/PtOEP/PMMA films (C_{DPA}= 25 wt%) as a function of sensitizer concentration.

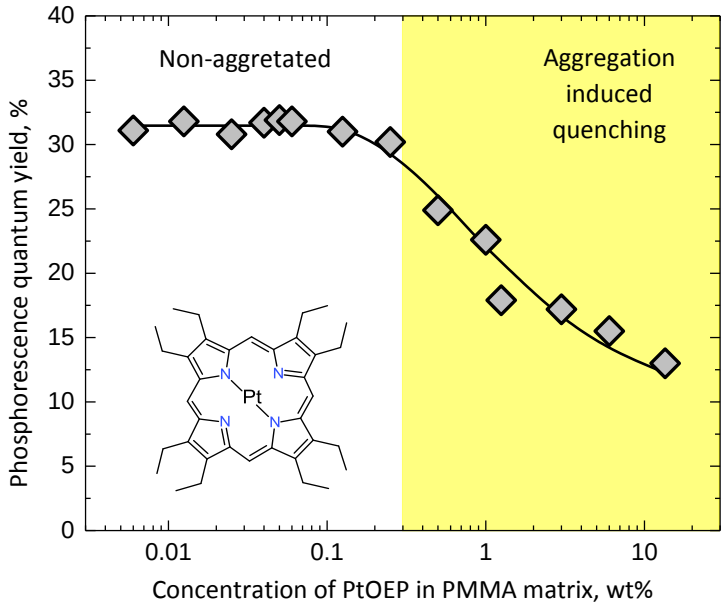

Fig. 46. Phosphorescence quantum yield as a function of PtOEP concentration in PMMA films. The region where PtOEP features aggregation is indicated. Line is a guide for the eyes.

concentration varying from 0.006 to 13.5 wt% is presented in Figure 46. Φ_{Ph} remains constant (31%) and is independent of concentration up to

0.25 wt% of PtOEP. This clearly indicated absence of aggregation of the sensitizer molecules up to this point. Meanwhile, further concentration increase triggers aggregation and diminishes Φ_{Ph}. Introduction of 10 wt% of PtOEP results in 2-fold lower Φ_{Ph}. Thus it can be concluded that TTA-UC intensity decrease up to 0.25 wt% is not related to aggregation of sensitizer molecules. However, at higher PtOEP concentrations, it may contribute to the quenching of TTA-UC. Φ_{FL} and Φ_{UC} of the same upconverting films with different PtOEP concentration were estimated by exciting them with 405 and 532 nm, respectively. The corresponding results are shown in Figure 47. Experimental data show that contrary to TTA-UC intensity (Fig. 45) Φ_{UC} monotonously decreases with increasing sensitizer concentration. Evidently, the initial UC intensity increase is due to increase of the absorbed light, however, further increasing sensitizer concentration results in strong TTA-UC quenching and thus reduces the intensity of TTA-UC (Fig. 45). Generally, Φ_{UC} trend *vs* PtOEP concentration

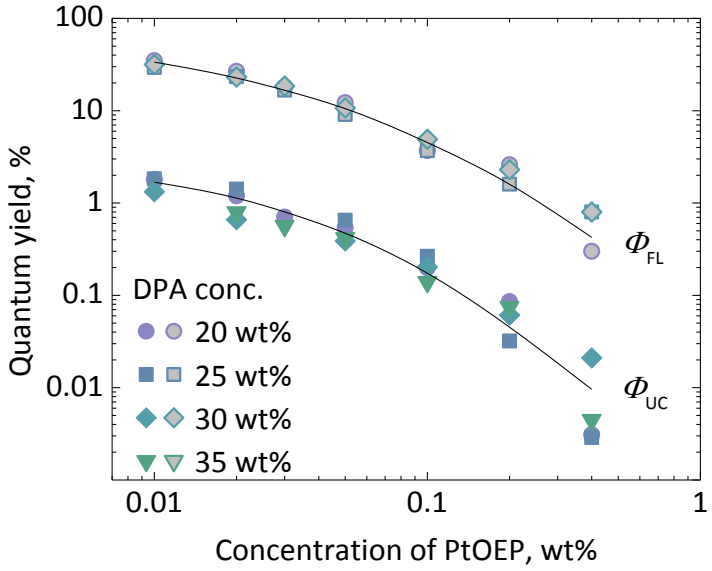

Fig. 47. Fluorescence and TTA-UC quantum yield of DPA/PtOEP/PMMA films as a function of PtOEP concentration at different DPA content (20 wt%, 25 wt%, 30 wt% and 35 wt%). For the fluorescence measurements excitation wavelength of 405 nm was used, for upconversion - 532 nm. Lines are guides for the eyes.

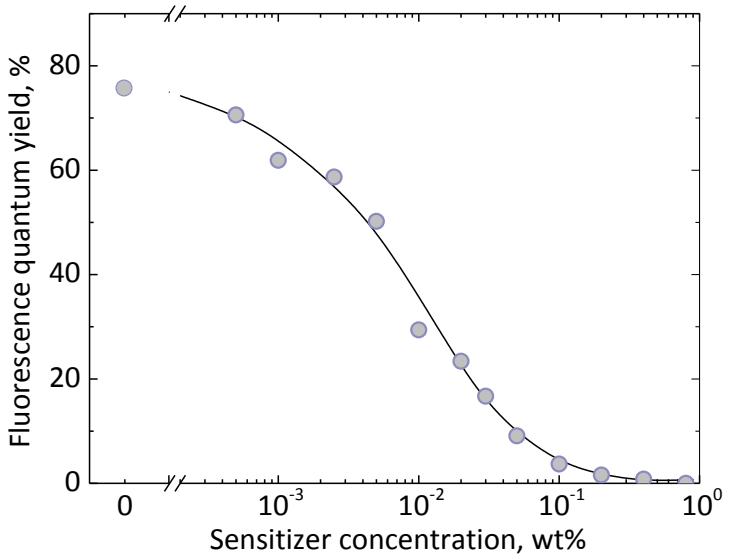

Fig. 48. Fluorescence quantum yield of DPA/PtOEP/PMMA films as a function of PtOEP concentration at fixed DPA content of 25 wt%. DPA was directly excited by 405 nm wavelength.

points out TTA-UC enhancement at the lowest sensitizer content. Therefore, by reducing PtOEP concentration down to 0.01 wt% in the DPA/PtOEP/PMMA films the Φ_{UC} up to 1.8% was achieved. Unfortunately, further reduction of the concentration conditioned very weak UC signal and Φ_{UC} measurements were not reliable. Φ_{UC} and Φ_{FL} displayed in Figure 47 have similar trends *vs* PtOEP concentration even at different DPA content (20 – 35 wt%) suggesting the same quenching mechanism for Φ_{UC} and Φ_{FL}, which is related to singlet exciton quenching.

Φ_{FL} measurements of the DPA/PtOEP/PMMA films with 25 wt% of DPA performed down to very low (0.0005 wt%) PtOEP concentrations (Fig. 48) unambiguously show noticeable fluorescence quenching. For instance, at 0.001 wt% of PtOEP Φ_{FL} drops down by ~20% as compared to that measured in the film without PtOEP (Fig. 48). Obviously, such fluorescence quenching is caused by the sensitizer molecules. However, emergence of the quenching at very low concentrations rules out the possible quenching by the PtOEP aggregation or DPA-PtOEP exciplex

formation. Thus, the most plausible explanation is singlet exciton transfer from DPA to sensitizer by FRET mechanism.

4.2.6 Singlet exciton diffusion in DPA/PMMA and DPA/PtOEP/PMMA films

Strong DPA fluorescence quenching by PtOEP sensitizer in polymeric films has been observed, however, the origins of this quenching are still unclear, and thus, detailed experimental studies are necessary. The feasible way for the DPA singlets to lose its energy is direct energy transfer from DPA to PtOEP by Förster transfer mechanism.[62] For this process to be effective, the distance between the singlet exciton generation and quenching sites should be within the Förster radius, which in organic materials typically is 2-10 nm.[135] Assuming that the singlet excitons might be created in the entire volume of the film, it is reasonable to compare Förster radius with the average distance between the sensitizer molecules, since it is closely connected to the probability of direct Förster energy transfer of singlet excitons. For PMMA films with 0.05 wt% of PtOEP and 25 wt% of DPA the average distance between PtOEP molecules was calculated to be 14 nm and is higher than the typical Förster radius. In this respect, effective energy transfer may occur only if singlet excitons can diffuse toward the porphyrin closer than Förster radius. To verify this statement, singlet exciton diffusion length in the DPA/PMMA films was evaluated. Diffusion of singlet as well as triplet excitons is known to be very sensitive to the intermolecular distance of DPA emitter. Therefore, the PMMA films with different DPA loadings (20 – 35 wt%), which imply variable intermolecular distance between DPA molecules, were fabricated for time-resolved fluorescence bulk-quenching experiments. Additionally, the analogous films containing 0.05 wt% of PtOEP were fabricated to assess the impact of sensitizer to singlet exciton

diffusion. Measured fluorescence transients of these two series of samples with different PCBM concentration allowed estimating relative fluorescence quenching efficiency, which is shown in Figure 49.

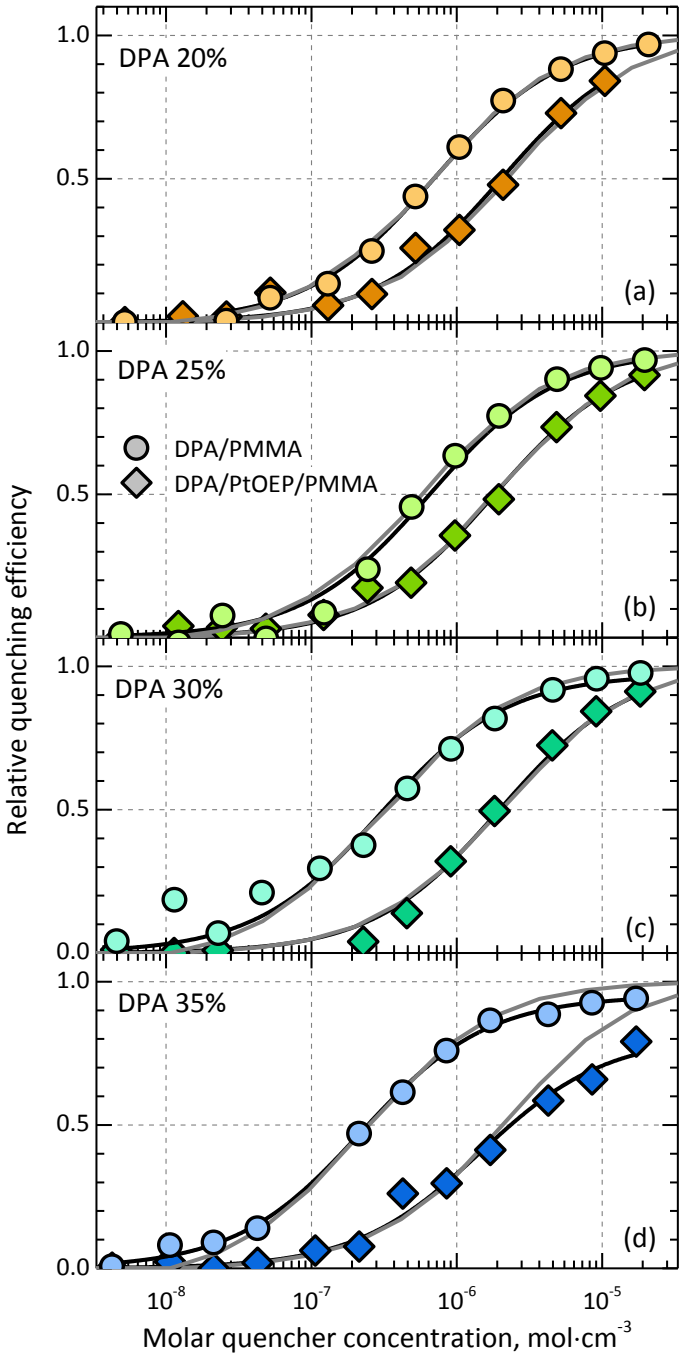

Fig. 49. Relative quenching efficiency *vs* molar quencher concentration of DPA/PMMA and DPA/PtOEP/PMMA films with 0.05% of PtOEP and different DPA load: (a) 20 wt%, (b) 25 wt%, (c) 30 wt%, (d) 35 wt%. Black and grey lines show Stern-Volmer and Monte Carlo fits, respectively.

Measured fluorescence transients and calculated relative quenching efficiencies allow applying Monte Carlo and Stern-Volmer volume quenching methods (Chapter 2) for evaluation of exciton diffusion length.[18,19,33] The main fitting parameters of both models, which gave very similar results, are presented in the Table 6.

Table 6. Monte Carlo and Stern-Volmer fitting parameters for singlet excitons.

DPA wt%	PtOEP wt%	Model	K_{SV} $cm^3 \times mol^{-1}$	k_q $cm^3 mol^{-1} s^{-1}$	D^* $cm^2 \times s^{-1}$	$<\tau>$ ns	L_D^* nm	f_a
DPA/PMMA films								
20	0	MC			2.1×10^{-4}	9.1	24.2	
		SV	1.4×10^{6}	1.6×10^{14}	2.1×10^{-4}		23.9	1.0
25	0	MC			2.8×10^{-4}	8.6	26.6	
		SV	1.5×10^{6}	1.8×10^{14}	2.4×10^{-4}		24.7	1.0
30	0	MC			4.4×10^{-4}	9.7	35.7	
		SV	3.4×10^{6}	3.5×10^{14}	4.6×10^{-4}		36.5	0.9
35	0	MC			6.5×10^{-4}	8.8	41.2	
		SV	4.5×10^{6}	5.2×10^{14}	6.8×10^{-4}		42.5	0.9
DPA/PtOEP/PMMA films								
20	0.05	MC			1.6×10^{-4}	3.7	13.4	
		SV	4.9×10^{5}	1.3×10^{14}	1.8×10^{-4}		14.0	1.0
25	0.05	MC			2.3×10^{-4}	3.3	15.2	
		SV	5.5×10^{5}	1.7×10^{14}	2.2×10^{-4}		14.8	1.0
30	0.05	MC			2.5×10^{-4}	2.8	14.5	
		SV	5.1×10^{5}	1.8×10^{14}	2.4×10^{-4}		14.2	0.9
35	0.05	MC			2.0×10^{-4}	3.1	13.8	
		SV	6.9×10^{5}	2.5×10^{14}	2.9×10^{-4}		16.5	0.8

* calculated assuming reaction radius of 1 nm.

Experimental results revealed that singlet exciton L_D increases from 24 up to 42 nm with increasing DPA loading from 20 to 35 wt%, respectively. Longer singlet exciton L_D at higher DPA concentrations clearly confirms the idea of exciton diffusion sensitivity to the intermolecular distance. Although L_D is enlarged with increasing DPA concentration, obtained L_D of 24 nm in the films with the lowest DPA load is relatively long. Typically singlet exciton L_D in amorphous organics films is only around 10 nm. This unusually long L_D was likely conditioned by the disregarded FRET from DPA to PCBM, i.e. assuming that the reaction

radius corresponds to the physical dimensions of exciton and quencher (1 nm). Since DPA fluorescence (Fig. 33a) overlaps with PCBM absorption (Fig. 1), it is essential to take into account FRET and thus include Förster radius (eq. 10) in the calculations. To calculate molar concentration in PMMA films material's densities of ρ_{PMMA}=1.18 g/cm^3, ρ_{DPA}=1.22 g/cm^3,[131] and ρ_{PCBM}=1.5 g/cm^3,[136] were used. The refraction index was set to 1.6, which is close to n_{PMMA}=1.5 and n_{DPA}=1.65.[137] Dipole orientation factor of κ=0.69 was used. Dipole orientation factor of κ=0.69 was used. Calculated Förster radius was found to slightly depend on the DPA concentration, i.e. it decreased from 5.7 to 5.5 nm with increasing DPA concentration from 20 to 35 wt%, respectively (Table 7).

Figure 50 and Table 7 present L_D as a function of DPA concentration in the PMMA films (with and without PtOEP) calculated with R_0 taken into account. Similarly to the previous calculations, the results show the same L_D trend *vs* DPA concentrations, however the L_D values are ~1.75 times lower (Table 6 and Table 7). These L_D values were

Table 7. Singlet D and L_D of DPA/PMMA films with and without PtOEP calculated by taking into account R_0 in Stern-Volmer model.

DPA	D	L_D	D	L_D	R_0
wt%	cm^2×s^{-1}	nm	cm^2×s^{-1}	nm	nm
	without PtOEP		With PtOEP		
20	6.7×10^{-5}	13.5	5.7×10^{-5}	7.9	5.72
25	7.8×10^{-5}	14.1	7.2×10^{-5}	8.5	5.61
30	1.5×10^{-4}	20.9	7.9×10^{-5}	8.1	5.61
35	2.3×10^{-4}	24.5	1.1×10^{-4}	9.5	5.52

also confirmed by Monte Carlo simulations with extended reaction radius. Interestingly, even with FRET taken into account L_D of up to 25 nm was obtained. This result can be explained on the basis of the work performed by S. M. Menke et al.[25] They have shown that L_D might be substantially extended by diluting molecules into wide bandgap matrix. Such increase of L_D originates from prolonged fluorescence lifetime, increased fluorescence quantum yield and enlarged spectral overlap after dilution.[25]

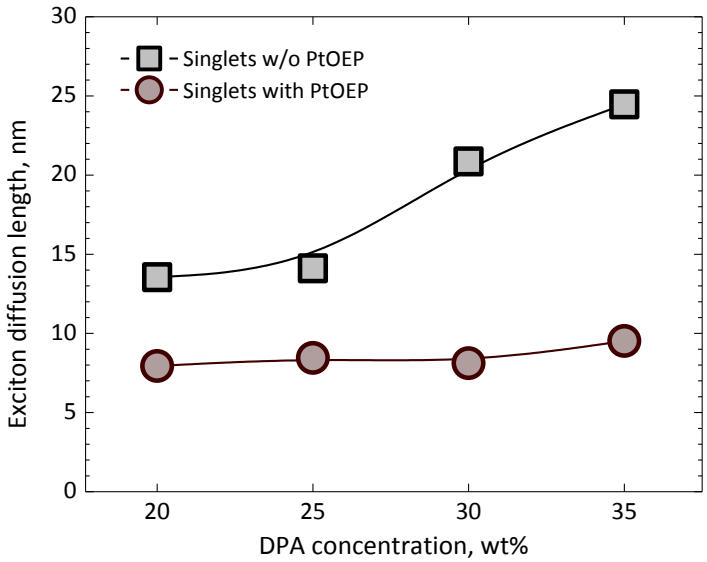

Fig. 50. Singlet exciton diffusion length as a function of DPA concentration in DPA/PMMA films with and without PtOEP sensitizer, taking into account R_0. Lines are guides for the eyes.

In this case, melt-processing technique enabled fabricating upconverting films with minimal concentration quenching, maintaining high Φ_{FL} and long lifetime. Moreover, increased DPA concentration reduced intermolecular distance between DPA, which made possible to

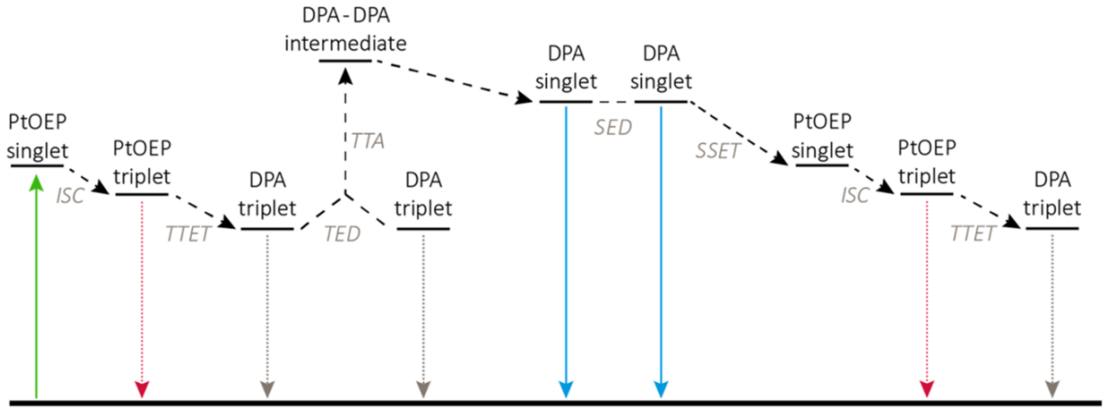

Fig. 51. TTA-UC energy diagram showing the various energy transfer steps between the PtOEP and DPA molecules: intersystem crossing (ISC), triplet-triplet energy transfer (TTET), triplet exciton diffusion (TED), triplet-triplet annihilation (TTA), singlet exciton diffusion (SED) and singlet-singlet energy transfer (SSET).

achieve singlet exciton L_D up to 25 nm (Fig. 49). Meanwhile, the films containing triplet exciton sensitizer showed different L_D behavior as a function of DPA concentration. L_D was found to be at least 1.7 times lower (~8 nm) and almost independent of the DPA concentration as compared to L_D measured in DPA/PMMA films (Fig. 50). Significantly reduced L_D suggests that PtOEP molecules in the films act as singlet exciton traps, severely limiting exciton diffusion length. This implies exciton diffusion towards the sensitizer and more efficient quenching by FRET prior their natural decay (Fig. 51). An example of trap limited exciton diffusion previously has been demonstrated by O. Mikhnenko et al. showing that exciton diffusion length is determined by the concentration of the defect sites.[138,139] The calculated average distance between PtOEP molecules (14 nm) fairly agrees with the double L_D in DPA/PtOEP/PMMA films, what corroborates trap limited exciton diffusion. These findings explain the origins of the c.a. 6-fold fluorescence quantum yield decrease in DPA/PMMA films in a presence of PtOEP sensitizer demonstrated in the section 4.2.5.

4.2.7 The enhancement of TTA-UC efficiency *via* singlet exciton sink approach

Long DPA triplet exciton diffusion length in glassy DPA/PtOEP/PMMA films ensures high probability for the triplets to encounter and subsequently in efficient triplet-triplet annihilation. Unfortunately, long L_D of singlet excitons is undesirable for the upconversion process, since this facilitates exciton back-transfer to PtOEP immediately after the TTA. Straightforward way to avoid such transfer is to reduce PtOEP concentration (Fig. 48), however in this case, the concentration of generated triplet excitons might be too low to attain linear regime, where TTA channel becomes dominant. On the other hand,

very low sensitizer concentration would result in very low light absorption severely limiting TTA-UC applications.

In fact light upconversion in organic molecules without triplet sensitizer has been demonstrated using single component system based on two photon absorption, yet, low two photon absorption cross section and low efficiency strongly impede utilization of such systems.[140,141]

To circumvent aforementioned problems related to large L_D of singlets, the singlet exciton sink approach is proposed. Intentionally introducing singlet exciton traps the problem of singlet energy back-transfer to the sensitizer can be resolved.[93,142,143] Importantly, in this case, singlet exciton traps (sinks) must be highly emissive. Generated *via* TTA singlet excitons featuring long L_D can be trapped by the sinks prior to reaching PtOEP. For the practical use, the singlet sink should possess the following features: i) energy level of the singlet state should be lower than DPA, to ensure energy transfer process into the sink, however, it should not be too low, as the principal of light upconversion is to generate light of higher energy as compared to the excitation wavelength; ii) Φ_{FL} of singlet sink should be as high as possible (desirably 100%); iii) lifetime of the singlet sink should be shorter than DPA singlet to ensure rapid emission; and iv) energy level of the triplet state of the singlet sink should be higher than DPA to avoid triplet exciton depopulation. To comply with the requirements for the singlet sink, the pyreneethynylene derivative (PE) was chosen (Fig. 52).[144] The lowest absorption band of this compound is at

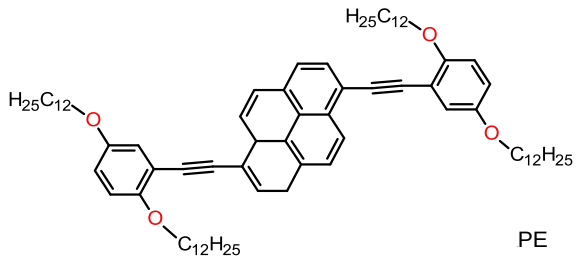

Fig. 52. Chemical structure of pyrene derivative employed as a singlet sink in light upconverting PMMA films.

435 nm,[144] which is very close to UC emission maximum of DPA (437 nm, section 4.2.2) (Fig. 53a). This ensures efficient singlet energy transfer from the DPA to the PE. The emission of the singlet sink has a maximum at 449 nm (Fig. 53a) and is redshifted as compared to the emission of DPA by approximately 12 nm. Thus, singlet energy level of PE is lower than DPA by ~75 meV and even at room temperature, the singlet excitons should be trapped at the PE sites. Φ_{FL} of 75% for PE was recorded in dilute (10^{-5} M) dichloromethane solutions[144] and slightly lower (69%) in melt-processed PMMA films at 0.01 wt% of PE.

Figure 53b depicts fluorescence decay at fluorescence maximum, which exhibit mono-exponential decay with time constant of 1.82 ns. 5 times faster fluorescence decay of PE as compared to that of DPA (Fig. 43, Table 6) ensures fast radiative relaxation of trapped excitons, low probability for energy back-transfer to DPA or exciton accumulation at sink sites.

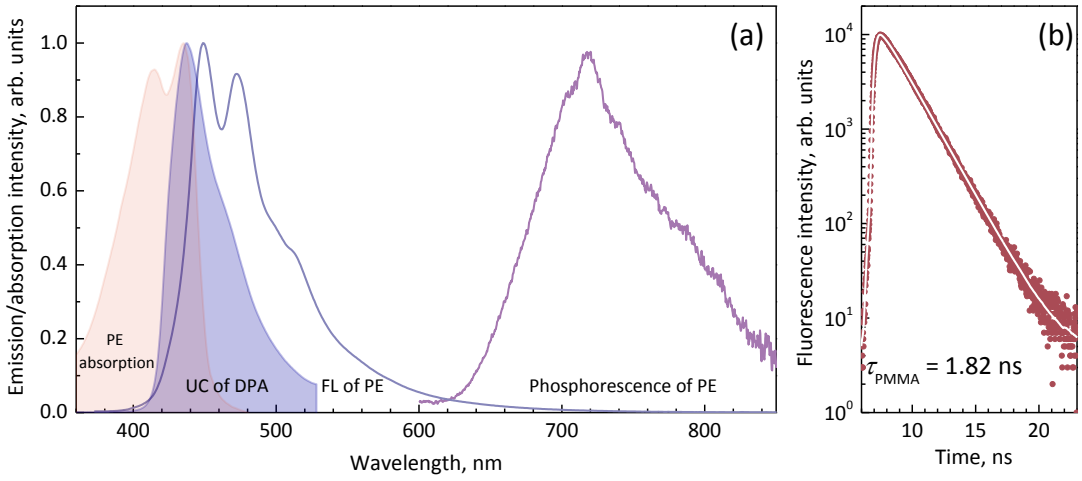

Fig. 53. Fluorescence and phosphorescence spectra (a) and fluorescence decay profile (b) of singlet sink in PMMA (C_{sink}=0.01 wt%). Also, absorption spectra of PE in THF at 10^{-5}M and UC of DPA/PtOEP/PMMA (C_{DPA}=25 wt%, C_{PtOEP}=0.01 wt%) are displayed in (a). Phosphorescence spectrum of PE in PMMA was obtained at 10K, at 0.15 wt% of PE.

Phosphorescence spectrum of the singlet sink is shown in Figure 53a. Phosphorescence was measured at 10 K in PMMA with slightly higher concentration of PE (0.15 wt%) to have sufficient intensity of the phosphorescence signal. The data revealed that the onset of PE phosphorescence is at ~630 nm. As compared to the phosphorescence of DPA at 685 nm, [145] the triplet energy level of PE is ~150 meV higher than that of DPA. This is important as it prevents triplet exciton transfer from DPA to PE.

To verify the proposed strategy of singlet exciton trapping, PMMA films containing 25 wt% of DPA, 0.01 wt% of PtOEP and variable concentration (0.001 – 1 wt%) of PE were fabricated. A typical emission spectrum of the films with 0.01 wt% of PE is shown in Figure 54. To elucidate the origin of TTA-UC emission in such film, UC spectrum of the films without singlet sink and fluorescence spectrum of the singlet sink is also displayed in Figure 54. The comparison of the emission spectra of DPA and PE, shows that UC emission originates from both molecular species. Therefore, to evaluate the contribution of emission of each species to the overall TTA-UC emission of DPA/PtOEP/PMMA doped with singlet sink film, the UC of DPA/PtOEP/PMMA and fluorescence of PE/PMMA was summed at appropriate ratios to reconstruct TTA-UC emission of DPA/PtOEP/PMMA:PE film (Fig. 54). Best fit of UC signal of DPA/PtOEP/PMMA:PE film was achieved with peak intensity coefficients of 0.775 and 0.325, respectively for DPA and PE emission spectra. While the integrated intensity of DPA and PE emission spectra gives a ratio of 2:1, which means that 1/3 of UC emission of the film with singlet sink originates from PE molecules.

To determine optimal singlet sink concentration in upconverting films, Φ_{UC} as a function of PE concentration in DPA/PtOEP/PMMA:PE films was measured. Φ_{UC} of the DPA/PtOEP/PMMA:PE films with 25 wt% of DPA, 0.01 wt% of PtOEP and

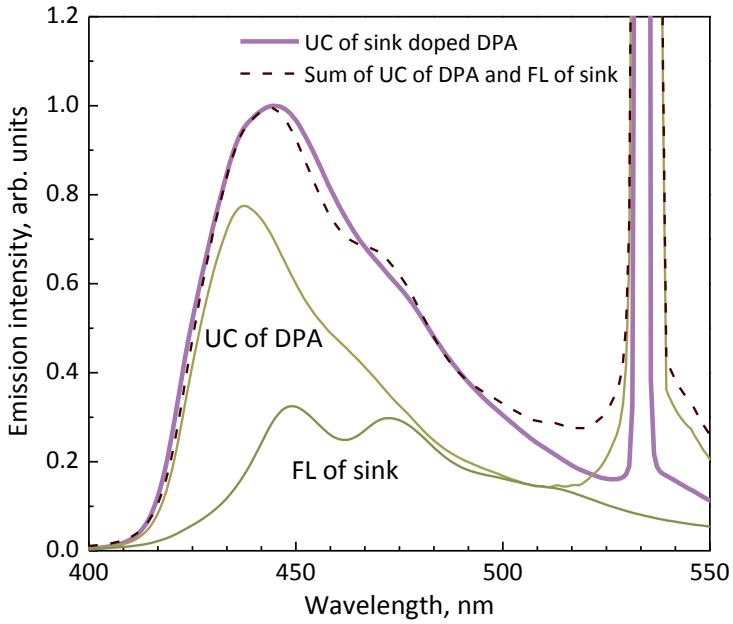

Fig. 54. Fluorescence spectrum of the singlet sink in the PMMA at 0.01 wt%, upconversion spectra of DPA/PtOEP/PMMA (C_{DPA}=25 wt%, C_{PtOEP}=0.01 wt%) with and without singlet sink (C_{sink}=0.01 wt%) and sum of upconversion of DPA/PtOEP/PMMA and fluorescence of singlet sink at the shown spectral intensities.

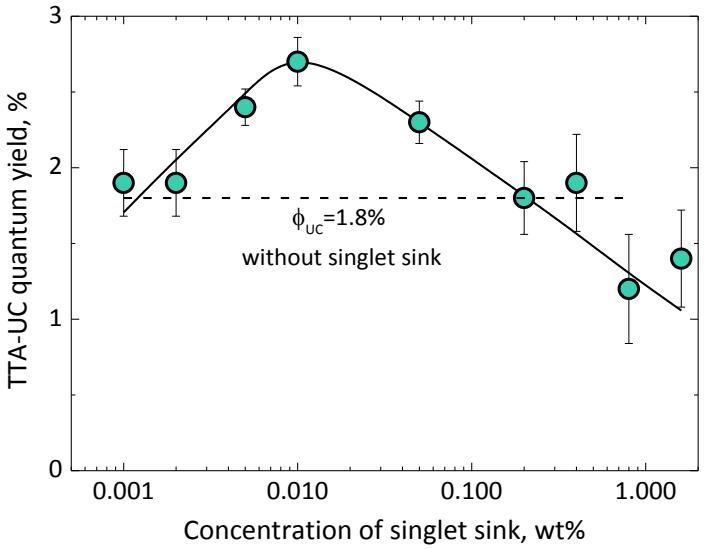

Fig. 55. Upconversion quantum yield in DPA/PtOEP/PMMA (C_{DPA}=25 wt%, C_{PtOEP}=0.01 wt%) as a function of singlet sink concentration. Note that theoretical maximum UC efficiency is 50%. Line is a guide for the eyes.

different PE concentration (0.001 – 1 wt%) is shown in Figure 55. Φ_{UC} data show only minor quantum yield increase in a presence of PE at the lowest

concentration as compared to the efficiency of the films without PE (Fig. 47), further increase of the concentration up to 0.01 wt%, i.e. the optimal concentration of PE enhances TTA-UC efficiency up to 2.7%. Beyond this point Φ_{UC} starts to degrade presumably due to PE aggregation. It is likely that for this particular singlet sink, which possess relatively flat molecular structure, fluorescence concentration quenching is responsible for this Φ_{UC} decrease. It was demonstrated before that PE does not show any glass transition, however well pronounced melting point at 112°C was observed.[144] Nevertheless, 1.5-fold higher TTA-UC quantum yield achieved at 0.01 wt% concentration of the singlet sink was recorded, which up to date is among the highest efficiencies reported so far in amorphous solid films.[146] The analysis of the spectral composition of TTA-UC spectrum of the films with singlet sink shows identical 1.5-fold increase in integrated emission intensity as compared to TTA-UC of the films without singlet sink (Φ_{UC}=1.8%). This explains that the enhancement of Φ_{UC} stems solely from the emission of singlet sink, which is being populated by the singlet excitons of DPA before they are quenched at PtOEP sites. Taking into

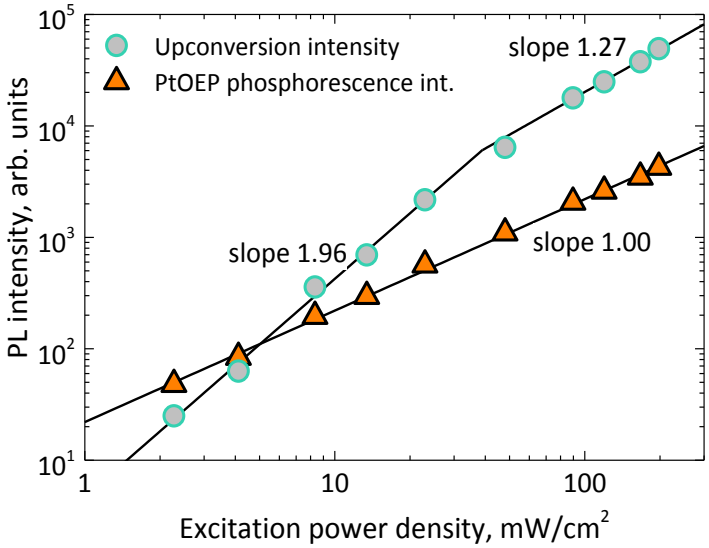

Fig. 56. TTA-UC and PtOEP phosphorescence intensity as a function of excitation power density (λ_{ex} = 532 nm) of the film DPA/PtOEP/sink/PMMA (C_{DPA} = 25 wt%, C_{PtOEP} = 0.01 wt%, C_{sink} = 0.01 wt%).

account that the presence of 0.01 wt% of PtOEP reduces Φ_{FL} of DPA by a factor of 2.5 (Fig. 48), Φ_{UC} of 1.8%×2.5=4.5% should be expected in the case PE could collect all the DPA singlets. Enhancement of Φ_{UC} only up to 2.7% indicated that exciton trapping at the sink sites is not completely efficient.

TTA-UC and residual PtOEP phosphorescence dependence on the excitation power density of the best performing film containing singlet sink is shown in Figure 56. The threshold at which TTA-UC dependence switches from quadratic to linear is estimated to be I_{th} = 39 mW/cm^2. This value being very close to the I_{th} values of the films without singlet sink indicates that singlet sink neither influences TTA process nor triplet exciton manifold. In the case excitons could populate PE triplet state the I_{th} should be noticeably reduced, due to contribution of PE to TTA and subsequently TTA mediated light upconversion.

4.2.8 Summary

The present study of a light upconverting model system consisting of an emitter-sensitizer pair (DPA-PtOEP) dispersed in glassy PMMA films allowed to investigate the factors limiting TTA-UC efficiency. The processes of fluorescence concentration quenching, triplet-triplet energy transfer, upconversion quenching by PtOEP, singlet and triplet exciton diffusion were investigated in great detail for evaluation of their contribution to TTA-UC efficiency.

High Dexter-type triplet energy transfer efficiency from the PtOEP to DPA (η_{TTET} >75% for DPA above 25 wt%), which were estimated from accelerated PtOEP phosphorescence decay measurements with increasing DPA concentration confirmed TTET process to be fairly efficient. High Φ_{FL} and minor concentration quenching of emitter even at

high loadings (up to 40 wt% in PMMA) achieved *via* melt-processing technique also proved to contribute only mildly to UC efficiency losses.

The special focus was placed on triplet exciton diffusion since the latter had been thought to be the major source of loss. The triplet exciton diffusion, i.e. diffusion coefficient and diffusion length in upconverting polymer glasses were evaluated by a time-resolved photoluminescence bulk-quenching technique followed by Stern-Volmer-type quenching analysis of obtained TTA-UC experimental data. The analysis has shown that continuous increase of DPA concentration from 20 wt% to 35 wt% in DPA/PtOEP/PMMA films causes monotonous enhancement of triplet L_D from 22 nm to 60 nm. However, increasing L_D does not result in steadily enhanced Φ_{UC}, which rapidly degrades above 25 wt% of DPA. This finding clearly implies the triplet exciton diffusion to be the non-governing loss mechanism of TTA-UC efficiency and points to alternate loss channel. Importantly, the accelerated UC intensity decay with increasing DPA content occurring on a millisecond time-scale unambiguously indicated that the dominant quenching mechanism is nevertheless governed by the triplet excitons in DPA. Moreover, this major loss channel is obviously facilitated by enhanced diffusion of long-lived triplets with increasing DPA content, thus causing increased probability for them to reach non-radiative decay sites.

Fluorescence quantum yield measurements revealed significant DPA fluorescence quenching by PtOEP even at low sensitizer concentrations. It was found that this quenching is determined by the effective singlet exciton back-transfer from DPA to PtOEP. Singlet exciton diffusion length in upconverting polymer glasses in a presence and absence of triplet sensitizer were evaluated by a time-resolved photoluminescence bulk-quenching technique followed by Stern-Volmer quenching analysis and additionally by Monte Carlo simulations. Experimental data revealed that, as in the case of triplet excitons, in the

absence of sensitizer the singlet exciton diffusion length effectively lengthens from 14 nm up to 25 nm with increasing concentration of the emitter from 20 wt% to 35 wt% in the PMMA films. Meanwhile in a presence of PtOEP L_D of the singlet excitons no longer depends on the concentration of the emitter. Insensitivity of L_D on emitter concentration signifies trap-limited exciton diffusion with triplet sensitizer acting as a singlet exciton trap. Reduction of the triplet sensitizer concentration down to 0.01 wt% resulted in reduced probability for the singlet excitons to be quenched at PtOEP site immediately after the TTA and increased TTA-UC efficiency up to 1.8%. The utilization of singlet sink approach with highly fluorescent pyreneethynylene molecules allowed trapping long L_D possessing singlet excitons prior to their quenching at PtOEP sites. The introduction of singlet sink at an optimal concentration (0.01 wt%) enhanced the integrated TTA-UC intensity by 50% and enabled to improve TTA-UC efficiency up to 2.7% in a glassy PMMA film.

5 Conclusions

1. Exciton is found to be localized on one of the sidearms of the TPA compounds independent of their number. Singlet exciton diffusion length in the films of TPA derivatives is improved from 3 nm to 12 nm with increasing number of phenylethenyl or naphthalimide sidearms. The improvement is a result of a dense network of the sidearms formed in the solid TPA film. Enlarged L_D well correlates with enhanced fluorescence quenching in the neat films of TPA compounds with higher number of sidearms. The approach for tuning exciton diffusion length is very attractive from the perspective of material design for the application in organic optoelectronic devices.

2. Triplet exciton diffusion length evaluated by measuring TTA-UC signal increases from 22 nm to 60 nm with increasing DPA content from 20 wt% to 35 wt%. Triplet L_D higher than the average distance between sensitizer molecules (14 nm) implies that triplet exciton diffusion is not the main limiting factor of TTA-UC efficiency in the solid films. However, decreasing Φ_{UC} with increasing emitter content above a certain point indicates diffusion-enhanced non-radiative decay of triplet excitons. These findings suggest that for further enhancement of light upconversion efficiency in the solid films the reduction of triplet exciton quenching is necessary.

3. Singlet exciton diffusion length increases from 14 nm to 25 nm with increasing DPA content from 20 wt% to 35 wt% in the films without triplet sensitizer. Singlet L_D longer than average distance between PtOEP molecules (14 nm) leads to effective fluorescence quenching by FRET to the triplet sensitizer and reduces upconversion efficiency.

In this case, L_D of ~8 nm is found in the films with 0.05 wt% of PtOEP and is virtually independent of the DPA content. The utilization of singlet sink approach with highly fluorescent sink allows trapping long L_D possessing singlet excitons prior to their quenching at PtOEP sites and improves TTA-UC efficiency by a factor of 1.5 (up to 2.7%) in a glassy PMMA film.

6 References

(1) *Organic Optoelectronics*; Hu, W., Ed.; Wiley-VCH Verlag GmbH & Co. KGaA: Weinheim, Germany, 2013.
(2) *Organic Electronics: Materials, Manufacturing and Applications*; Klauk, H., Ed.; Wiley-VCH: Weinheim, 2006.
(3) *Organic Electronics II: More Materials and Applications*; Klauk, H., Ed.; Wiley-VCH-Verl: Weinheim, 2012.
(4) Takeda, Y.; Hayasaka, K.; Shiwaku, R.; Yokosawa, K.; Shiba, T.; Mamada, M.; Kumaki, D.; Fukuda, K.; Tokito, S. Fabrication of Ultra-Thin Printed Organic TFT CMOS Logic Circuits Optimized for Low-Voltage Wearable Sensor Applications. *Sci. Rep.* **2016**, *6*.
(5) Sasabe, H.; Kido, J. Development of High Performance OLEDs for General Lighting. *J. Mater. Chem. C* **2013**, *1* (9), 1699–1707.
(6) OLED Info | The OLED Experts https://www.oled-info.com/ (accessed Jun 2, 2017).
(7) Torsi, L.; Magliulo, M.; Manoli, K.; Palazzo, G. Organic Field-Effect Transistor Sensors: A Tutorial Review. *Chem. Soc. Rev.* **2013**, *42* (22), 8612–8628.
(8) Borsenberger, P. M.; Weiss, D. S. *Organic Photoreceptors for Xerography*; Marcel Dekker: New York, 1998.
(9) Hedley, G. J.; Ruseckas, A.; Samuel, I. D. W. Light Harvesting for Organic Photovoltaics. *Chem. Rev.* **2017**, *117* (2), 796–837.
(10) Ostroverkhova, O. Organic Optoelectronic Materials: Mechanisms and Applications. *Chem. Rev.* **2016**, *116* (22), 13279–13412.
(11) Heliatek – The future is light http://www.heliatek.com/en/ (accessed Jun 2, 2017).
(12) Terao, Y.; Sasabe, H.; Adachi, C. Correlation of Hole Mobility, Exciton Diffusion Length, and Solar Cell Characteristics in Phthalocyanine/Fullerene Organic Solar Cells. *Appl. Phys. Lett.* **2007**, *90* (10), 103515.
(13) Schulze, T. F.; Schmidt, T. W. Photochemical Upconversion: Present Status and Prospects for Its Application to Solar Energy Conversion. *Energy Environ. Sci.* **2015**, *8* (1), 103–125.
(14) Baluschev, S.; Miteva, T.; Yakutkin, V.; Nelles, G.; Yasuda, A.; Wegner, G. Up-Conversion Fluorescence: Noncoherent Excitation by Sunlight. *Phys. Rev. Lett.* **2006**, *97* (14), 143903.
(15) Monguzzi, A.; Tubino, R.; Hoseinkhani, S.; Campione, M.; Meinardi, F. Low Power, Non-Coherent Sensitized Photon up-Conversion: Modelling and Perspectives. *Phys. Chem. Chem. Phys.* **2012**, *14* (13), 4322.
(16) Dzebo, D.; Börjesson, K.; Gray, V.; Moth-Poulsen, K.; Albinsson, B. Intramolecular Triplet–Triplet Annihilation Upconversion in 9,10-Diphenylanthracene Oligomers and Dendrimers. *J. Phys. Chem. C* **2016**, *120* (41), 23397–23406.
(17) Gregg, B. A.; Sprague, J.; Peterson, M. W. Long-Range Singlet Energy Transfer in Perylene Bis(phenethylimide) Films. *J. Phys. Chem. B* **1997**, *101* (27), 5362–5369.

(18) Mikhnenko, O. V.; Azimi, H.; Scharber, M.; Morana, M.; Blom, P. W. M.; Loi, M. A. Exciton Diffusion Length in Narrow Bandgap Polymers. *Energy Environ. Sci.* **2012**, *5* (5), 6960–6965.
(19) Hsu, H.-Y.; Vella, J. H.; Myers, J. D.; Xue, J.; Schanze, K. S. Triplet Exciton Diffusion in Platinum Polyyne Films. *J. Phys. Chem. C* **2014**, *118* (42), 24282–24289.
(20) Shaw, P. E.; Ruseckas, A.; Peet, J.; Bazan, G. C.; Samuel, I. D. W. Exciton–Exciton Annihilation in Mixed-Phase Polyfluorene Films. *Adv. Funct. Mater.* **2010**, *20* (1), 155–161.
(21) Tabachnyk, M.; Ehrler, B.; Bayliss, S.; Friend, R. H.; Greenham, N. C. Triplet Diffusion in Singlet Exciton Fission Sensitized Pentacene Solar Cells. *Appl. Phys. Lett.* **2013**, *103* (15), 153302.
(22) Yang, C. L.; Tang, Z. K.; Ge, W. K.; Wang, J. N.; Zhang, Z. L.; Jian, X. Y. Exciton Diffusion in Light-Emitting Organic Thin Films Studied by Photocurrent Spectra. *Appl. Phys. Lett.* **2003**, *83* (9), 1737–1739.
(23) Kroeze, J. E.; Savenije, T. J.; Vermeulen, M. J. W.; Warman, J. M. Contactless Determination of the Photoconductivity Action Spectrum, Exciton Diffusion Length, and Charge Separation Efficiency in Polythiophene-Sensitized TiO2 Bilayers. *J. Phys. Chem. B* **2003**, *107* (31), 7696–7705.
(24) Irkhin, P.; Biaggio, I. Direct Imaging of Anisotropic Exciton Diffusion and Triplet Diffusion Length in Rubrene Single Crystals. *Phys. Rev. Lett.* **2011**, *107* (1), 017402.
(25) Menke, S. M.; Luhman, W. A.; Holmes, R. J. Tailored Exciton Diffusion in Organic Photovoltaic Cells for Enhanced Power Conversion Efficiency. *Nat. Mater.* **2013**, *12* (2), 152–157.
(26) Lin, J. D. A.; Mikhnenko, O. V.; Chen, J.; Masri, Z.; Ruseckas, A.; Mikhailovsky, A.; Raab, R. P.; Liu, J.; Blom, P. W. M.; Loi, M. A.; et al. Systematic Study of Exciton Diffusion Length in Organic Semiconductors by Six Experimental Methods. *Mater. Horiz.* **2014**, *1* (2), 280–285.
(27) Mikhnenko, O. V. *Dynamics of Singlet and Triplet Excitons in Organic Semiconductors*; Groningen, 2012.
(28) Mikhnenko, O. V.; Cordella, F.; Sieval, A. B.; Hummelen, J. C.; Blom, P. W. M.; Loi, M. A. Temperature Dependence of Exciton Diffusion in Conjugated Polymers. *J. Phys. Chem. B* **2008**, *112* (37), 11601–11604.
(29) Fŏrster, T. 10th Spiers Memorial Lecture. Transfer Mechanisms of Electronic Excitation. *Discuss. Faraday Soc.* **1959**, *27* (0), 7–17.
(30) Maksimov, M. Z.; Rozman, I. M. On Energy Transfer in Solid Solutions. *Opt. Spectrosc.* **1962**, *12*, 337.
(31) Powell, R. C.; Soos, Z. G. Singlet Exciton Energy Transfer in Organic Solids. *J. Lumin.* **1975**, *11* (1–2), 1–45.
(32) Lunt, R. R.; Giebink, N. C.; Belak, A. A.; Benziger, J. B.; Forrest, S. R. Exciton Diffusion Lengths of Organic Semiconductor Thin Films Measured by Spectrally Resolved Photoluminescence Quenching. *J. Appl. Phys.* **2009**, *105* (5), 053711.
(33) Chen, J.; Lin, J. D. A.; Nguyen, T.-Q. Towards a Unified Macroscopic Description of Exciton Diffusion in Organic Semiconductors. *Commun. Comput. Phys.* **2016**, *20* (3), 754–772.
(34) Cheng, Y. Y.; Fückel, B.; Khoury, T.; Clady, R. G. C. R.; Tayebjee, M. J. Y.; Ekins-Daukes, N. J.; Crossley, M. J.; Schmidt, T. W. Kinetic Analysis of

Photochemical Upconversion by Triplet–Triplet Annihilation: Beyond Any Spin Statistical Limit. *J. Phys. Chem. Lett.* **2010**, *1* (12), 1795–1799.
(35) Köhler, A.; Bässler, H. Triplet States in Organic Semiconductors. *Mater. Sci. Eng. R Rep.* **2009**, *66* (4–6), 71–109.
(36) Adams, M. J.; Highfield, J. G.; Kirkbright, G. F. Determination of Absolute Fluorescence Quantum Efficiency of Quinine Bisulfate in Aqueous Medium by Optoacoustic Spectrometry. *Anal. Chem.* **1977**, *49* (12), 1850–1852.
(37) de Mello, J. C.; Wittmann, H. F.; Friend, R. H. An Improved Experimental Determination of External Photoluminescence Quantum Efficiency. *Adv. Mater.* **1997**, *9* (3), 230–232.
(38) Iwan, A.; Sek, D. Polymers with Triphenylamine Units: Photonic and Electroactive Materials. *Prog. Polym. Sci.* **2011**, *36* (10), 1277–1325.
(39) Agarwala, P.; Kabra, D. A Review on Triphenylamine (TPA) Based Organic Hole Transport Materials (HTMs) for Dye Sensitized Solar Cells (DSSCs) and Perovskite Solar Cells (PSCs): Evolution and Molecular Engineering. *J. Mater. Chem. A* **2017**, *5* (4), 1348–1373.
(40) Rybakiewicz, R.; Zagorska, M.; Pron, A. Triphenylamine-Based Electroactive Compounds: Synthesis, Properties and Application to Organic Electronics. *Chem. Pap.* **2017**, *71* (2), 243–268.
(41) Duan, L.; Hou, L.; Lee, T.-W.; Qiao, J.; Zhang, D.; Dong, G.; Wang, L.; Qiu, Y. Solution Processable Small Molecules for Organic Light-Emitting Diodes. *J. Mater. Chem.* **2010**, *20* (31), 6392–6407.
(42) Tao, Y.; Yang, C.; Qin, J. Organic Host Materials for Phosphorescent Organic Light-Emitting Diodes. *Chem. Soc. Rev.* **2011**, *40* (5), 2943–2970.
(43) Yen, H.-J.; Lin, H.-Y.; Liou, G.-S. Novel Starburst Triarylamine-Containing Electroactive Aramids with Highly Stable Electrochromism in Near-Infrared and Visible Light Regions. *Chem. Mater.* **2011**, *23* (7), 1874–1882.
(44) Zhao, Z.; Li, Z.; Lam, J. W. Y.; Maldonado, J.-L.; Ramos-Ortiz, G.; Liu, Y.; Yuan, W.; Xu, J.; Miao, Q.; Tang, B. Z. High Hole Mobility of 1,2-bis[4′-(Diphenylamino)biphenyl-4-Yl]-1,2-Diphenylethene in Field Effect Transistor. *Chem. Commun.* **2011**, *47* (24), 6924–6926.
(45) Yasuda, T.; Shinohara, Y.; Matsuda, T.; Han, L.; Ishi-i, T. Improved Power Conversion Efficiency of Bulk-Heterojunction Organic Solar Cells Using a Benzothiadiazole–triphenylamine Polymer. *J. Mater. Chem.* **2012**, *22* (6), 2539–2544.
(46) Metri, N.; Sallenave, X.; Plesse, C.; Beouch, L.; Aubert, P.-H.; Goubard, F.; Chevrot, C.; Sini, G. Processable Star-Shaped Molecules with Triphenylamine Core as Hole-Transporting Materials: Experimental and Theoretical Approach. *J. Phys. Chem. C* **2012**, *116* (5), 3765–3772.
(47) Choi, H.; Park, S.; Paek, S.; Ekanayake, P.; Khaja Nazeeruddin, M.; Ko, J. Efficient Star-Shaped Hole Transporting Materials with Diphenylethenyl Side Arms for an Efficient Perovskite Solar Cell. *J. Mater. Chem. A* **2014**, *2* (45), 19136–19140.
(48) Malinauskas, T.; Tomkute-Luksiene, D.; Daskeviciene, M.; Jankauskas, V.; Juska, G.; Gaidelis, V.; Arlauskas, K.; Getautis, V. One Small Step in Synthesis, a Big Leap in Charge Mobility: Diphenylethenyl Substituted Triphenylamines. *Chem. Commun.* **2011**, *47* (27), 7770–7772.
(49) Malinauskas, T.; Daskeviciene, M.; Bubniene, G.; Petrikyte, I.; Raisys, S.; Kazlauskas, K.; Gaidelis, V.; Jankauskas, V.; Maldzius, R.; Jursenas, S.; et al.

Phenylethenyl-Substituted Triphenylamines: Efficient, Easily Obtainable, and Inexpensive Hole-Transporting Materials. *Chem. – Eur. J.* **2013**, *19* (44), 15044–15056.
(50) Cekaviciute, M.; Simokaitiene, J.; Jankauskas, V.; Raisys, S.; Kazlauskas, K.; Jursenas, S.; Grazulevicius, J. V. Structure-Properties Relationship of Phenylethenyl-Substituted Triphenylamines. *J. Phys. Chem. C* **2013**, *117* (16), 7973–7980.
(51) Reghu, R. R.; Simokaitiene, J.; Grazulevicius, J. V.; Raisys, S.; Kazlauskas, K.; Jursenas, S.; Jankauskas, V.; Reina, A. Synthesis and Properties of Hole-Transporting Triphenylamine-Derived Dendritic Compounds. *Dyes Pigments* **2015**, *115*, 135–142.
(52) Gudeika, D.; Michaleviciute, A.; Grazulevicius, J. V.; Lygaitis, R.; Grigalevicius, S.; Jankauskas, V.; Miasojedovas, A.; Jursenas, S.; Sini, G. Structure Properties Relationship of Donor–Acceptor Derivatives of Triphenylamine and 1,8-Naphthalimide. *J. Phys. Chem. C* **2012**, *116* (28), 14811–14819.
(53) Gudeika, D.; Grazulevicius, J. V.; Sini, G.; Bucinskas, A.; Jankauskas, V.; Miasojedovas, A.; Jursenas, S. New Derivatives of Triphenylamine and Naphthalimide as Ambipolar Organic Semiconductors: Experimental and Theoretical Approach. *Dyes Pigments* **2014**, *106*, 58–70.
(54) Halls, J. J. M.; Walsh, C. A.; Greenham, N. C.; Marseglia, E. A.; Friend, R. H.; Moratti, S. C.; Holmes, A. B. Efficient Photodiodes from Interpenetrating Polymer Networks. *Nature* **1995**, *376* (6540), 498–500.
(55) Peumans, P.; Yakimov, A.; Forrest, S. R. Small Molecular Weight Organic Thin-Film Photodetectors and Solar Cells. *J. Appl. Phys.* **2003**, *93* (7), 3693–3723.
(56) Scully, S. R.; McGehee, M. D. Effects of Optical Interference and Energy Transfer on Exciton Diffusion Length Measurements in Organic Semiconductors. *J. Appl. Phys.* **2006**, *100* (3), 034907.
(57) Shaw, P. E.; Ruseckas, A.; Samuel, I. D. W. Exciton Diffusion Measurements in Poly(3-Hexylthiophene). *Adv. Mater.* **2008**, *20* (18), 3516–3520.
(58) Najafov, H.; Lee, B.; Zhou, Q.; Feldman, L. C.; Podzorov, V. Observation of Long-Range Exciton Diffusion in Highly Ordered Organic Semiconductors. *Nat. Mater.* **2010**, *9* (11), 938–943.
(59) Luhman, W. A.; Holmes, R. J. Investigation of Energy Transfer in Organic Photovoltaic Cells and Impact on Exciton Diffusion Length Measurements. *Adv. Funct. Mater.* **2011**, *21* (4), 764–771.
(60) Sun, Y.; Welch, G. C.; Leong, W. L.; Takacs, C. J.; Bazan, G. C.; Heeger, A. J. Solution-Processed Small-Molecule Solar Cells with 6.7% Efficiency. *Nat. Mater.* **2012**, *11* (1), 44–48.
(61) Ruseckas, A.; Shaw, P. E.; Samuel, I. D. W. Probing the Nanoscale Phase Separation in Binary Photovoltaic Blends of poly(3-Hexylthiophene) and Methanofullerene by Energy Transfer. *Dalton Trans.* **2009**, No. 45, 10040–10043.
(62) Ward, A. J.; Ruseckas, A.; Samuel, I. D. W. A Shift from Diffusion Assisted to Energy Transfer Controlled Fluorescence Quenching in Polymer–Fullerene Photovoltaic Blends. *J. Phys. Chem. C* **2012**, *116* (45), 23931–23937.
(63) Kirkpatrick, J.; Keivanidis, P. E.; Bruno, A.; Ma, F.; Haque, S. A.; Yarstev, A.; Sundstrom, V.; Nelson, J. Ultrafast Transient Optical Studies of Charge Pair

Generation and Recombination in Poly-3-Hexylthiophene(P3ht):[6,6]Phenyl C61 Butyric Methyl Acid Ester (PCBM) Blend Films. *J. Phys. Chem. B* **2011**, *115* (51), 15174–15180.
(64) Masri, Z.; Ruseckas, A.; Emelianova, E. V.; Wang, L.; Bansal, A. K.; Matheson, A.; Lemke, H. T.; Nielsen, M. M.; Nguyen, H.; Coulembier, O.; et al. Molecular Weight Dependence of Exciton Diffusion in Poly(3-Hexylthiophene). *Adv. Energy Mater.* **2013**, *3* (11), 1445–1453.
(65) Rand, B. P.; Girotto, C.; Mityashin, A.; Hadipour, A.; Genoe, J.; Heremans, P. Photocurrent Enhancement in Polymer:fullerene Bulk Heterojunction Solar Cells Doped with a Phosphorescent Molecule. *Appl. Phys. Lett.* **2009**, *95* (17), 173304–173304–3.
(66) Lunt, R. R.; Benziger, J. B.; Forrest, S. R. Relationship between Crystalline Order and Exciton Diffusion Length in Molecular Organic Semiconductors. *Adv. Mater.* **2010**, *22* (11), 1233–1236.
(67) Sun, Y.; Giebink, N. C.; Kanno, H.; Ma, B.; Thompson, M. E.; Forrest, S. R. Management of Singlet and Triplet Excitons for Efficient White Organic Light-Emitting Devices. *Nature* **2006**, *440* (7086), 908–912.
(68) Meijer, G.; Berden, G.; Meerts, W. L.; Hunziker, H. E.; de Vries, M. S.; Wendt, H. R. Spectroscopy on Triphenylamine and Its van Der Waals Complexes. *Chem. Phys.* **1992**, *163* (2), 209–222.
(69) Bansal, A. K.; Penzkofer, A. Linear and Nonlinear Optical Spectroscopic Characterisation of Triphenylamine and 1,2,3-tris(3-Methylphenylphenylamino)benzene. *Chem. Phys.* **2008**, *352* (1–3), 48–56.
(70) Waldeck, D. H. Photoisomerization Dynamics of Stilbenes. *Chem. Rev.* **1991**, *91* (3), 415–436.
(71) Karpicz, R.; Puzinas, S.; Krotkus, S.; Kazlauskas, K.; Jursenas, S.; Grazulevicius, J. V.; Grigalevicius, S.; Gulbinas, V. Impact of Intramolecular Twisting and Exciton Migration on Emission Efficiency of Multifunctional Fluorene-Benzothiadiazole-Carbazole Compounds. *J. Chem. Phys.* **2011**, *134* (20), 204508.
(72) Tong, H.; Dong, Y.; Hong, Y.; Häussler, M.; Lam, J. W. Y.; Sung, H. H.-Y.; Yu, X.; Sun, J.; Williams, I. D.; Kwok, H. S.; et al. Aggregation-Induced Emission: Effects of Molecular Structure, Solid-State Conformation, and Morphological Packing Arrangement on Light-Emitting Behaviors of Diphenyldibenzofulvene Derivatives. *J. Phys. Chem. C* **2007**, *111* (5), 2287–2294.
(73) Katan, C.; Terenziani, F.; Mongin, O.; Werts, M. H. V.; Porrès, L.; Pons, T.; Mertz, J.; Tretiak, S.; Blanchard-Desce, M. Effects of (Multi)branching of Dipolar Chromophores on Photophysical Properties and Two-Photon Absorption. *J. Phys. Chem. A* **2005**, *109* (13), 3024–3037.
(74) Terenziani, F.; Sissa, C.; Painelli, A. Symmetry Breaking in Octupolar Chromophores: Solvatochromism and Electroabsorption. *J. Phys. Chem. B* **2008**, *112* (16), 5079–5087.
(75) Keruckas, J.; Lygaitis, R.; Simokaitiene, J.; Grazulevicius, J. V.; Jankauskas, V.; Sini, G. Influence of Methoxy Groups on the Properties of 1,1-bis(4-Aminophenyl)cyclohexane Based Arylamines: Experimental and Theoretical Approach. *J. Mater. Chem.* **2012**, *22* (7), 3015–3027.
(76) Kersting, R.; Mollay, B.; Rusch, M.; Wenisch, J.; Leising, G.; Kauffmann, H. F. Femtosecond Site-Selective Probing of Energy Relaxing Excitons in

Poly(phenylenevinylene): Luminescence Dynamics and Lifetime Spectra. *J. Chem. Phys.* **1997**, *106* (7), 2850–2864.
(77) Krotkus, S.; Kazlauskas, K.; Miasojedovas, A.; Gruodis, A.; Tomkeviciene, A.; Grazulevicius, J. V.; Jursenas, S. Pyrenyl-Functionalized Fluorene and Carbazole Derivatives as Blue Light Emitters. *J. Phys. Chem. C* **2012**, *116* (13), 7561–7572.
(78) Xiang, H.-F.; Xu, Z.-X.; Roy, V. A. L.; Che, C.-M.; Lai, P. T. Method for Measurement of the Density of Thin Films of Small Organic Molecules. *Rev. Sci. Instrum.* **2007**, *78* (3), 034104.
(79) Banerjee, S.; Parhi, A. P.; Iyer, S. S. K.; Kumar, S. Method of Determining the Exciton Diffusion Length Using Optical Interference Effect in Schottky Diode. *Appl. Phys. Lett.* **2009**, *94* (22), 223303.
(80) Healy, A. T.; Boudouris, B. W.; Frisbie, C. D.; Hillmyer, M. A.; Blank, D. A. Intramolecular Exciton Diffusion in Poly(3-Hexylthiophene). *J. Phys. Chem. Lett.* **2013**, *4* (20), 3445–3449.
(81) Markov, D. E.; Tanase, C.; Blom, P. W. M.; Wildeman, J. Simultaneous Enhancement of Charge Transport and Exciton Diffusion in Poly(p-Phenylene Vinylene) Derivatives. *Phys. Rev. B* **2005**, *72* (4), 045217.
(82) Burlakov, V. M.; Kawata, K.; Assender, H. E.; Briggs, G. A. D.; Ruseckas, A.; Samuel, I. D. W. Discrete Hopping Model of Exciton Transport in Disordered Media. *Phys. Rev. B* **2005**, *72* (7), 075206.
(83) Athanasopoulos, S.; Emelianova, E. V.; Walker, A. B.; Beljonne, D. Exciton Diffusion in Energetically Disordered Organic Materials. *Phys. Rev. B* **2009**, *80* (19), 195209.
(84) Richert, R.; Ries, B.; Bässler, H. Time-Dependent Non-Equilibrium Exciton Diffusion in an Organic Glass. *Philos. Mag. Part B* **1984**, *49* (3), L25–L30.
(85) Sajjad, M. T.; Ward, A. J.; Kästner, C.; Ruseckas, A.; Hoppe, H.; Samuel, I. D. W. Controlling Exciton Diffusion and Fullerene Distribution in Photovoltaic Blends by Side Chain Modification. *J. Phys. Chem. Lett.* **2015**, *6* (15), 3054–3060.
(86) Mullenbach, T. K.; McGarry, K. A.; Luhman, W. A.; Douglas, C. J.; Holmes, R. J. Connecting Molecular Structure and Exciton Diffusion Length in Rubrene Derivatives. *Adv. Mater.* **2013**, *25* (27), 3689–3693.
(87) Yuan, W. Z.; Hu, R.; Lam, J. W. Y.; Xie, N.; Jim, C. K. W.; Tang, B. Z. Conjugated Hyperbranched Poly(aryleneethynylene)s: Synthesis, Photophysical Properties, Superquenching by Explosive, Photopatternability, and Tunable High Refractive Indices. *Chem. – Eur. J.* **2012**, *18* (10), 2847–2856.
(88) Tod Rieger, P.; Palese, S. P.; Dwayne Miller, R. J. On the Förster Model: Computational and Ultrafast Studies of Electronic Energy Transport. *Chem. Phys.* **1997**, *221* (1–2), 85–102.
(89) Fennel, F.; Lochbrunner, S. Long Distance Energy Transfer in a Polymer Matrix Doped with a Perylene Dye. *Phys. Chem. Chem. Phys.* **2011**, *13* (8), 3527–3533.
(90) Gray, V.; Dzebo, D.; Abrahamsson, M.; Albinsson, B.; Moth-Poulsen, K. Triplet–triplet Annihilation Photon-Upconversion: Towards Solar Energy Applications. *Phys. Chem. Chem. Phys.* **2014**, *16* (22), 10345.
(91) Schmidt, T. W.; Ekins-Daukes, N. J. A Molecular Approach to the Intermediate Band Solar Cell: The Symmetric Case. *Appl. Phys. Lett.* **2008**, *93* (6), 063507.

(92) Khnayzer, R. S.; Blumhoff, J.; Harrington, J. A.; Haefele, A.; Deng, F.; Castellano, F. N. Upconversion-Powered Photoelectrochemistry. *Chem Commun* **2012**, *48* (2), 209–211.
(93) Lin, B.-Y.; Easley, C. J.; Chen, C.-H.; Tseng, P.-C.; Lee, M.-Z.; Sher, P.-H.; Wang, J.-K.; Chiu, T.-L.; Lin, C.-F.; Bardeen, C. J.; et al. Exciplex-Sensitized Triplet-Triplet Annihilation in Heterojunction Organic Thin-Film. *ACS Appl. Mater. Interfaces* **2017**.
(94) Chiang, C.-J.; Kimyonok, A.; Etherington, M. K.; Griffiths, G. C.; Jankus, V.; Turksoy, F.; Monkman, A. P. Ultrahigh Efficiency Fluorescent Single and Bi-Layer Organic Light Emitting Diodes: The Key Role of Triplet Fusion. *Adv. Funct. Mater.* **2013**, *23* (6), 739–746.
(95) Wohnhaas, C.; Mailänder, V.; Dröge, M.; Filatov, M. A.; Busko, D.; Avlasevich, Y.; Baluschev, S.; Miteva, T.; Landfester, K.; Turshatov, A. Triplet-Triplet Annihilation Upconversion Based Nanocapsules for Bioimaging under Excitation by Red and Deep-Red Light. *Macromol. Biosci.* **2013**, *13* (10), 1422–1430.
(96) Liu, Q.; Feng, W.; Yang, T.; Yi, T.; Li, F. Upconversion Luminescence Imaging of Cells and Small Animals. *Nat. Protoc.* **2013**, *8* (10), 2033–2044.
(97) Simon, Y. C.; Weder, C. Low-Power Photon Upconversion through Triplet–triplet Annihilation in Polymers. *J. Mater. Chem.* **2012**, *22* (39), 20817–20830.
(98) Zhou, J.; Liu, Q.; Feng, W.; Sun, Y.; Li, F. Upconversion Luminescent Materials: Advances and Applications. *Chem. Rev.* **2015**, *115* (1), 395–465.
(99) Bagnich, S. A.; Bässler, H. Origin of Delayed Fluorescence of a Ladder-Type Methyl-Poly(para-Phenylene) Doped with Pt(II)octaethylporphyrin. *Chem. Phys. Lett.* **2003**, *381* (3–4), 464–470.
(100) Keivanidis, P. e.; Baluschev, S.; Miteva, T.; Nelles, G.; Scherf, U.; Yasuda, A.; Wegner, G. Up-Conversion Photoluminescence in Polyfluorene Doped with Metal(II)–Octaethyl Porphyrins. *Adv. Mater.* **2003**, *15* (24), 2095–2098.
(101) Islangulov, R. R.; Lott, J.; Weder, C.; Castellano, F. N. Noncoherent Low-Power Upconversion in Solid Polymer Films. *J. Am. Chem. Soc.* **2007**, *129* (42), 12652–12653.
(102) Kim, J.-H.; Deng, F.; Castellano, F. N.; Kim, J.-H. High Efficiency Low-Power Upconverting Soft Materials. *Chem. Mater.* **2012**, *24* (12), 2250–2252.
(103) Monguzzi, A.; Mauri, M.; Bianchi, A.; Dibbanti, M. K.; Simonutti, R.; Meinardi, F. Solid-State Sensitized Upconversion in Polyacrylate Elastomers. *J. Phys. Chem. C* **2016**, *120* (5), 2609–2614.
(104) Vadrucci, R.; Weder, C.; C. Simon, Y. Organogels for Low-Power Light Upconversion. *Mater. Horiz.* **2015**, *2* (1), 120–124.
(105) Duan, P.; Yanai, N.; Nagatomi, H.; Kimizuka, N. Photon Upconversion in Supramolecular Gel Matrixes: Spontaneous Accumulation of Light-Harvesting Donor–Acceptor Arrays in Nanofibers and Acquired Air Stability. *J. Am. Chem. Soc.* **2015**, *137* (5), 1887–1894.
(106) Svagan, A. J.; Busko, D.; Avlasevich, Y.; Glasser, G.; Baluschev, S.; Landfester, K. Photon Energy Upconverting Nanopaper: A Bioinspired Oxygen Protection Strategy. *ACS Nano* **2014**, *8* (8), 8198–8207.
(107) Monguzzi, A.; Mauri, M.; Frigoli, M.; Pedrini, J.; Simonutti, R.; Larpent, C.; Vaccaro, G.; Sassi, M.; Meinardi, F. Unraveling Triplet Excitons Photophysics in Hyper-Cross-Linked Polymeric Nanoparticles: Toward the Next

Generation of Solid-State Upconverting Materials. *J. Phys. Chem. Lett.* **2016**, *7* (14), 2779–2785.
(108) Merkel, P. B.; Dinnocenzo, J. P. Low-Power Green-to-Blue and Blue-to-UV Upconversion in Rigid Polymer Films. *J. Lumin.* **2009**, *129* (3), 303–306.
(109) Monguzzi, A.; Tubino, R.; Meinardi, F. Multicomponent Polymeric Film for Red to Green Low Power Sensitized Up-Conversion. *J. Phys. Chem. A* **2009**, *113* (7), 1171–1174.
(110) Lee, S. H.; Lott, J. R.; Simon, Y. C.; Weder, C. Melt-Processed Polymer Glasses for Low-Power Upconversion via Sensitized Triplet–triplet Annihilation. *J. Mater. Chem. C* **2013**, *1* (33), 5142–5148.
(111) Lee, S. H.; Ayer, M. A.; Vadrucci, R.; Weder, C.; Simon, Y. C. Light Upconversion by Triplet–triplet Annihilation in Diphenylanthracene-Based Copolymers. *Polym. Chem.* **2014**, *5* (24), 6898–6904.
(112) Vadrucci, R.; Weder, C.; Simon, Y. C. Low-Power Photon Upconversion in Organic Glasses. *J. Mater. Chem. C* **2014**, *2* (16), 2837–2841.
(113) Marsico, F.; Turshatov, A.; Peköz, R.; Avlasevich, Y.; Wagner, M.; Weber, K.; Donadio, D.; Landfester, K.; Baluschev, S.; Wurm, F. R. Hyperbranched Unsaturated Polyphosphates as a Protective Matrix for Long-Term Photon Upconversion in Air. *J. Am. Chem. Soc.* **2014**, *136* (31), 11057–11064.
(114) Simon, Y. C.; Weder, C. Metal-Organic Frameworks: Framing Upconversion Materials. *Nat. Mater.* **2015**, *14* (9), 864–865.
(115) Serevičius, T.; Komskis, R.; Adomėnas, P.; Adomėnienė, O.; Jankauskas, V.; Gruodis, A.; Kazlauskas, K.; Juršėnas, S. Non-Symmetric 9,10-Diphenylanthracene-Based Deep-Blue Emitters with Enhanced Charge Transport Properties. *Phys. Chem. Chem. Phys.* **2014**, *16* (15), 7089–7101.
(116) Rothe, C.; Monkman, A. P. Triplet Exciton Migration in a Conjugated Polyfluorene. *Phys. Rev. B* **2003**, *68* (7), 075208.
(117) Hirayama, H.; Sugawara, Y.; Miyashita, Y.; Mitsuishi, M.; Miyashita, T. Direct Observation of Back Energy Transfer in Blue Phosphorescent Materials for Organic Light Emitting Diodes by Time-Resolved Optical Waveguide Spectroscopy. *Appl. Phys. Lett.* **2013**, *102* (8).
(118) Haefele, A.; Blumhoff, J.; Khnayzer, R. S.; Castellano, F. N. Getting to the (Square) Root of the Problem: How to Make Noncoherent Pumped Upconversion Linear. *J. Phys. Chem. Lett.* **2012**, *3* (3), 299–303.
(119) Monguzzi, A.; Mezyk, J.; Scotognella, F.; Tubino, R.; Meinardi, F. Upconversion-Induced Fluorescence in Multicomponent Systems: Steady-State Excitation Power Threshold. *Phys. Rev. B* **2008**, *78* (19), 195112.
(120) Schlenker, C. W.; Chen, K.-S.; Yip, H.-L.; Li, C.-Z.; Bradshaw, L. R.; Ochsenbein, S. T.; Ding, F.; Li, X. S.; Gamelin, D. R.; Jen, A. K.-Y.; et al. Polymer Triplet Energy Levels Need Not Limit Photocurrent Collection in Organic Solar Cells. *J. Am. Chem. Soc.* **2012**, *134* (48), 19661–19668.
(121) Mikhnenko, O. V.; Blom, P. W. M.; Nguyen, T.-Q. Exciton Diffusion in Organic Semiconductors. *Energy Environ. Sci.* **2015**, *8* (7), 1867–1888.
(122) Schwartz, G.; Reineke, S.; Rosenow, T. C.; Walzer, K.; Leo, K. Triplet Harvesting in Hybrid White Organic Light-Emitting Diodes. *Adv. Funct. Mater.* **2009**, *19* (9), 1319–1333.
(123) Shao, Y.; Yang, Y. Efficient Organic Heterojunction Photovoltaic Cells Based on Triplet Materials. *Adv. Mater.* **2005**, *17* (23), 2841–2844.

(124) Rand, B. P.; Schols, S.; Cheyns, D.; Gommans, H.; Girotto, C.; Genoe, J.; Heremans, P.; Poortmans, J. Organic Solar Cells with Sensitized Phosphorescent Absorbing Layers. *Org. Electron.* **2009**, *10* (5), 1015–1019.
(125) Kroeze, J. E.; Savenije, T. J.; Candeias, L. P.; Warman, J. M.; Siebbeles, L. D. A. Triplet Exciton Diffusion and Delayed Interfacial Charge Separation in a Tio2/PdTPPC Bilayer: Monte Carlo Simulations. *Sol. Energy Mater. Sol. Cells* **2005**, *85* (2), 189–203.
(126) Mikhnenko, O. V.; Ruiter, R.; Blom, P. W. M.; Loi, M. A. Direct Measurement of the Triplet Exciton Diffusion Length in Organic Semiconductors. *Phys. Rev. Lett.* **2012**, *108* (13), 137401.
(127) Avakian, P.; Merrifield, R. E. Experimental Determination of the Diffusion Length of Triplet Excitons in Anthracene Crystals. *Phys. Rev. Lett.* **1964**, *13* (18), 541–543.
(128) Mahato, P.; Monguzzi, A.; Yanai, N.; Yamada, T.; Kimizuka, N. Fast and Long-Range Triplet Exciton Diffusion in Metal-Organic Frameworks for Photon Upconversion at Ultralow Excitation Power. *Nat. Mater.* **2015**, *14* (9), 924–930.
(129) Tamai, Y.; Ohkita, H.; Benten, H.; Ito, S. Exciton Diffusion in Conjugated Polymers: From Fundamental Understanding to Improvement in Photovoltaic Conversion Efficiency. *J. Phys. Chem. Lett.* **2015**, *6* (17), 3417–3428.
(130) Menke, S. M.; Holmes, R. J. Exciton Diffusion in Organic Photovoltaic Cells. *Energy Env. Sci* **2014**, *7* (2), 499–512.
(131) Adams, J. M.; Ramdas, S. The Crystal Structure of Solution-Grown 9,10-Diphenylanthracene. A Combined Computational and X-Ray Study. *Acta Crystallogr. B* **1979**, *35* (3), 679–683.
(132) Gray, V.; Börjesson, K.; Dzebo, D.; Abrahamsson, M.; Albinsson, B.; Moth-Poulsen, K. Porphyrin–Anthracene Complexes: Potential in Triplet–Triplet Annihilation Upconversion. *J. Phys. Chem. C* **2016**, *120* (34), 19018–19026.
(133) Karpicz, R.; Puzinas, S.; Gulbinas, V.; Vakhnin, A.; Kadashchuk, A.; Rand, B. P. Exciton Dynamics in an Energy up-Converting Solid State System Based on Diphenylanthracene Doped with Platinum Octaethylporphyrin. *Chem. Phys.* **2014**, *429*, 57–62.
(134) Jankus, V.; Snedden, E. W.; Bright, D. W.; Whittle, V. L.; Williams, J. A. G.; Monkman, A. Energy Upconversion via Triplet Fusion in Super Yellow PPV Films Doped with Palladium Tetraphenyltetrabenzoporphyrin: A Comprehensive Investigation of Exciton Dynamics. *Adv. Funct. Mater.* **2013**, *23* (3), 384–393.
(135) Lakowicz, J. R. *Principles of Fluorescence Spectroscopy*; Springer Science & Business Media, 2007.
(136) Kirschner, S. B.; Smith, N. P.; Wepasnick, K. A.; Katz, H. E.; Kirby, B. J.; Borchers, J. A.; Reich, D. H. X-Ray and Neutron Reflectivity and Electronic Properties of PCBM-Poly(bromo)styrene Blends and Bilayers with poly(3-Hexylthiophene). *J. Mater. Chem.* **2012**, *22* (10), 4364–4370.
(137) Muthuraja, A.; Kalainathan, S. 9,10-Diphenylanthracene (DPA) Single Crystals Grown by Conventional Slow Evaporation Method and Its Characterisation. *Mater. Res. Innov.* **2016**, *20* (5), 358–364.

(138) Mikhnenko, O. V.; Kuik, M.; Lin, J.; van der Kaap, N.; Nguyen, T.-Q.; Blom, P. W. M. Trap-Limited Exciton Diffusion in Organic Semiconductors. *Adv. Mater.* **2014**, *26* (12), 1912–1917.
(139) Curtin, I. J.; Blaylock, W. D.; Holmes, R. J. Role of Impurities in Determining the Exciton Diffusion Length in Organic Semiconductors. *Appl. Phys. Lett.* **2016**, *108* (16), 163301.
(140) Liu, H.; Yan, F.; Li, W.; Lee, C.-S.; Chu, B.; Chen, Y.; Li, X.; Han, L.; Su, Z.; Zhu, J.; et al. Up-Conversion Luminescence of Crystalline Rubrene without Any Sensitizers. *Org. Electron.* **2010**, *11* (5), 946–950.
(141) Ye, C.; Zhou, L.; Wang, X.; Liang, Z. Photon Upconversion: From Two-Photon Absorption (TPA) to Triplet–triplet Annihilation (TTA). *Phys. Chem. Chem. Phys.* **2016**, *18* (16), 10818–10835.
(142) Lee, J.-H.; Ho, Y.-H.; Lin, T.-C.; Wu, C.-F. High-Efficiency Fluorescent Blue Organic Light-Emitting Device with Balanced Carrier Transport. *J. Electrochem. Soc.* **2007**, *154* (7), 226–228.
(143) Wu, M.; Congreve, D. N.; Wilson, M. W. B.; Jean, J.; Geva, N.; Welborn, M.; Van Voorhis, T.; Bulović, V.; Bawendi, M. G.; Baldo, M. A. Solid-State Infrared-to-Visible Upconversion Sensitized by Colloidal Nanocrystals. *Nat. Photonics* **2016**, *10* (1), 31–34.
(144) Gupta, J.; Vadukumpully, S.; Valiyaveettil, S. Synthesis and Property Studies of Linear and Kinked Poly(pyreneethynylene)s. *Polymer* **2010**, *51* (22), 5078–5086.
(145) Goudarzi, H.; Keivanidis, P. E. All-Solution-Based Aggregation Control in Solid-State Photon Upconverting Organic Model Composites. *ACS Appl. Mater. Interfaces* **2017**, *9* (1), 845–857.
(146) Turshatov, A.; Busko, D.; Kiseleva, N.; Grage, S. L.; Howard, I. A.; Richards, B. S. Room-Temperature High-Efficiency Solid-State Triplet-Triplet Annihilation Up-Conversion in Amorphous Poly(olefin Sulfone)s. *ACS Appl. Mater. Interfaces* **2017**.